Galaxy Clusters and the IntraCluster Medium

Rashid Sunyaev

Yakov Zeldovich

The Observation of Relic Radiation as a Test of the Nature of X-Ray Radiation from the Clusters of Galaxies

Introduction

The x-ray radiation from a number of clusters of galaxies (Coma, Virgo, Perseus) was discovered recently.[1] It is assumed that clusters of galaxies form an important class of powerful x-ray sources, possibly giving the main contribution to the x-ray background radiation of the Universe.[2] What is the nature of these sources? What physical mechanisms give the observed x-ray radiation?

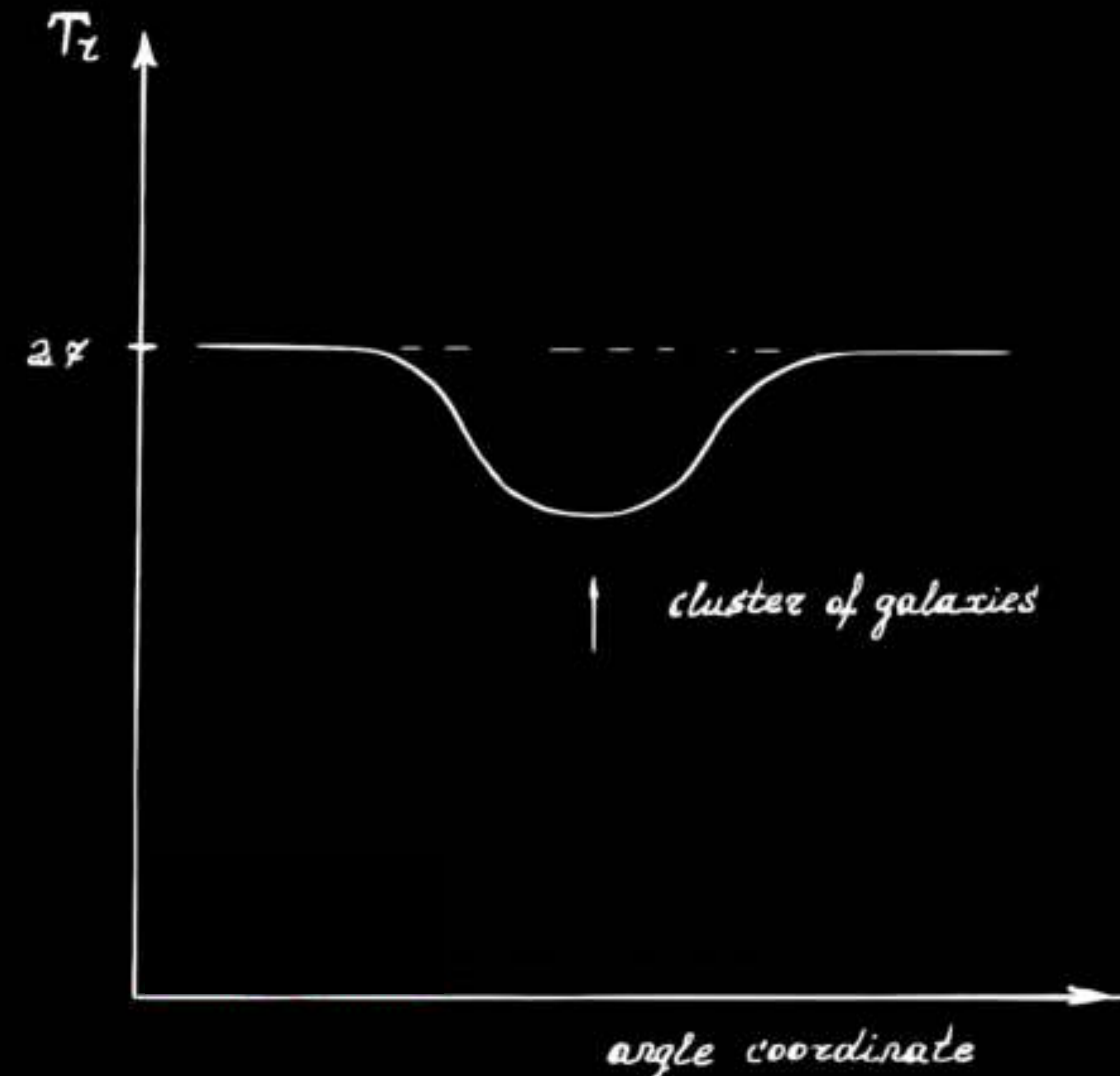

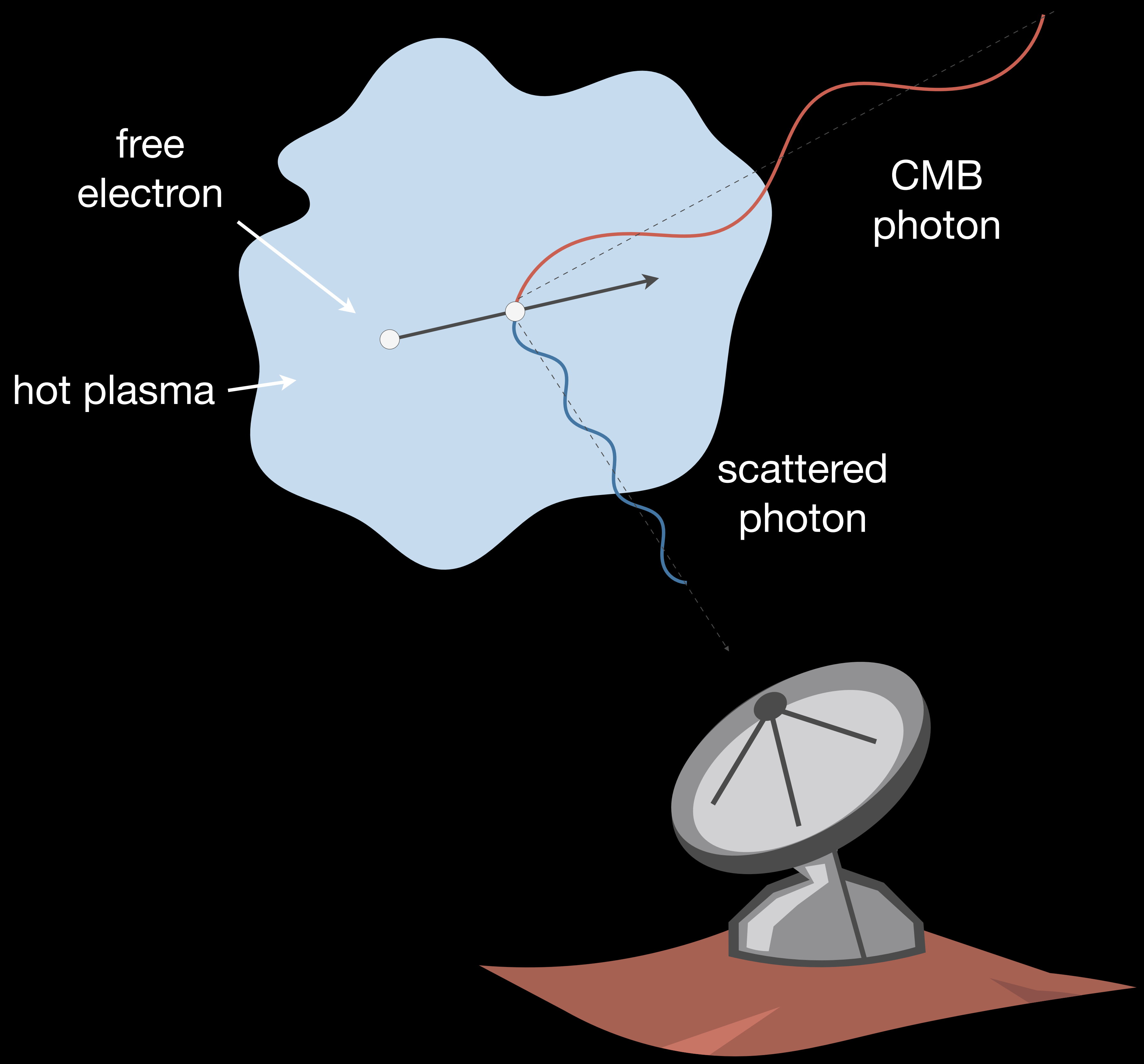
free
electron
hot plasma
CMB
photon
scattered
photon

CMB spectral distortion

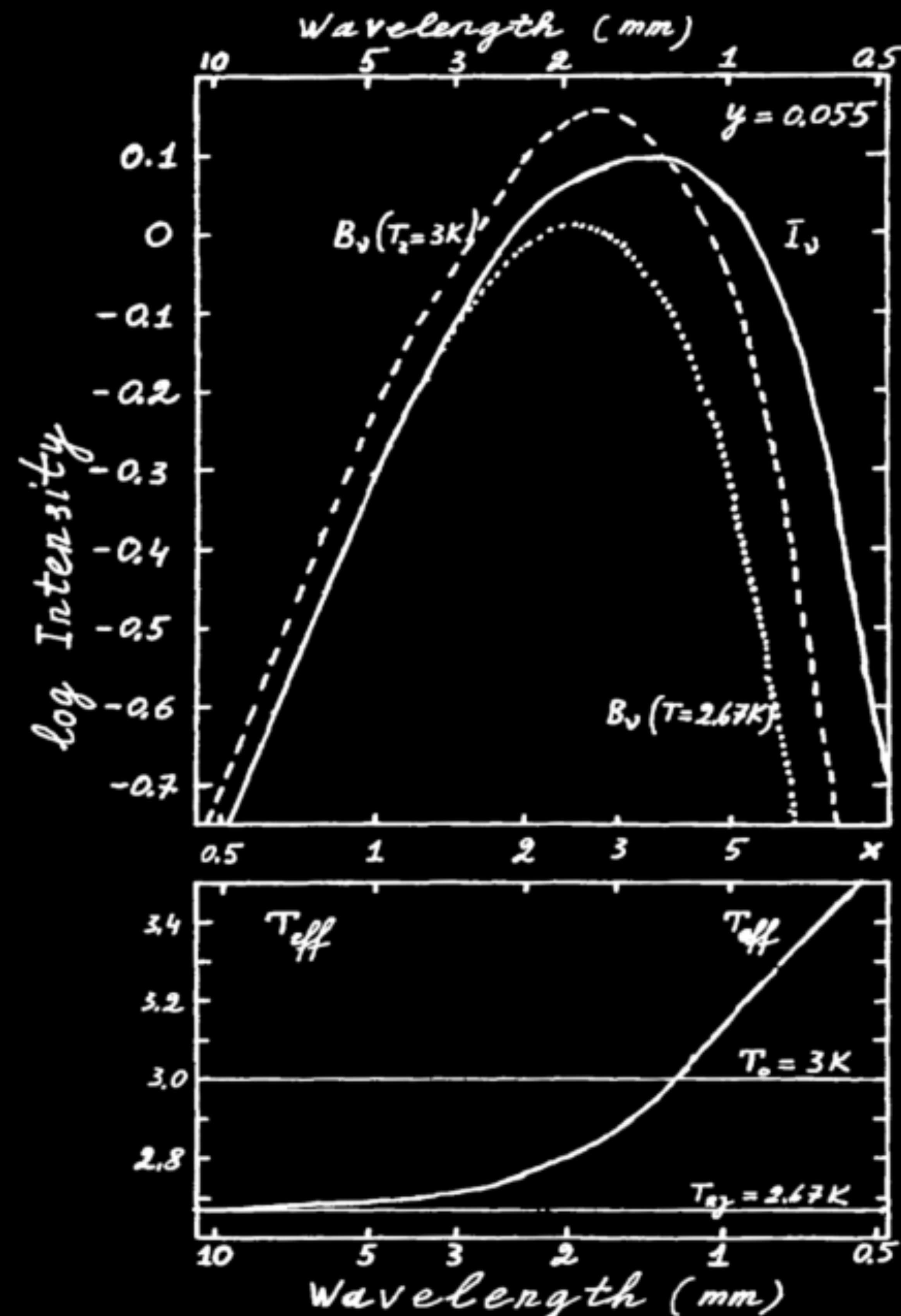

Sunyaev & Zeldovich, ARA&A, 18, 1980

Some useful equations

$$\delta I_\nu \approx \frac{2(k_\mathrm{B}T_\mathrm{CMB})^3}{(h\nu)^2}\frac{x^4e^x}{(e^x-1)^2}\left[x\frac{e^x+1}{e^x-1}-4\right]y \qquad x=\frac{h\nu}{k_\mathrm{B}T_\mathrm{CMB}}$$

$$\delta T \approx T_\mathrm{CMB}\left[x\frac{e^x+1}{e^x-1}-4\right]y \qquad y=\frac{\sigma_\mathrm{T}}{m_ec^2}\int n_eT_e\mathrm{d}l$$

peculiar spectral signature

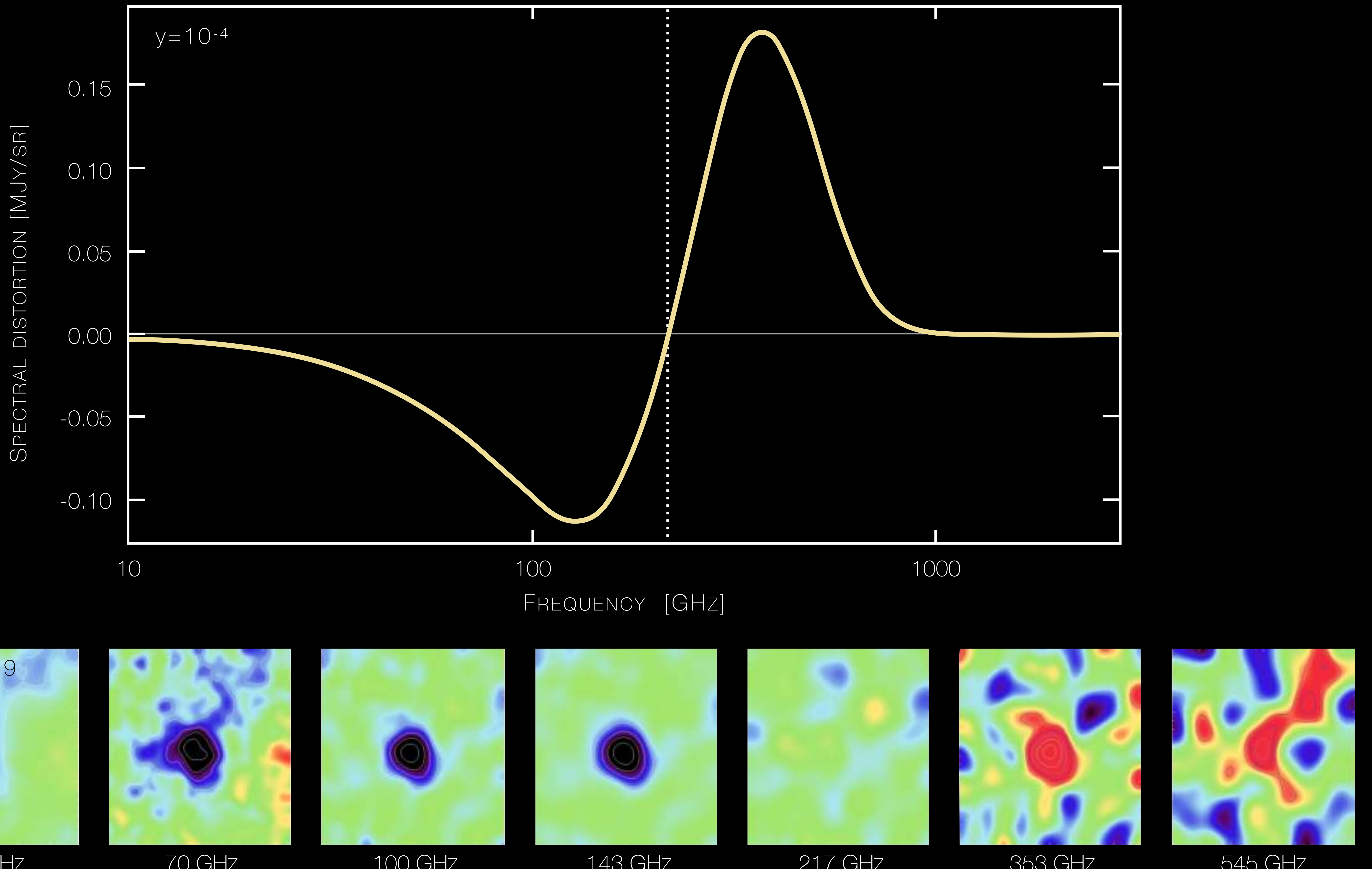

y=10-4
Spectral distortion [MJy/sr]
0.15
0.10
0.05
0.00
-0.05
-0.10
10
100
1000
Frequency [GHz]
Abell 2319
44 GHz
70 GHz
100 GHz
143 GHz
217 GHz
353 GHz
545 GHz

Some useful equations

$$\delta I_\nu \approx \frac{2(k_\mathrm{B} T_\mathrm{CMB})^3}{(h\nu)^2} \frac{x^4 e^x}{(e^x - 1)^2} \left[x \frac{e^x + 1}{e^x - 1} - 4 \right] y \qquad x = \frac{h\nu}{k_\mathrm{B} T_\mathrm{CMB}}$$

$$\delta T \approx T_\mathrm{CMB} \left[x \frac{e^x + 1}{e^x - 1} - 4 \right] y \qquad y = \frac{\sigma_\mathrm{T}}{m_e c^2} \int n_e T_e \mathrm{d}l$$

peculiar spectral signature
no redshift dependence

no redshift dependence

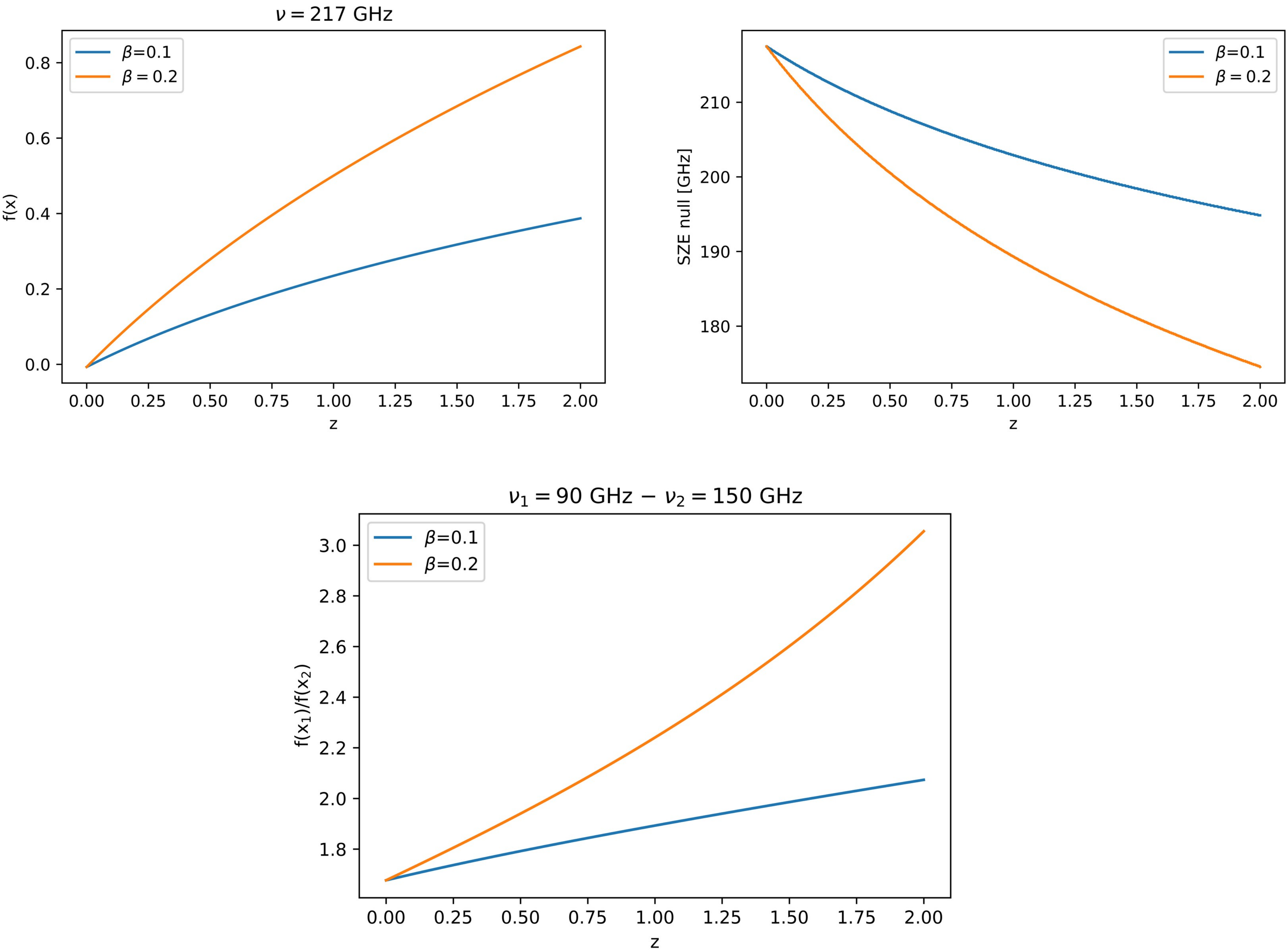

ν = 217 GHz
β=0.1
β = 0.2
0.8
0.6
0.4
0.2
0.0
f(x)
0.00
0.25
0.50
0.75
1.00
1.25
1.50
1.75
2.00
z
β=0.1
β = 0.2
210
200
190
180
SZE null [GHz]
0.00
0.25
0.50
0.75
1.00
1.25
1.50
1.75
2.00
z
ν1 = 90 GHz − ν2 = 150 GHz
β=0.1
β=0.2
3.0
2.8
2.6
2.4
2.2
2.0
1.8
f(x1)/f(x2)
0.00
0.25
0.50
0.75
1.00
1.25
1.50
1.75
2.00
z

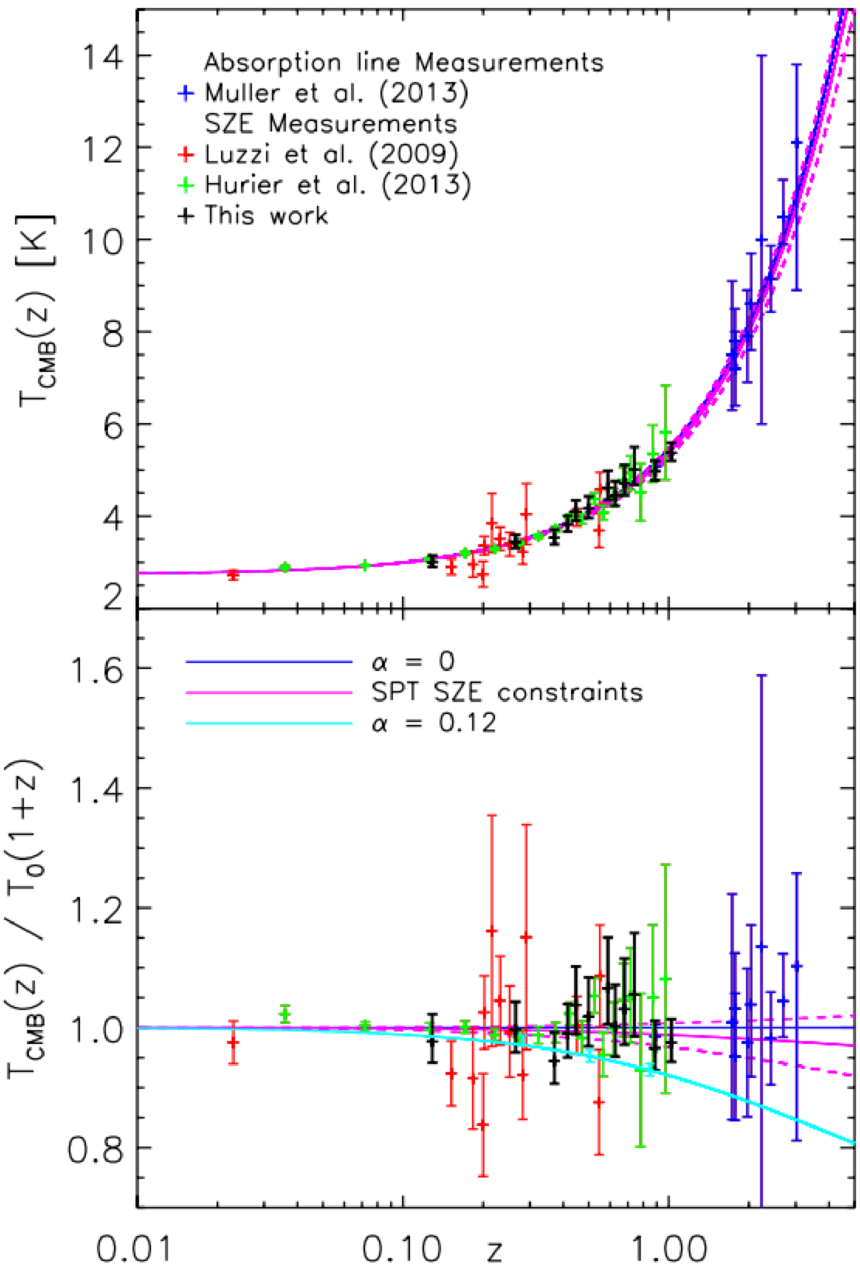

Saro et al. 2014

Method	Reference	z	N	T_{CMB} (K)	β	Label
SZ effect towards clusters	Saro et al. (2014) [18]	0.055 – 1.350	158	-	0.017 ± 0.030	[a]
		0.3 – 1.350		-	0.016 ± 0.031	[b]
	de Martino et al. (2015) [15]	< 0.3	481	-	-0.007 ± 0.013	[c]
	Luzzi et al. (2015) [16]	0.011 – 0.972	103	-	0.012 ± 0.016	[d]
		0.011 – 0.972	99	-	0.014 ± 0.016	[e]
		0.3 – 0.972	33	-	0.020 ± 0.017	[f]
	Luzzi et al. (2009) [14]	0.023 – 0.546	13	-	0.065 ± 0.080	[g]
		0.200 – 0.546	7	-	0.044 ± 0.087	[h]
		0.3 – 0.546	2	-	0.05 ± 0.14	[i]
	Hurier et al. (2014) [17]	0 – 1	813	-	0.009 ± 0.017	[j]
		0.30 – 0.35	81	3.562 ± 0.050	-0.006 ± 0.022	[k]
		0.35 – 0.40	50	3.717 ± 0.063		
		0.40 – 0.45	45	3.971 ± 0.071		
		0.45 – 0.50	26	3.943 ± 0.112		
		0.50 – 0.55	20	4.380 ± 0.119		
		0.55 – 0.60	18	4.075 ± 0.156		
		0.60 – 0.65	12	4.404 ± 0.194		
		0.65 – 0.70	6	4.779 ± 0.278		
		0.70 – 0.75	5	4.933 ± 0.371		
		0.75 – 0.80	2	4.515 ± 0.621		
		0.85 – 0.90	1	5.356 ± 0.617		
		0.95 – 1.00	1	5.813 ± 1.025		
QSO absorption lines	Muller et al. (2013) [19]	0.89	1	$5.0791^{+0.0993}_{-0.0994}$	0.005 ± 0.022	[l]
	Noterdeame et al. (2011) [20]	1.7293	1	$7.5^{+1.6}_{-1.2}$		
		1.7738	1	$7.8^{+0.7}_{-0.6}$		
		2.0377	1	$8.6^{+1.1}_{-1.0}$		
	Cui et al. (2005) [21]	1.77654	1	7.2 ± 0.8		
	Ge et al. (2001) [22]	1.9731	1	7.9 ± 1.0		
	Srianand et al. (2000) [23]	2.33771	1	6 – 14		
	Srianand (2008) [24]	2.4184	1	9.15 ± 0.72		
	Noterdaeme et al. (2010) [25]	2.6896	1	$10.5^{+0.8}_{-0.6}$		
	Molaro et al. (2002) [26]	3.025	1	$12.1^{+1.7}_{-3.2}$		

Avgoustidis et al. 2019

H_0 constraints from X-ray and SZE observations

- Very simple idea that traces back to the work Cavaliere et al. (1977)
- It is based on a distance-measuring techniques that depend on a comparison of 2 observables:

$$E \propto \int n_e^2 dl$$

$$A \propto \int n_e dl$$

- A^2/E is a 'Density-weighted' measure of the path-length through the gas [dimensions of a length]
- If the structure of the gas is known, and if we can measure the angular size θ then the angular diameter distance is $D_a(z)=A^2/(E\,\Theta)$

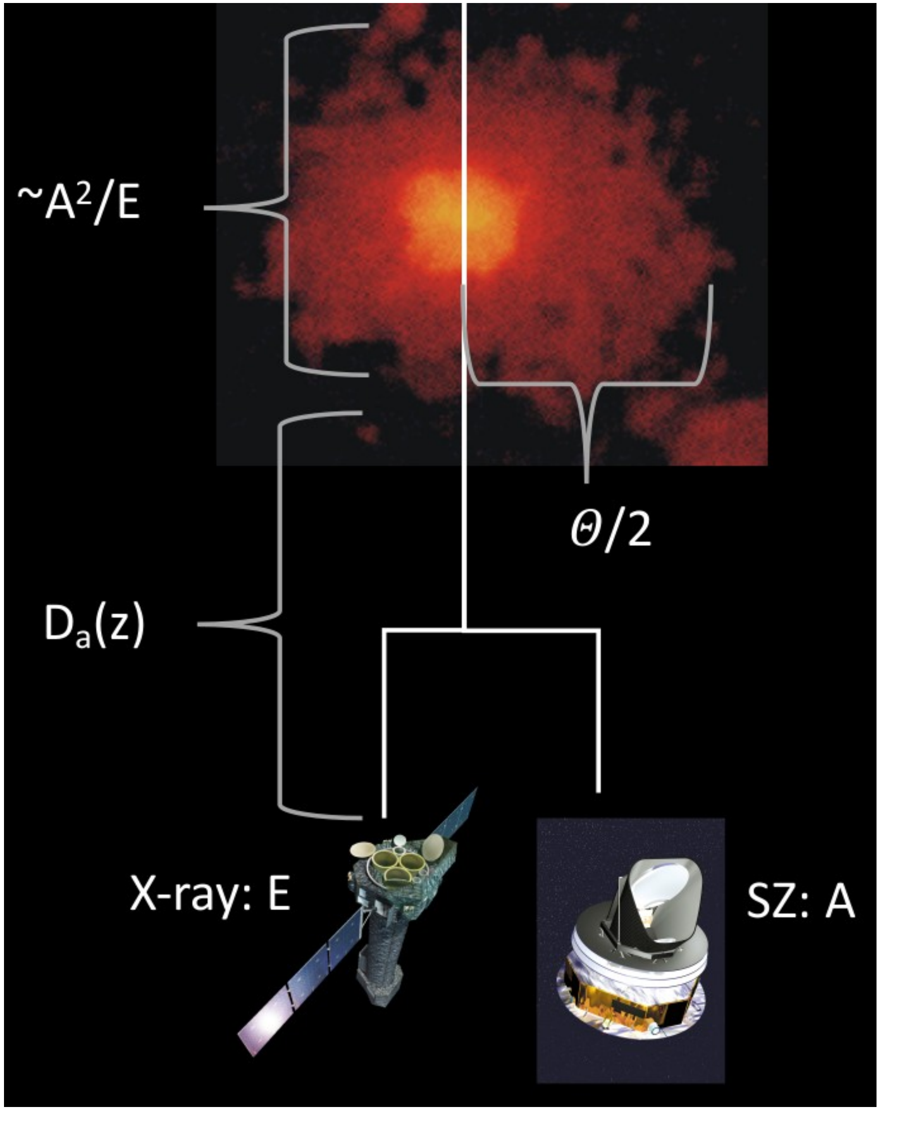

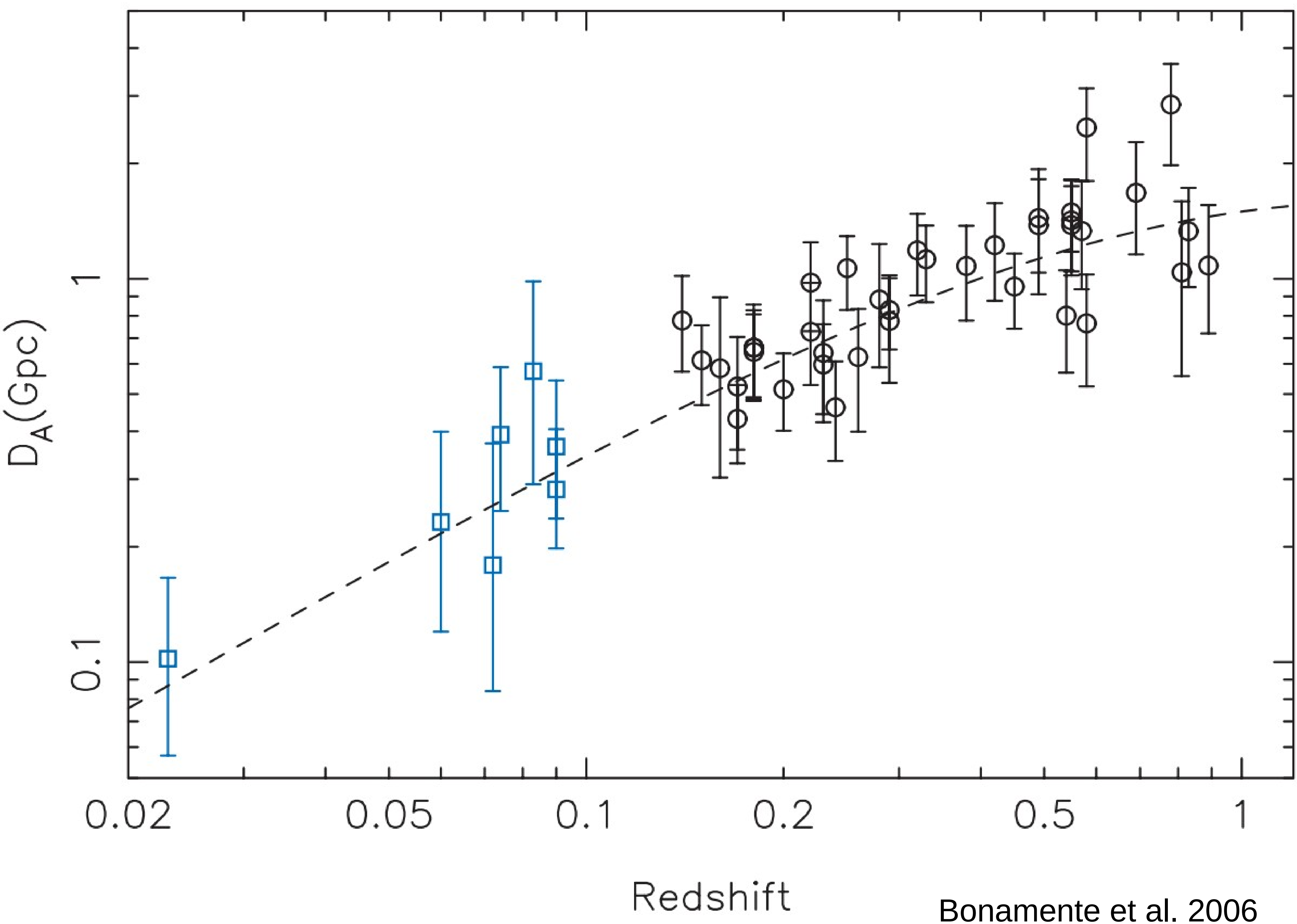

Bonamente et al. 2006

- Birkinshaw (1979)
- Reese et al. (2000)
- Patel et al. (2000)
- Mason et al. (2001)
- Reese et al. (2002)
- Sereno (2003)
- Udomprasert et al. (2004)
- Reese et al. (2004)
- Schmidt et al. (2004)
- Jones et al. (2005)
- Bonamente et al. (2006)
- Kozmanyan et al. (2019)

SZ measurements from RT, OVRO and BIMA, X-ray from ROSAT

26 clusters z < 0.78

H_0 = 61±3(stat.)±18(sys.) km/s/Mpc

SZ measurements from OVRO, BIMA and X-ray from Chandra

38 clusters 0.14< z< 0.89

H_0 = 76.9±4(stat.) ±9(sys.) km/s/Mpc

Three regular clusters

z=0.088, 0.2523, and 0.451

H_0 = 68±8(stat.) km/s/Mpc

SZ measurments from Planck and X-ray from XMM

61 nearby systems (z<0.5)

H_0 = 67± 3km/s/Mpc

Article	Number	redshift	Ω_m, Ω_Λ	value	SZ data source	X-ray data source
Reese et al. (2000)	2	0.55	0.3, 0.7	$63^{+12}_{-9}{}^{+21}_{-21}$	OVRO, BIMA	ROSAT
Patel et al. (2000)	1	0.322	0.3, 0.7	$52.2^{+11.4}_{-11.9}{}^{+18.5}_{-17.7}$	OVRO, BIMA, MMT[2]	ROSAT, ASCA[3]
Mason et al. (2001)	7	< 0.1	0.3, 0.7	$66^{+14}_{-11}{}^{+15}_{-15}$	OVRO	ROSAT
Grainge et al. (2002a)	1	0.143	1, 0	57^{+23}_{-16}	RT	ROSAT, ASCA
Reese et al. (2002)	18	0.14 – 0.78	0.3, 0.7	$60^{+4}_{-4}{}^{+13}_{-18}$	OVRO, BIMA	ROSAT
Saunders et al. (2003)	1	0.217	0.3, 0.7	85^{+20}_{-17}	RT	ROSAT, ASCA
Reese (2004)	26	0 – 0.78	0.3, 0.7	$61 \pm 3 \pm 18$	RT, OVRO, BIMA	ROSAT
Battistelli et al. (2003)	1	0.0231	0.27, 0.73	84 ± 26	OVRO, WMAP[4], MITO[5]	ROSAT
Udomprasert et al. (2004)	7	< 0.1	0.3, 0.7	$67^{+30}_{-18}{}^{+15}_{-6}$	CBI	ROSAT, ASCA, BeppoSAX[6]
Schmidt et al. (2004)	3	0.09 – 0.45	0.3, 0.7	69 ± 8	various	Chandra
Jones et al. (2005)	5	0.14 – 0.3	0.3, 0.7	$66^{+11}_{-10}{}^{+9}_{-8}$	RT	ROSAT, ASCA
Bonamente et al. (2006)	38	0.14 – 0.89	0.3, 0.7		OVRO, BIMA	Chandra
	double β-model with HSE			$76.9^{+3.9}_{-3.4}{}^{+10.0}_{-8.0}$		
	isothermal β-model			$73.7^{+4.6}_{-3.8}{}^{+9.5}_{-7.6}$		
	isothermal β-model with excised core			$77.6^{+4.8}_{-4.3}{}^{+10.1}_{-8.2}$		

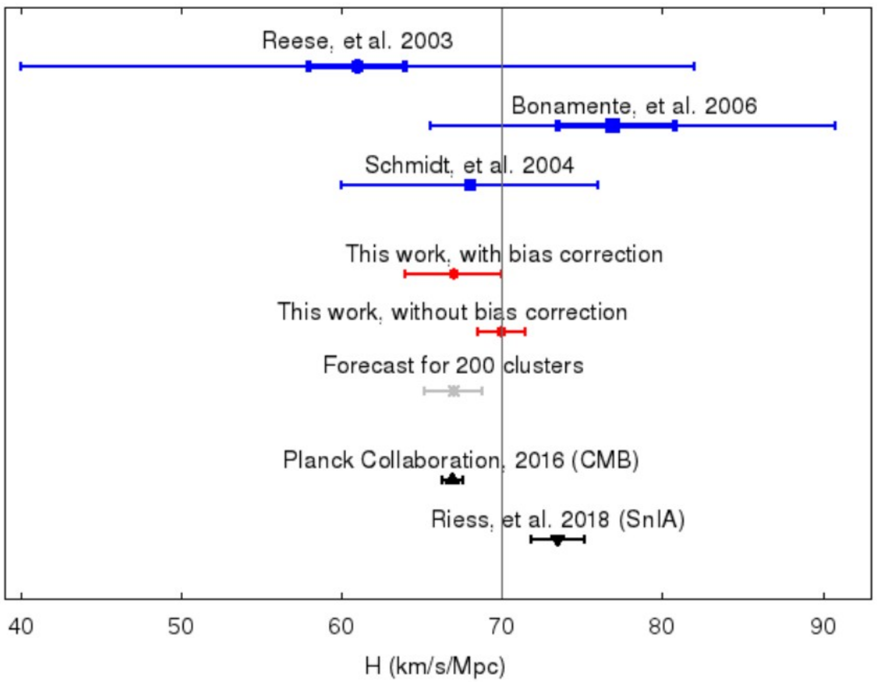

61 galaxy clusters with redshifts up to $z < 0.5$ observed with Planck and XMM-Newton: $H_0 = 67 \pm 3 \mathrm{km\ s^{-1}\ Mpc^{-1}}$

Kozmanyan et al. 2019

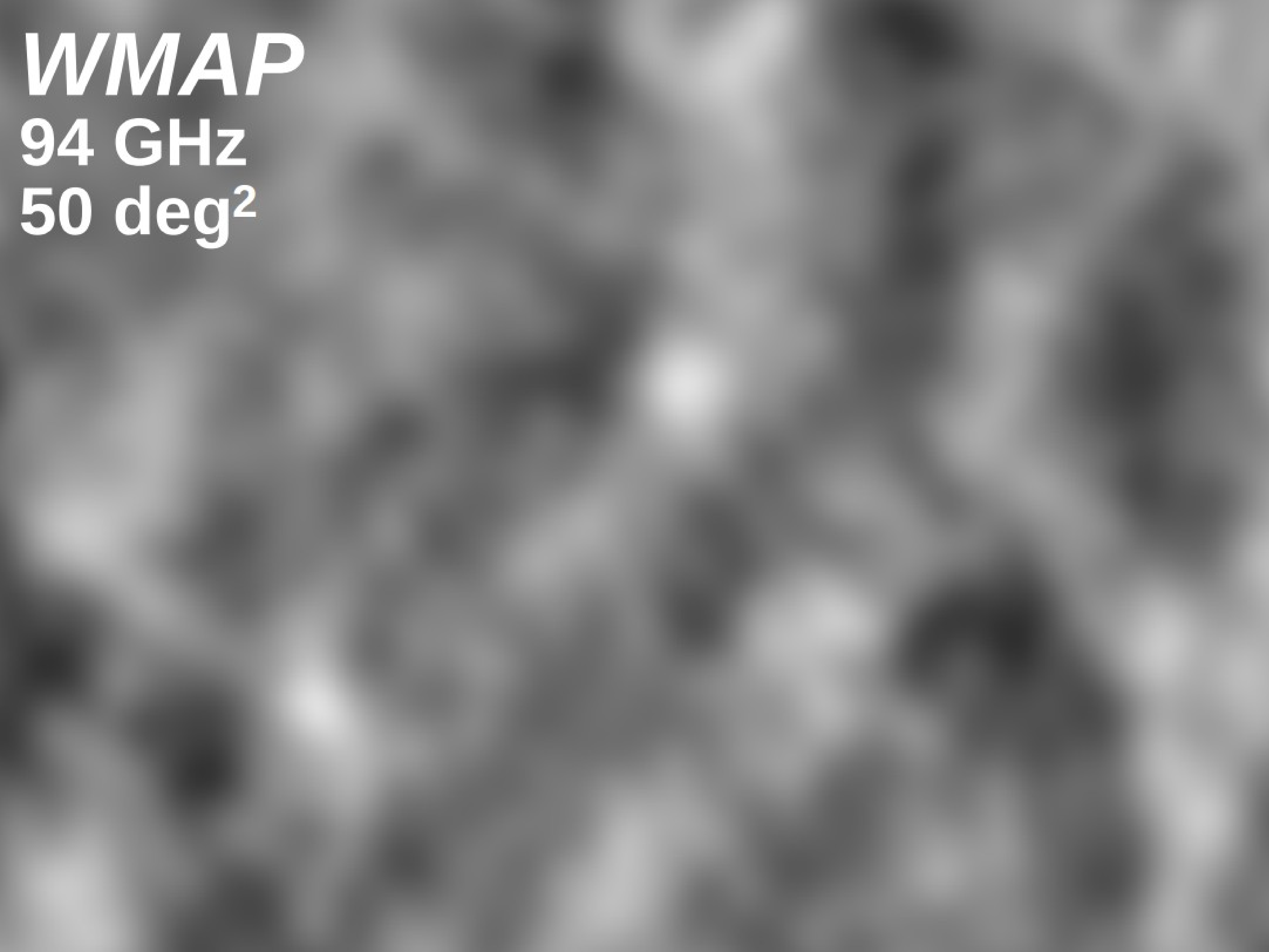
WMAP
94 GHz
50 deg2

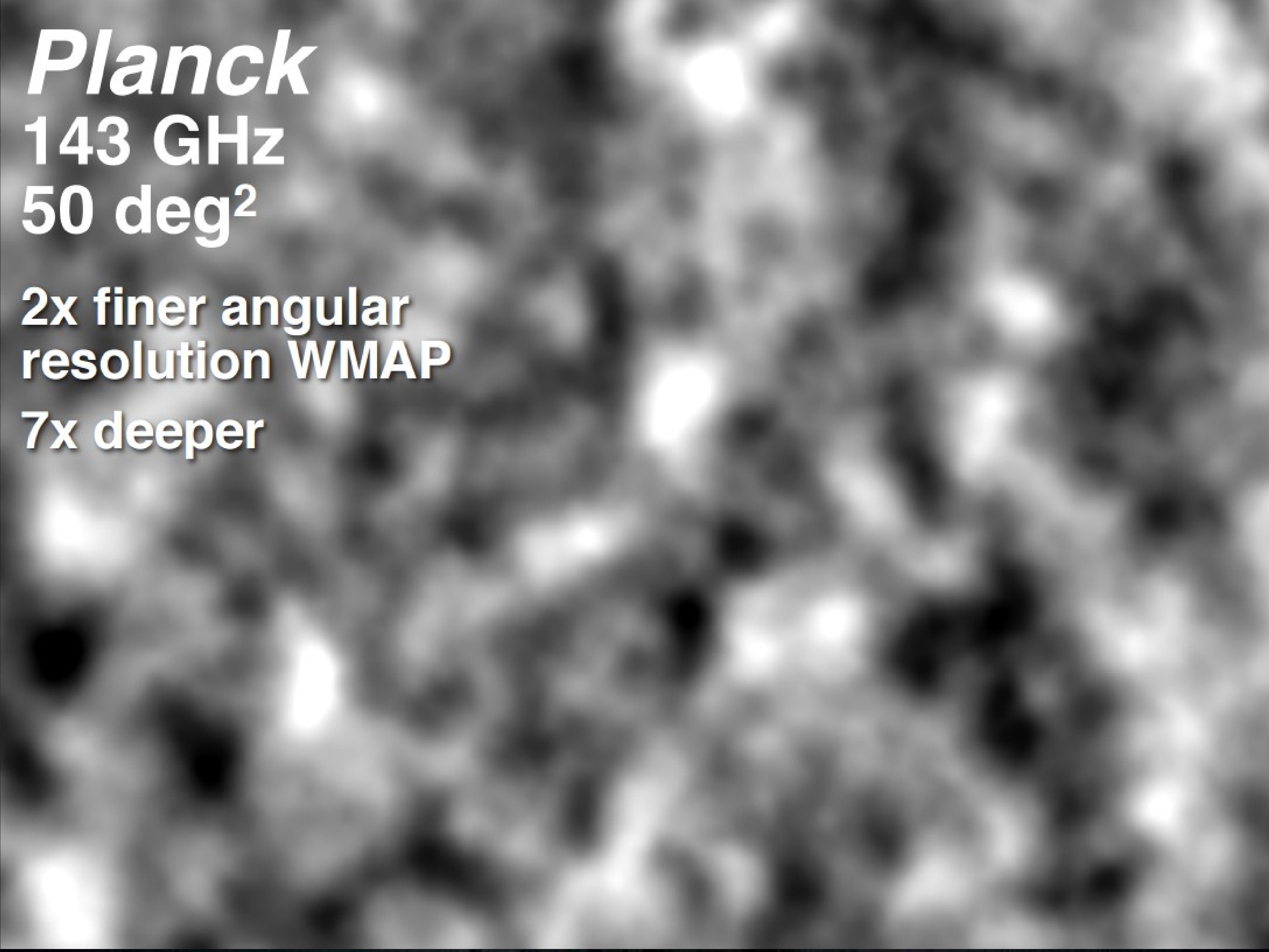
Planck
143 GHz
50 deg²
2x finer angular resolution WMAP
7x deeper

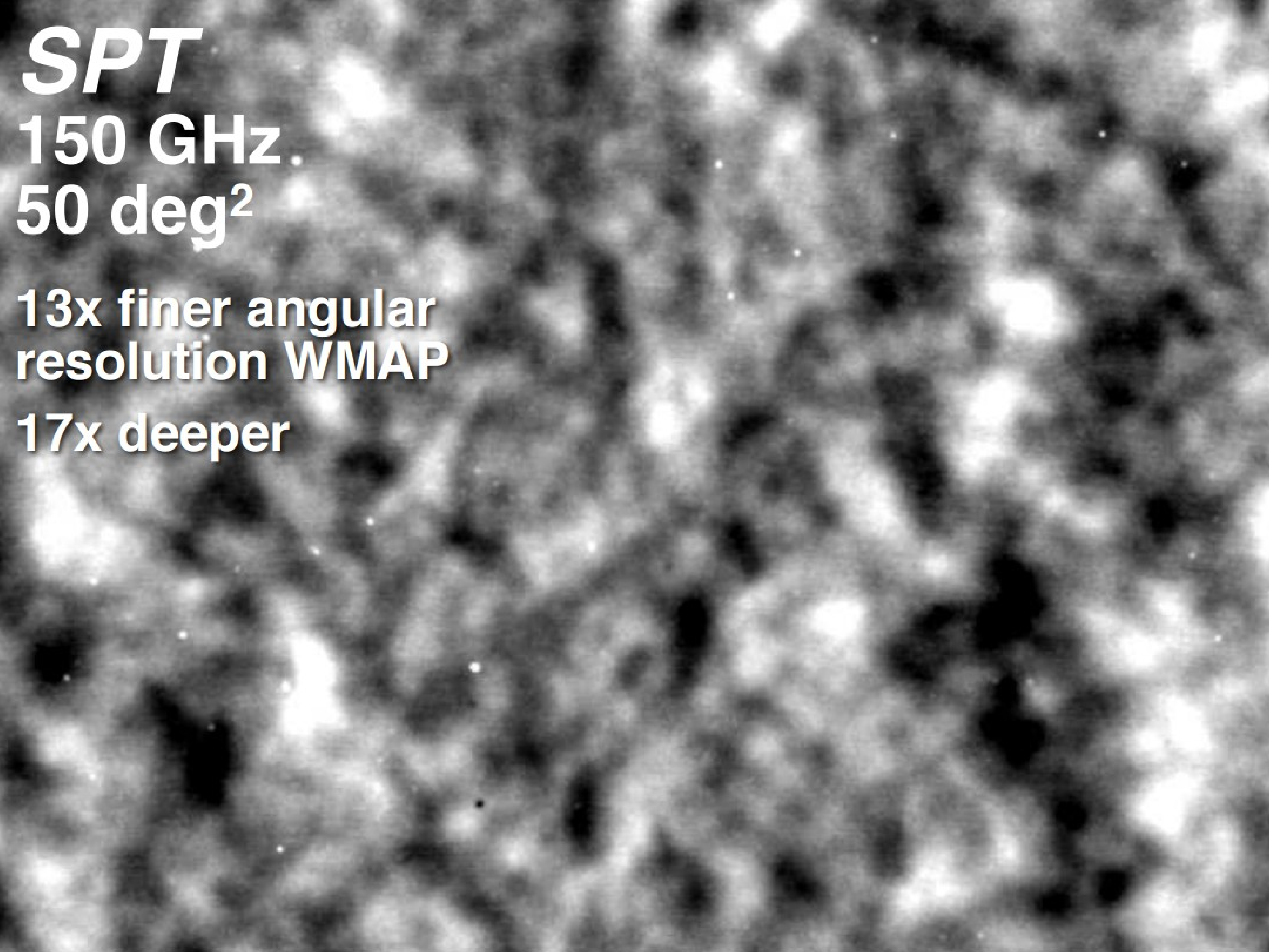
SPT
150 GHz
50 deg²
13x finer angular
resolution WMAP
17x deeper

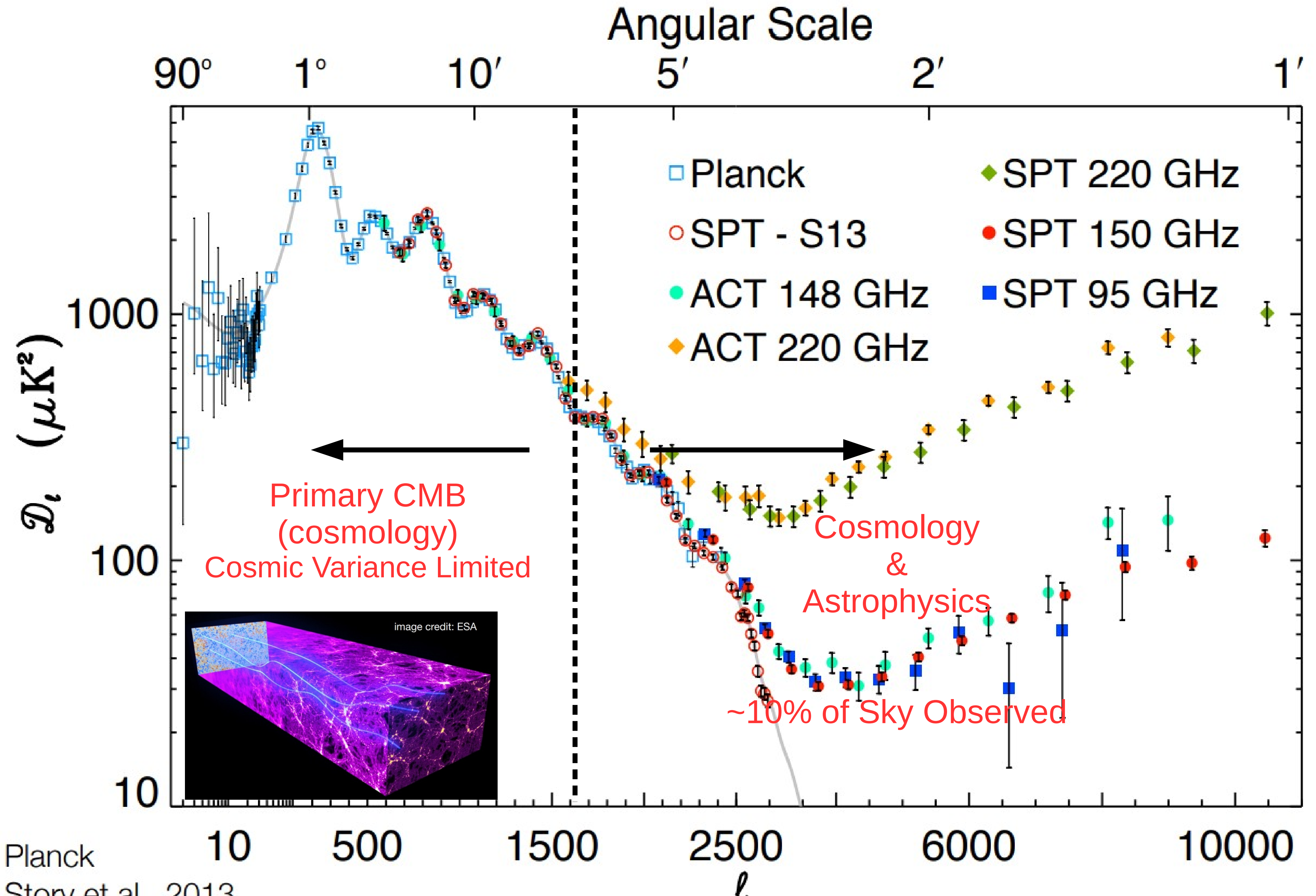

Planck
Story et al., 2013
George et al., 2014
Das et al., 2014

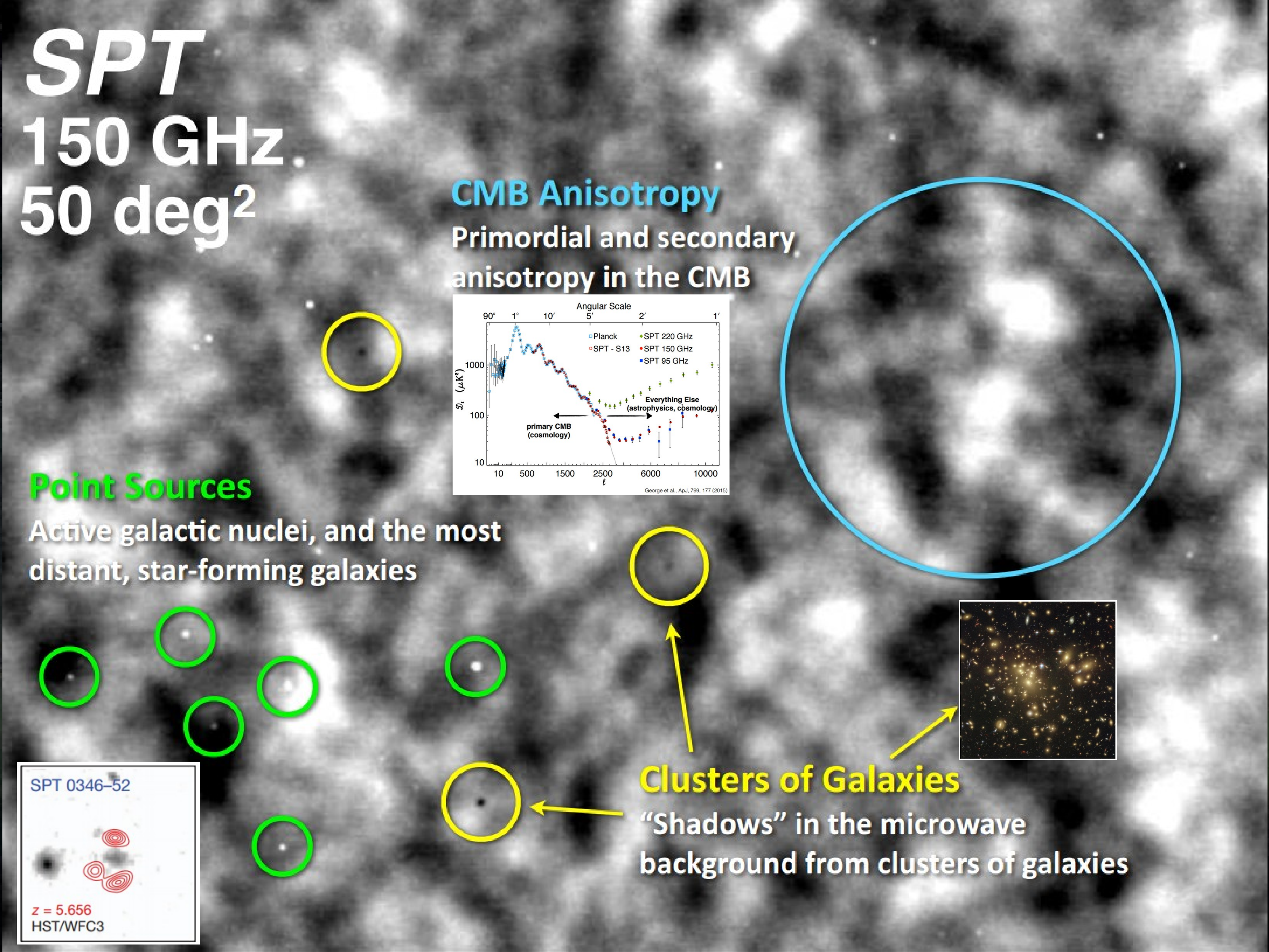
SPT
150 GHz
50 deg²
CMB Anisotropy
Primordial and secondary anisotropy in the CMB
Angular Scale
90° 1° 10′ 5′ 2′ 1′
Planck
SPT - S13
SPT 220 GHz
SPT 150 GHz
SPT 95 GHz
Everything Else (astrophysics, cosmology)
primary CMB (cosmology)
10 500 1500 2500 6000 10000
ℓ
George et al., ApJ, 799, 177 (2015)
Point Sources
Active galactic nuclei, and the most distant, star-forming galaxies
SPT 0346–52
z = 5.656
HST/WFC3
Clusters of Galaxies
"Shadows" in the microwave background from clusters of galaxies

Table 1. Conversion factors for tSZ Compton parameter y to CMB temperature units and the FWHM of the beam of the *Planck* channel maps.

Frequency [GHz]	$T_{\rm CMB}\ g(\nu)$ [$K_{\rm CMB}$]	FWHM [arcmin]
100	−4.031	9.66
143	−2.785	7.27
217	0.187	5.01
353	6.205	4.86
545	14.455	4.84
857	26.335	4.63

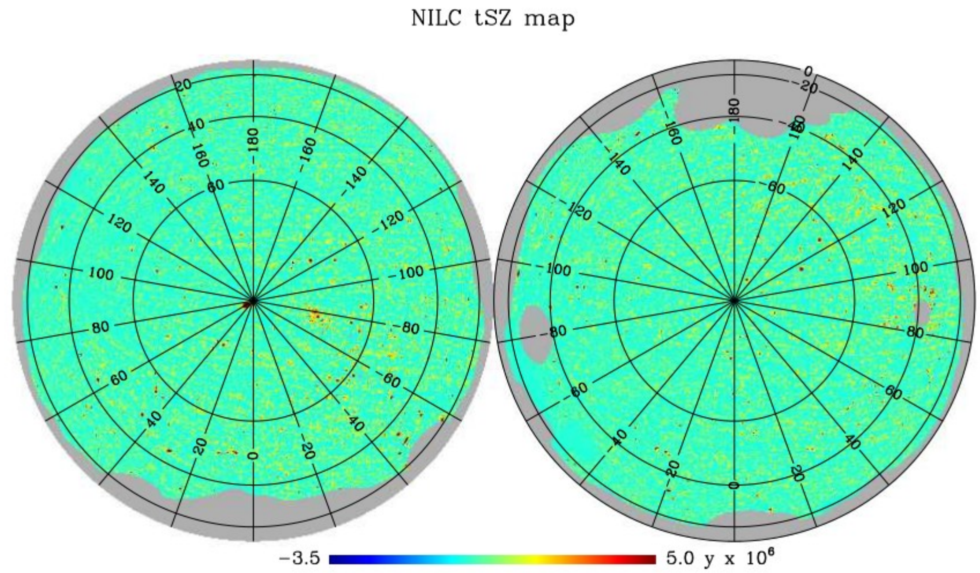

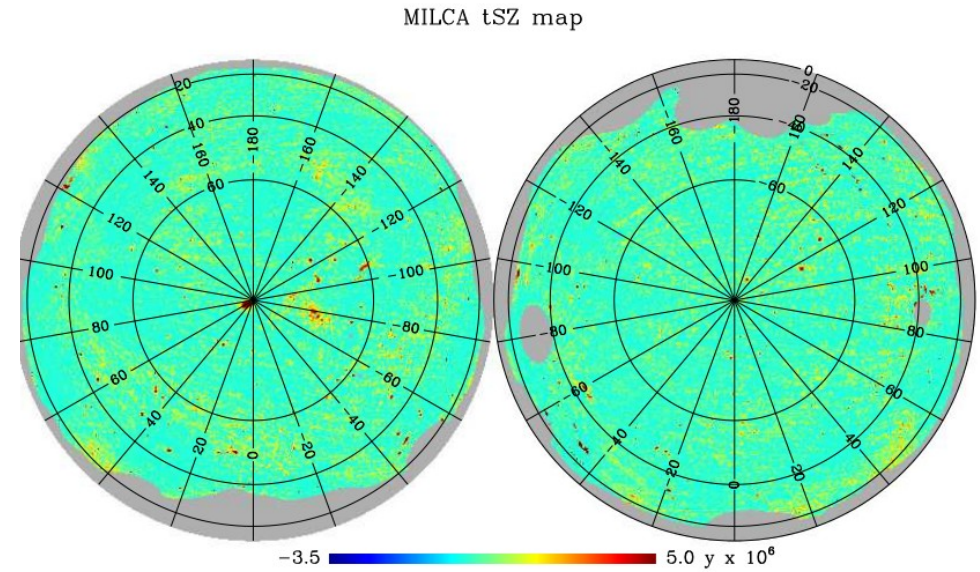

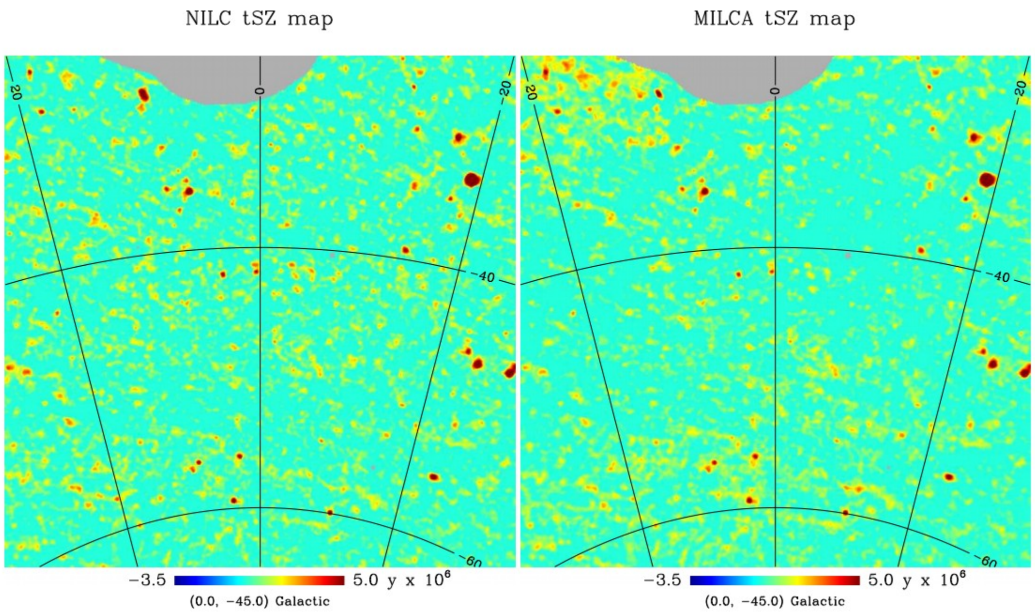

Planck 2013 results. XXI

Planck "y-map"

Planck papers 2013, 2015

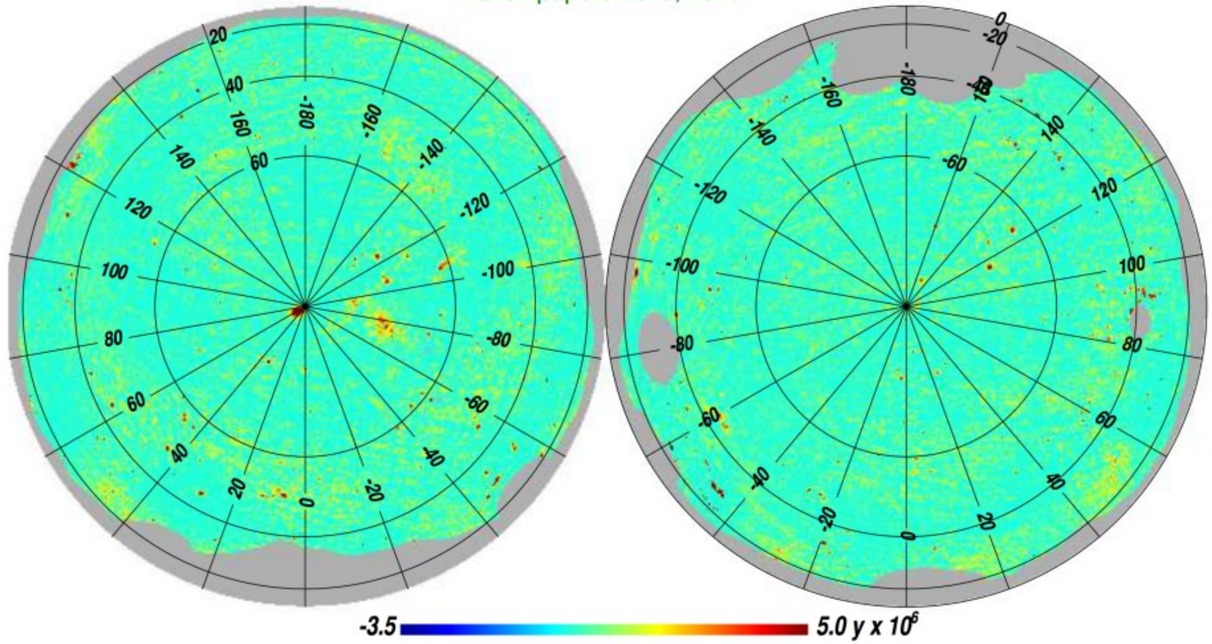

…. still contains foreground contaminants…

y^2 = tSZ + CIB + RS + IR

Power spectrum of the Compton y-parameter

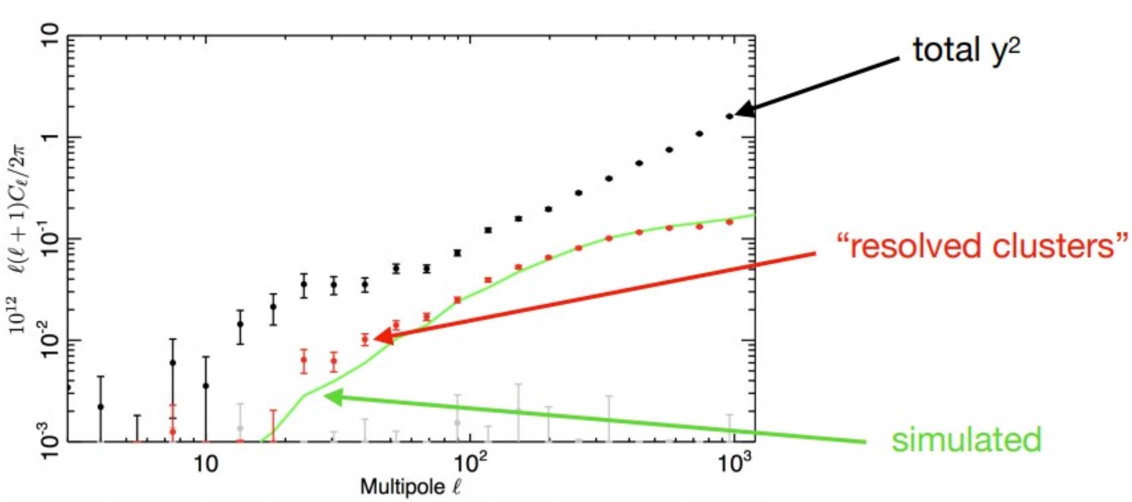

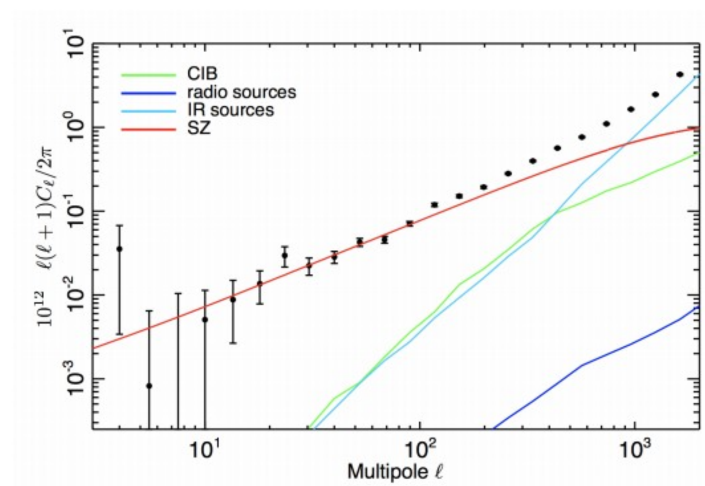

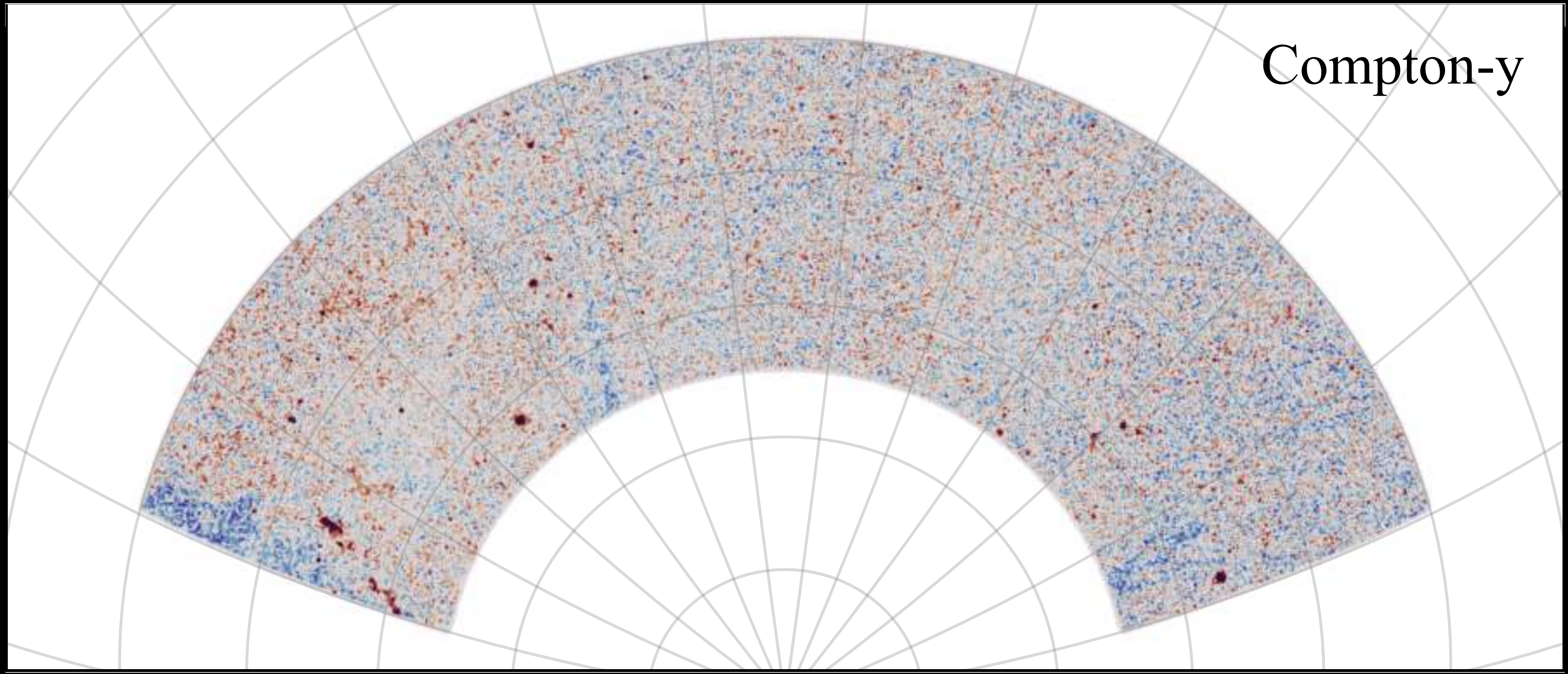

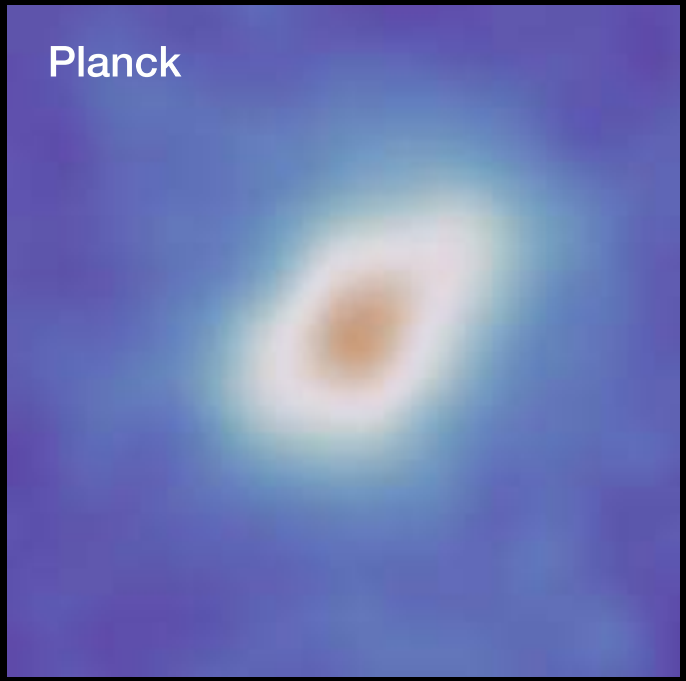

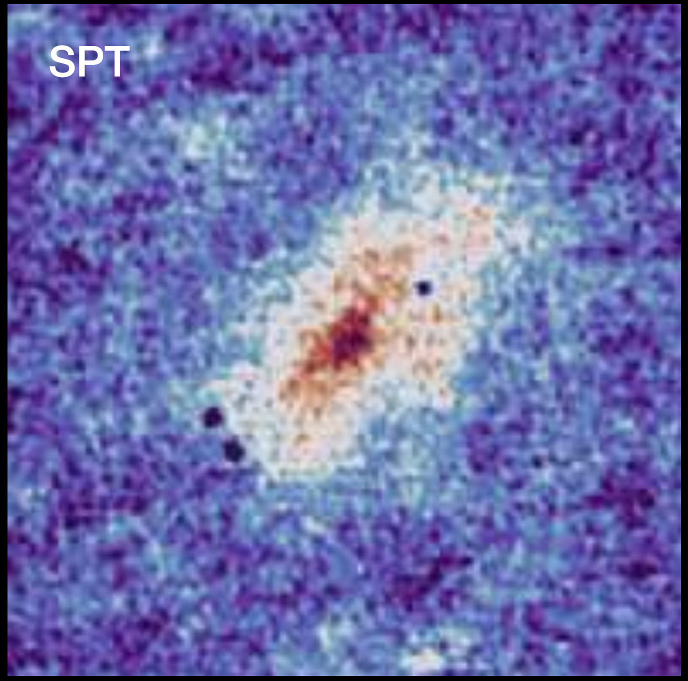

L. Bleem et al., ApJ, 258, 2, 36, 2022

Dependence on cosmological parameters

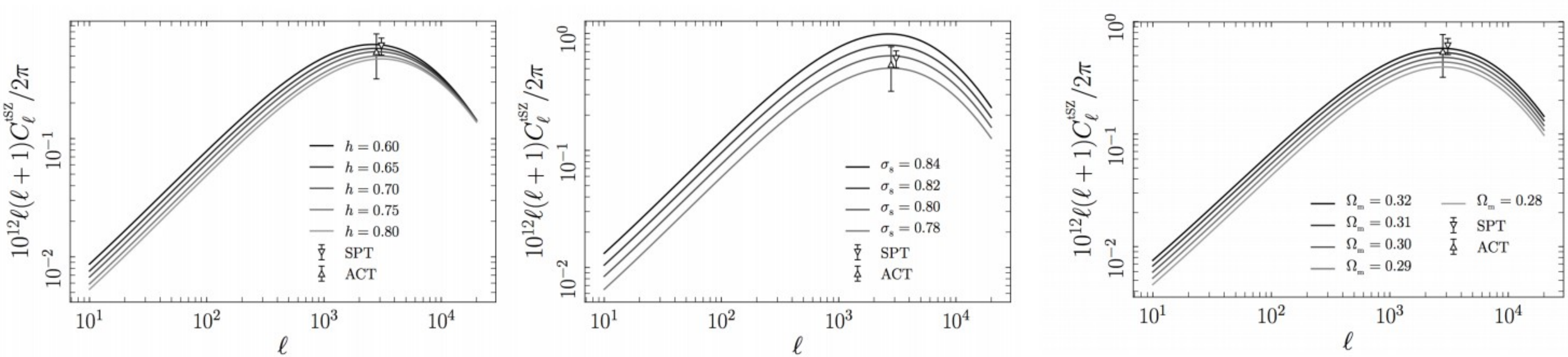

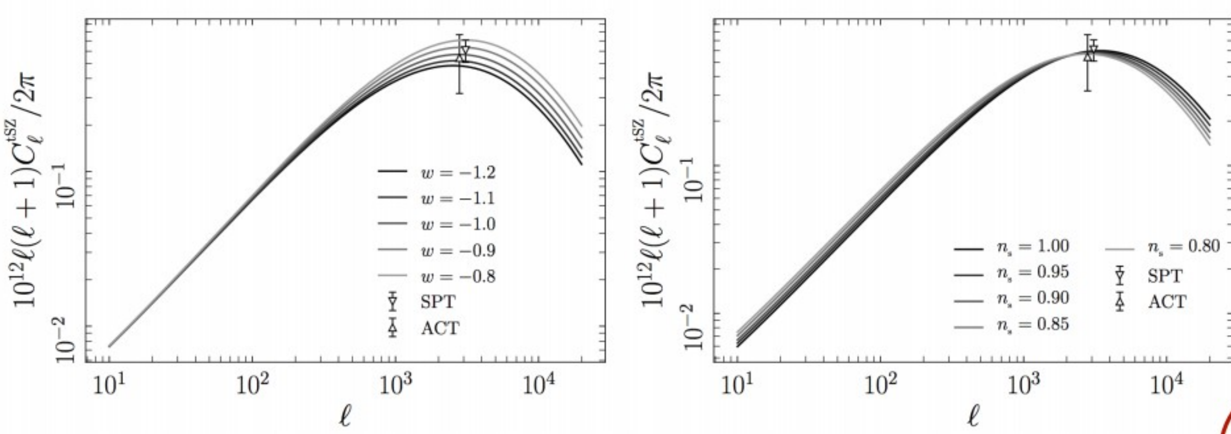

Scaling on **large scales**:

$$C_\ell^{\rm tSZ} \propto \sigma_8^{8.1}\Omega_{\rm m}^{3.2}B^{-3.2}h^{-1.7}$$

We constrain the parameter "F"

$$F \equiv \sigma_8\left(\Omega_{\rm m}/B\right)^{0.40}h^{-0.21}$$

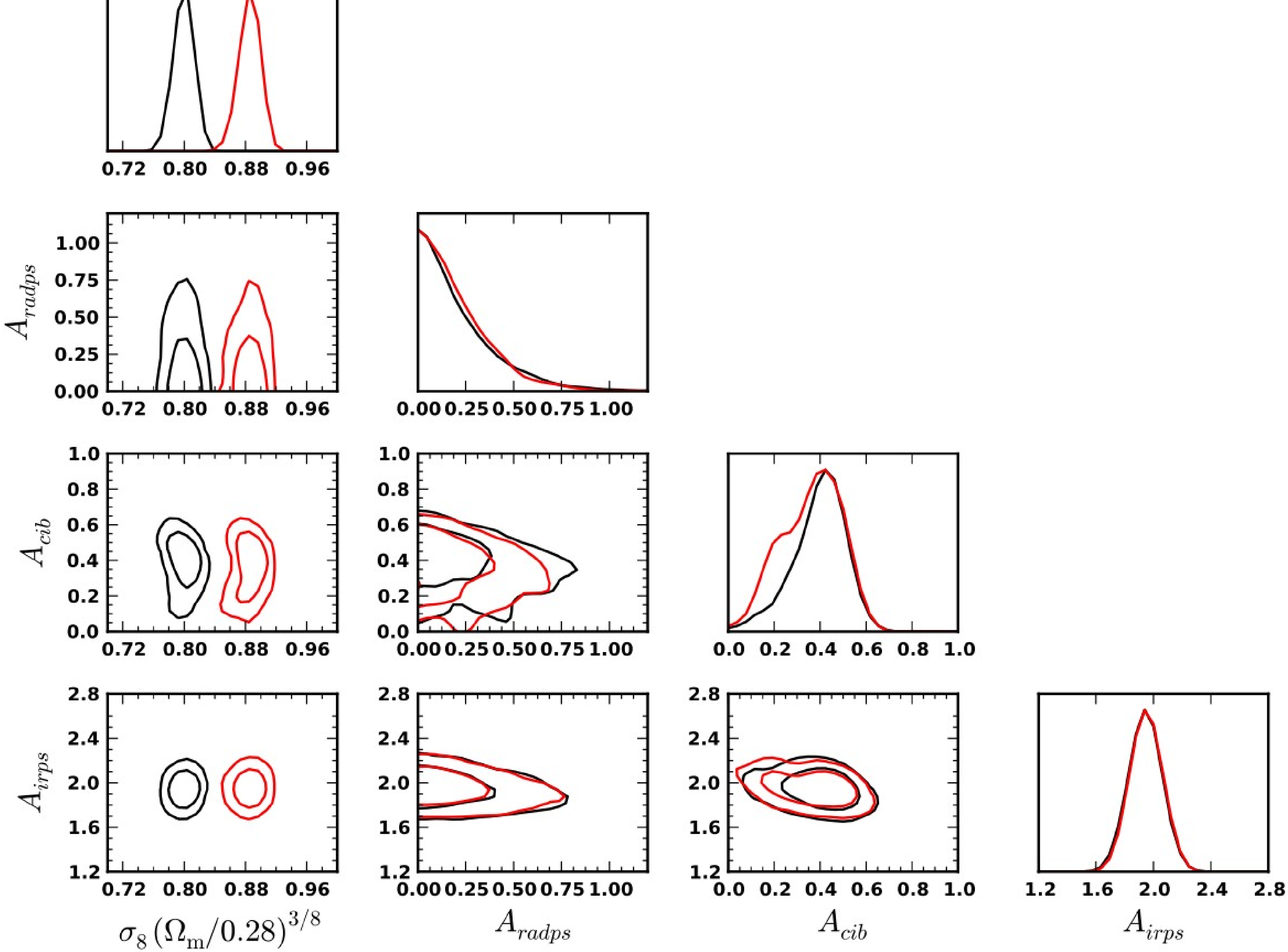

Fig. 16: 2D and 1D likelihood distributions for the combination of cosmological parameters $\sigma_8(\Omega_m/0.28)^{3/8}$, and for the foreground parameters $A_{\rm Rad.PS}$, $A_{\rm CIB}$ and $A_{\rm IR.PS}$. We show the 68.3% and 95.4% C.L. contours. The red and black contours correspond to a fixed mass bias of 0.2 and 0.4 respectively.

Planck 15 XXII

∷∷ The SZ effect(s)

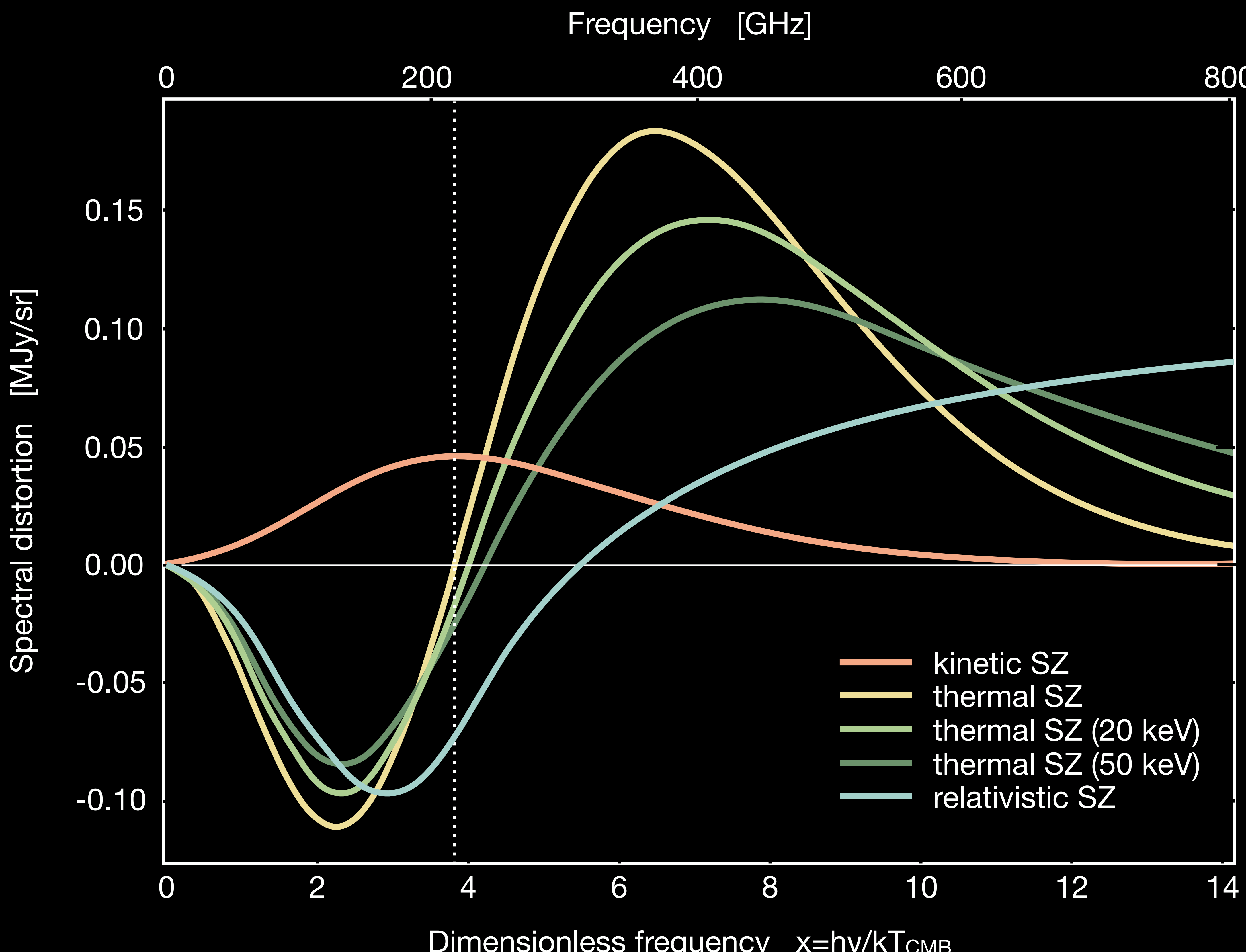

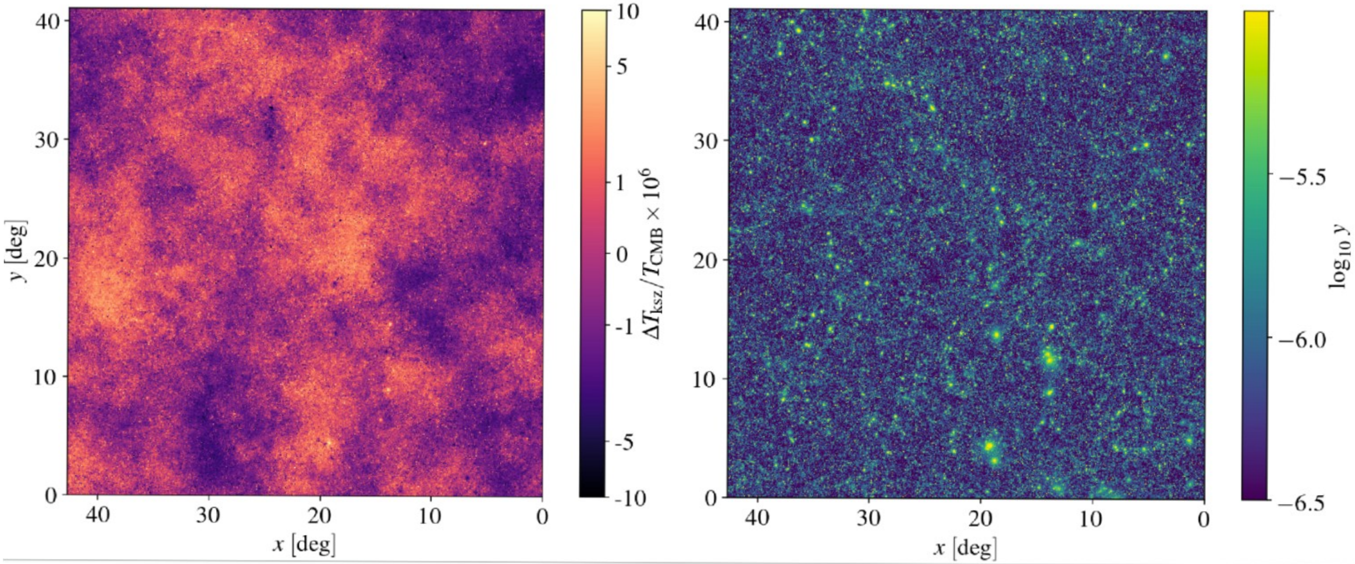

Soergel et al. 2016

4.2 sigma detection with ~6700 clusters

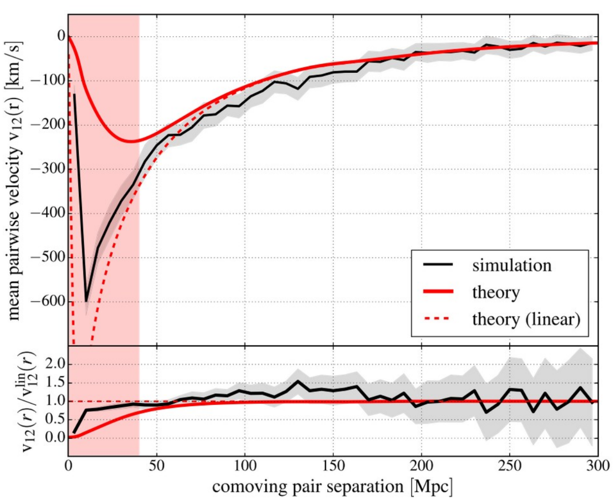

Figure 4. Mean pairwise velocity $v_{12}(r)$ from simulations: Top: we show in black the measurement from the clusters in our mock catalogue, where the shaded regions indicate the 1σ uncertainties. The solid red line shows the mean pairwise velocity model of equation (9) evaluated at the median redshift of $z_\mathrm{m} \simeq 0.5$, whereas the dashed red line represents the leading-order term (the numerator of equation 9). Bottom: we show here the residuals of the upper panel with respect to linear theory. In both panels, the red shaded region ($r < 40$ Mpc) indicates scales that we exclude from our analysis, as the simulations deviate by more than 2σ from the theoretical models.

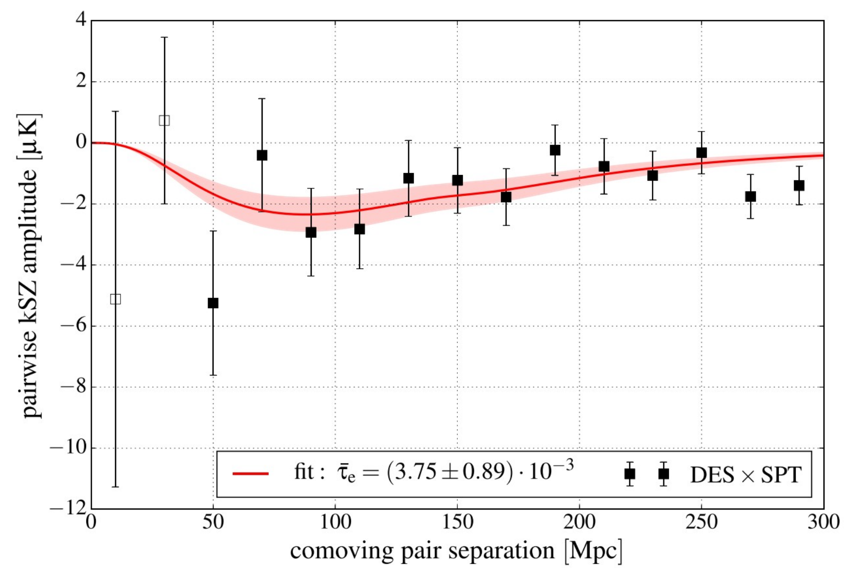

Figure 7. Pairwise kSZ amplitude measured from the DES Y1 redMaPPer catalogue and the SPT-SZ temperature maps, using the baseline sample of clusters with $20 < \tilde{\lambda} < 60$. The solid red line shows the analytic pairwise velocity template (equation 11) scaled with the best-fitting optical depth $\bar{\tau}_e$; the shaded regions are the corresponding 1σ uncertainties. As before, the two lowest separation points shown with empty symbols are excluded from the fit, as on these scales perturbation theory is not valid.

Planck's view of galaxy clusters

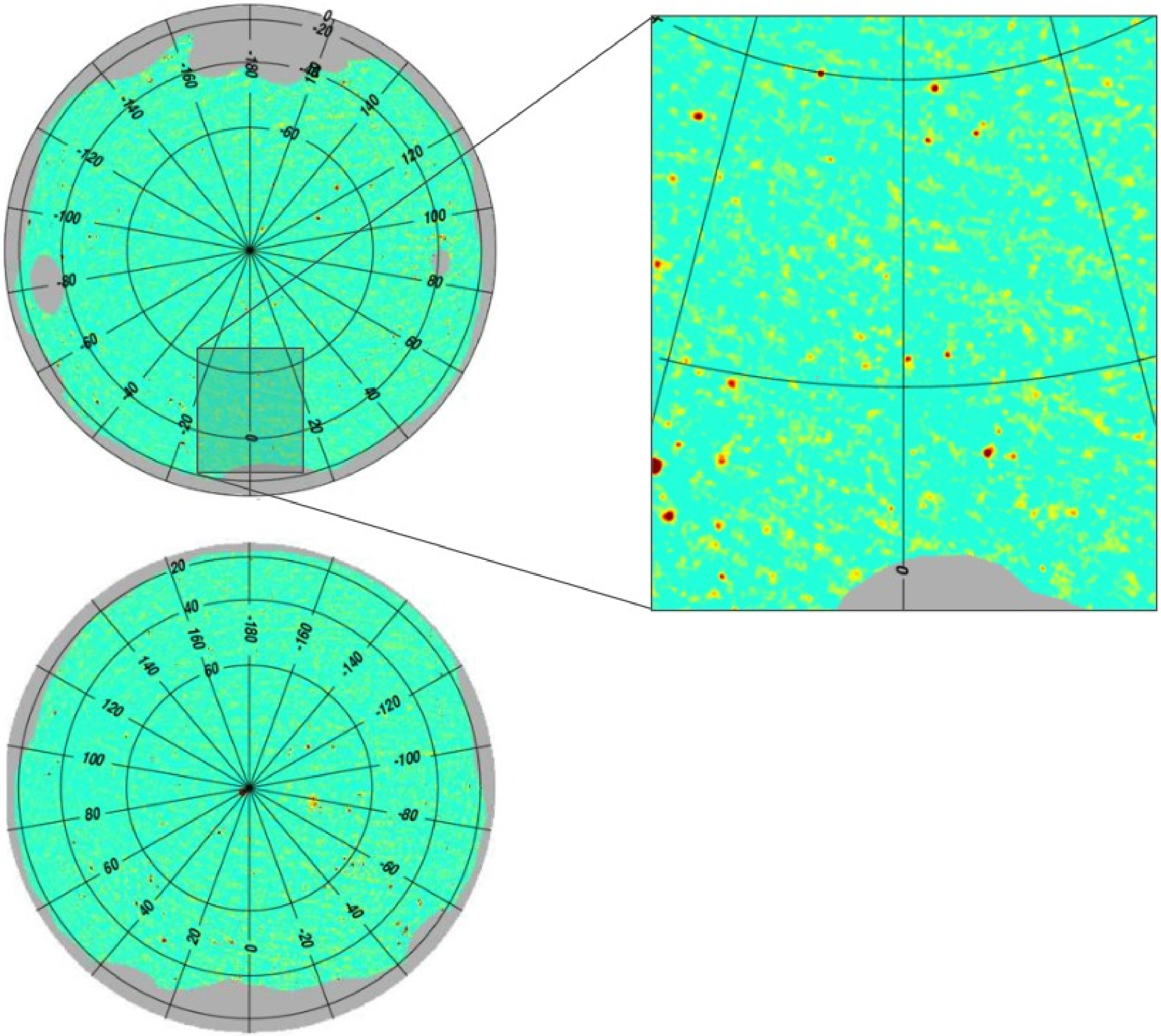

Adapted from Planck 2015 XXII

Observing the SZ effect

Planck's view of galaxy clusters

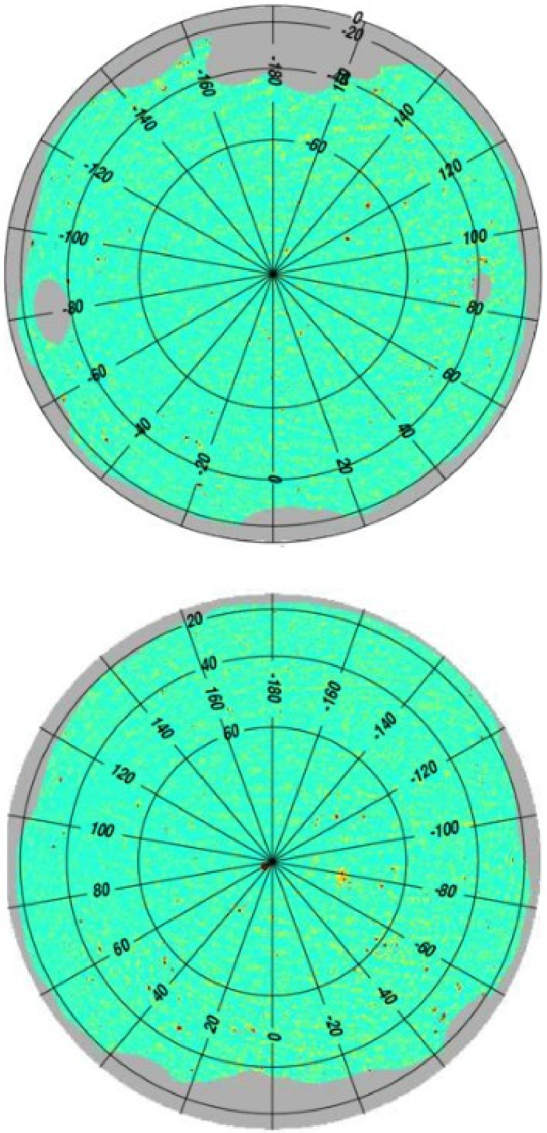

Adapted from Planck 2015 XXII

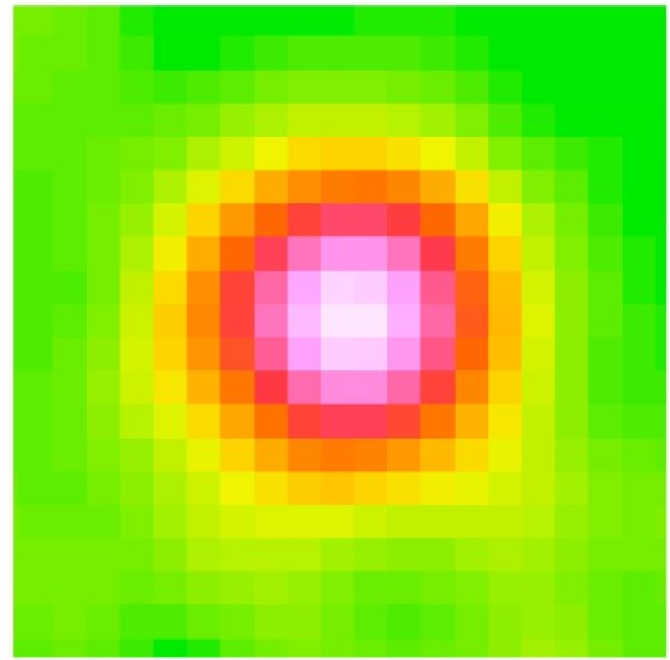

Planck Legacy Archive

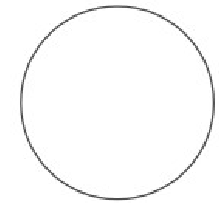

10 arcmin

Planck's view of galaxy clusters

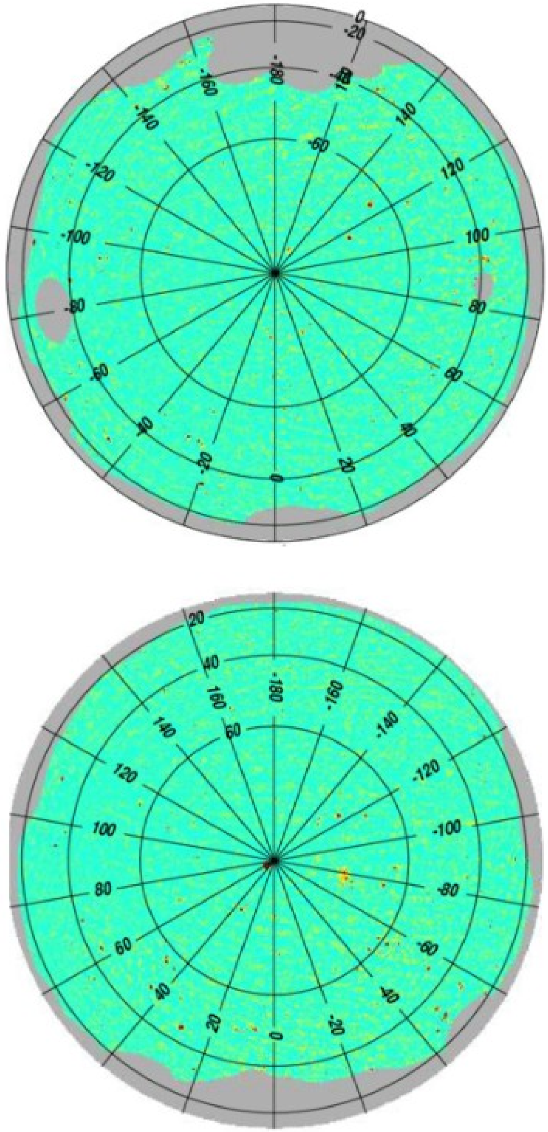

Adapted from Planck 2015 XXII

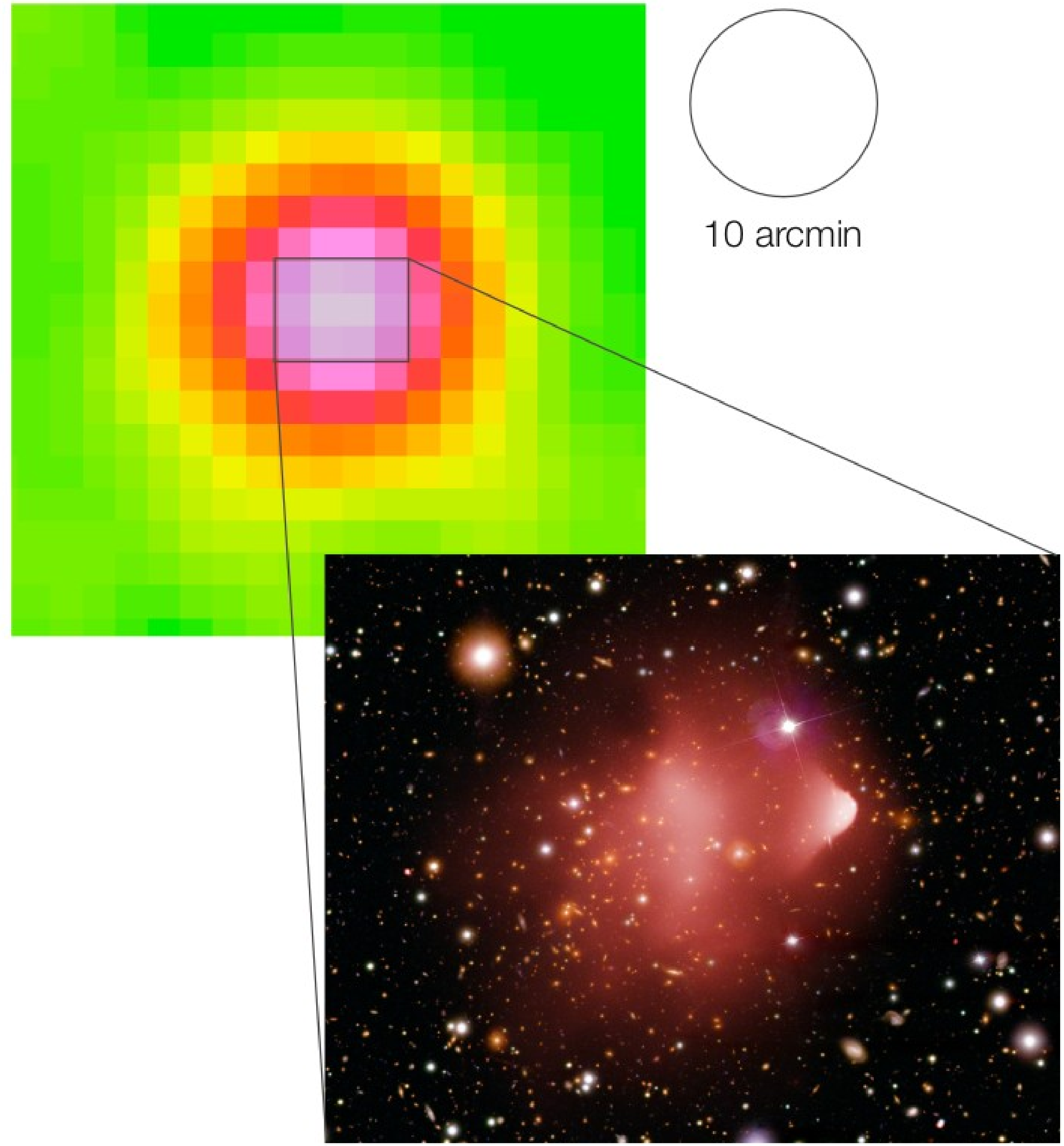

Chandra+HST

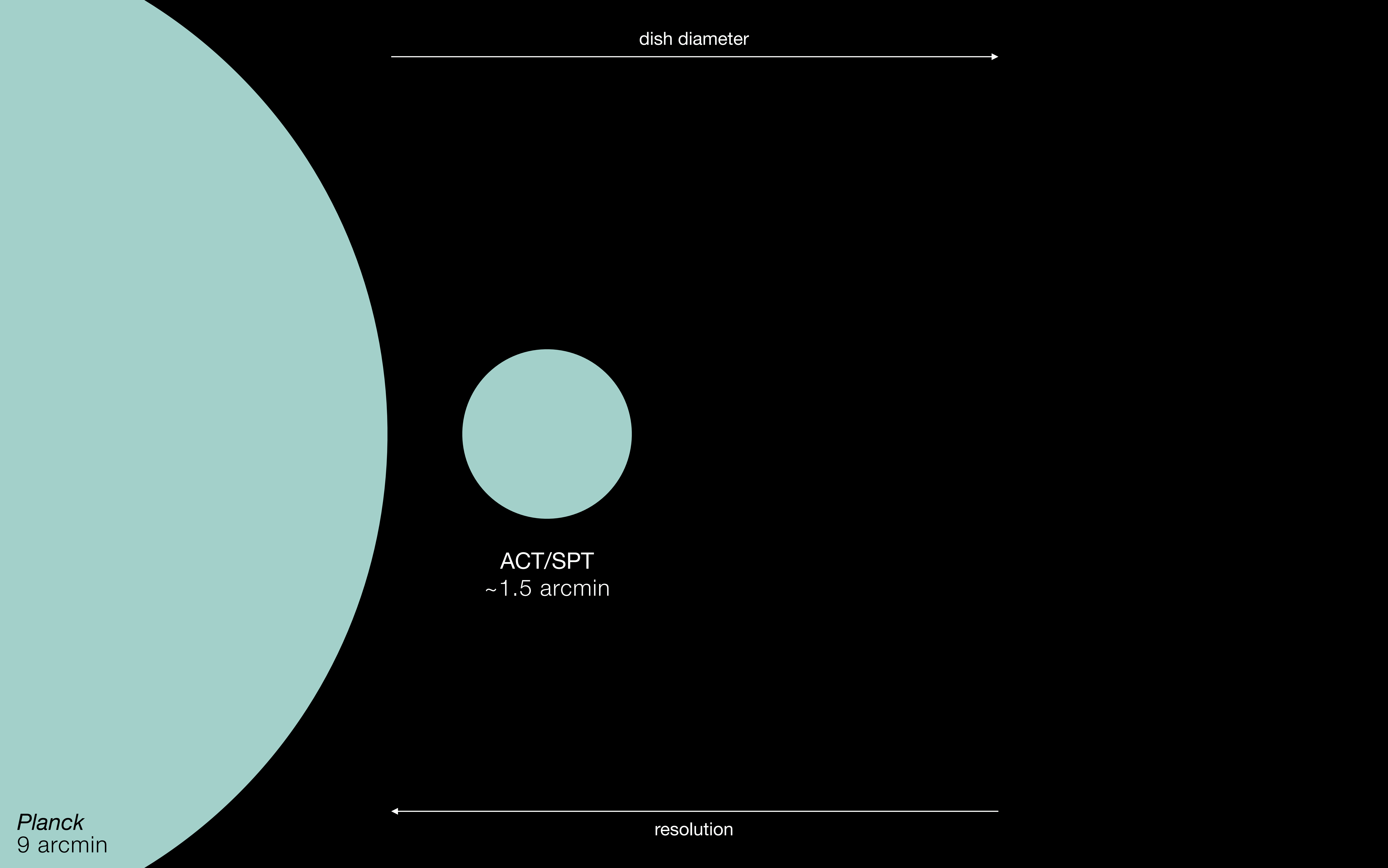
dish diameter
ACT/SPT
~1.5 arcmin
resolution
Planck
9 arcmin

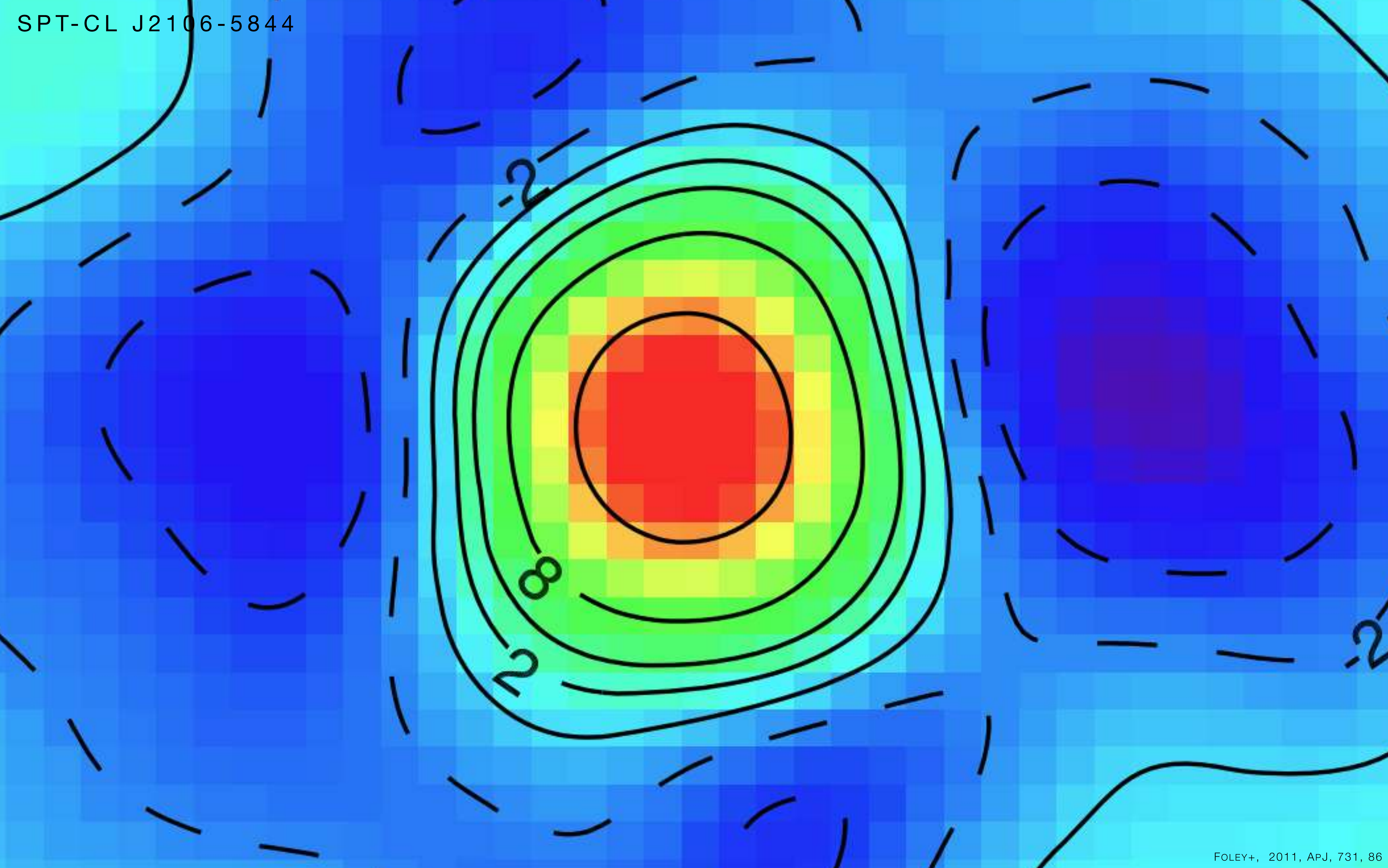
SPT-CL J2106-5844
-2
8
2
-2
FOLEY+, 2011, APJ, 731, 86

Discovered by SPT, and, for a long time, the most massive cluster at z>1

SPT

evidence of a strongly cooling core

X-ray luminous core near BCG

low central temperature

potential X-ray cavities or sloshing

several hints for merger activity

disturbed X-ray morphology

skewed velocity distribution

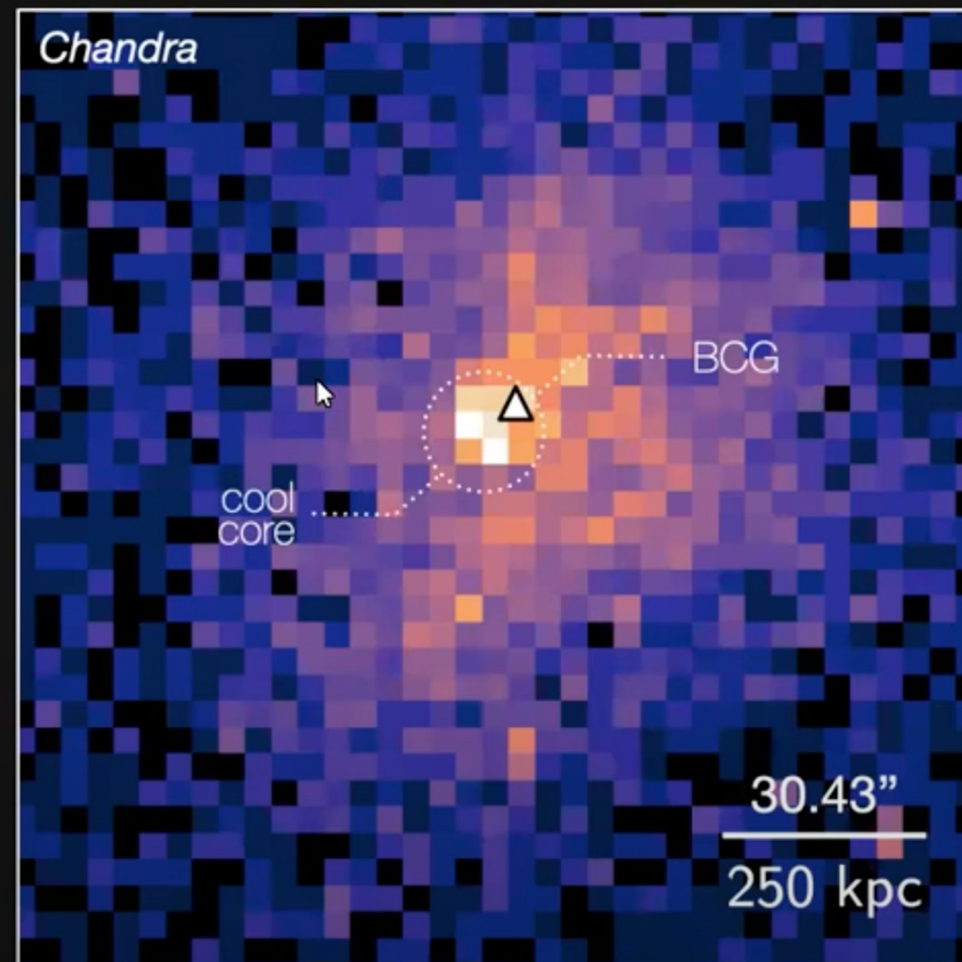

Foley et al., 2011, ApJ, 731, 86
Di Mascolo et al., 2021, A&A, 650, A153

Discovered by SPT, and, for a long time, the most massive cluster at z>1

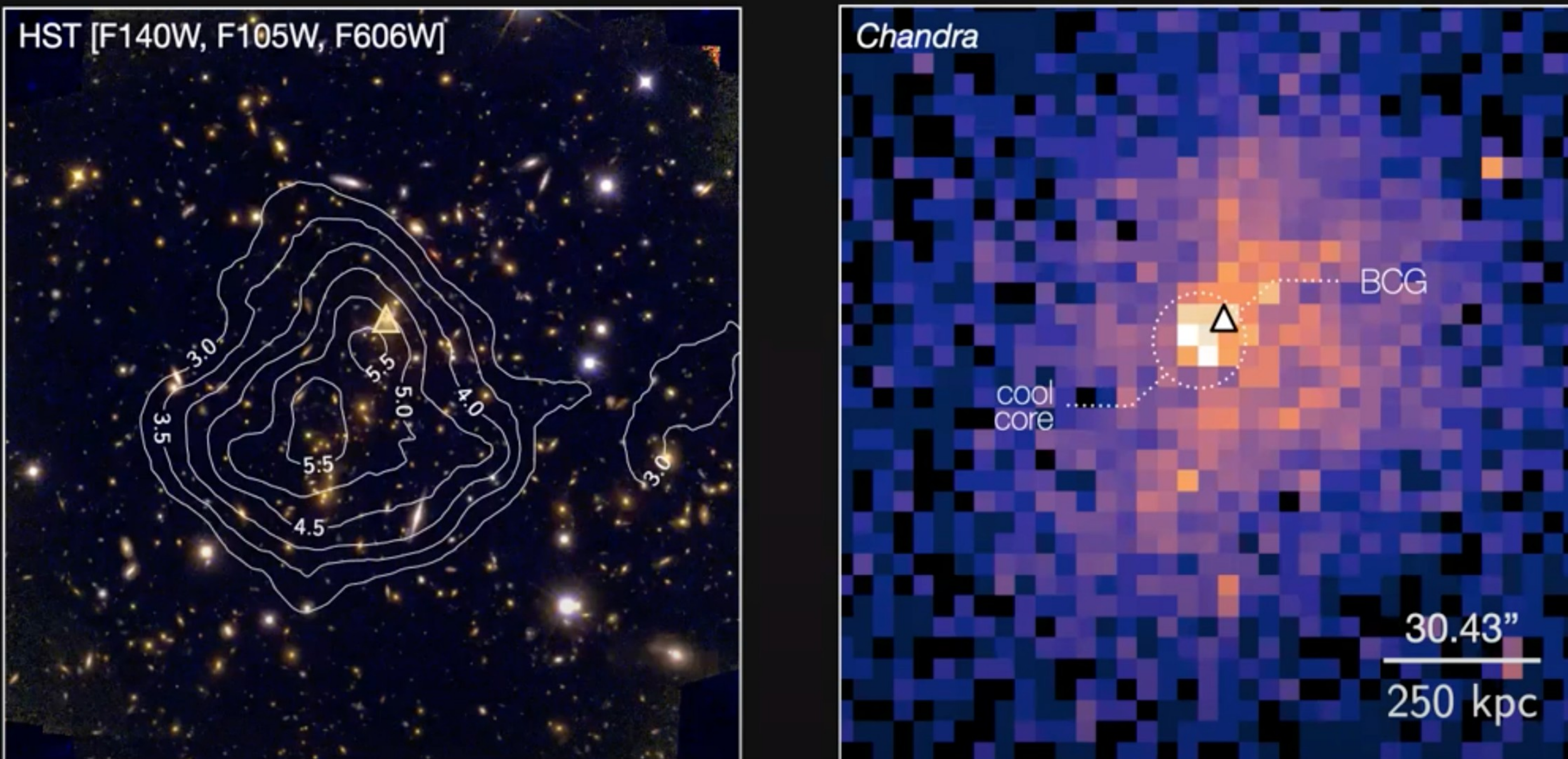

Di Mascolo et al., 2021, A&A, 650, A153

ACA	Band 3	107.8 μJy	ALMA	Band 3	27.9 μJy
	Band 4	99.4 μJy		Band 4	15.2 μJy

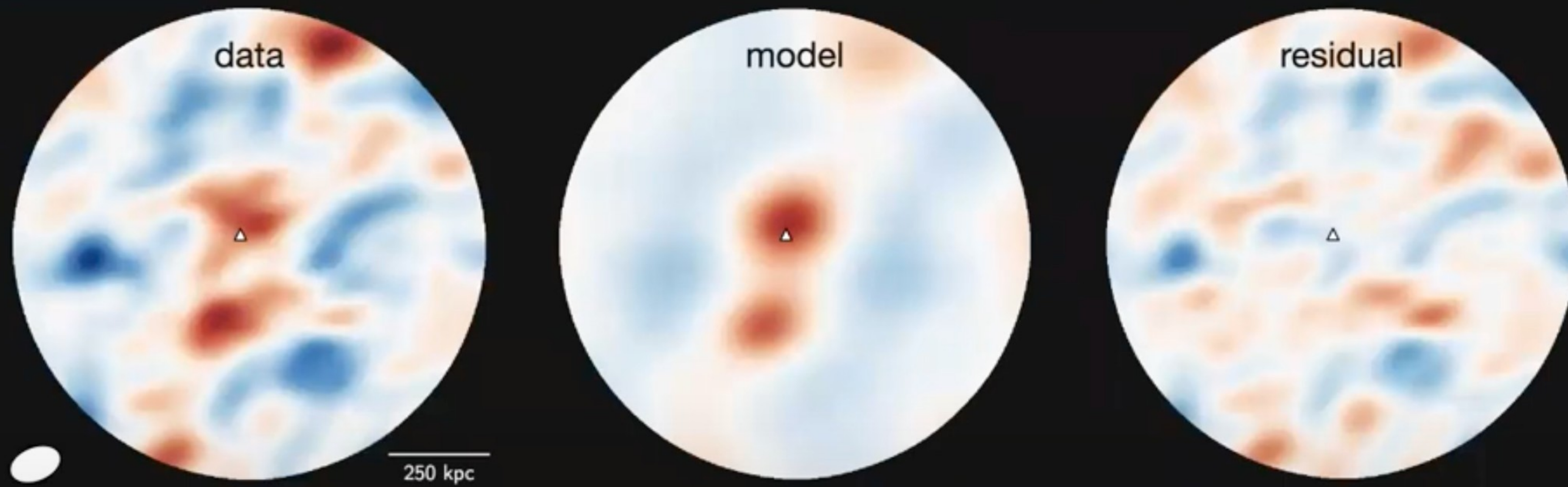

Model reconstruction performed entirely in *uv* space

Two-components favoured over one at the 9.9σ level and independently of priors

DI MASCOLO ET AL., 2021, A&A, 650, A153

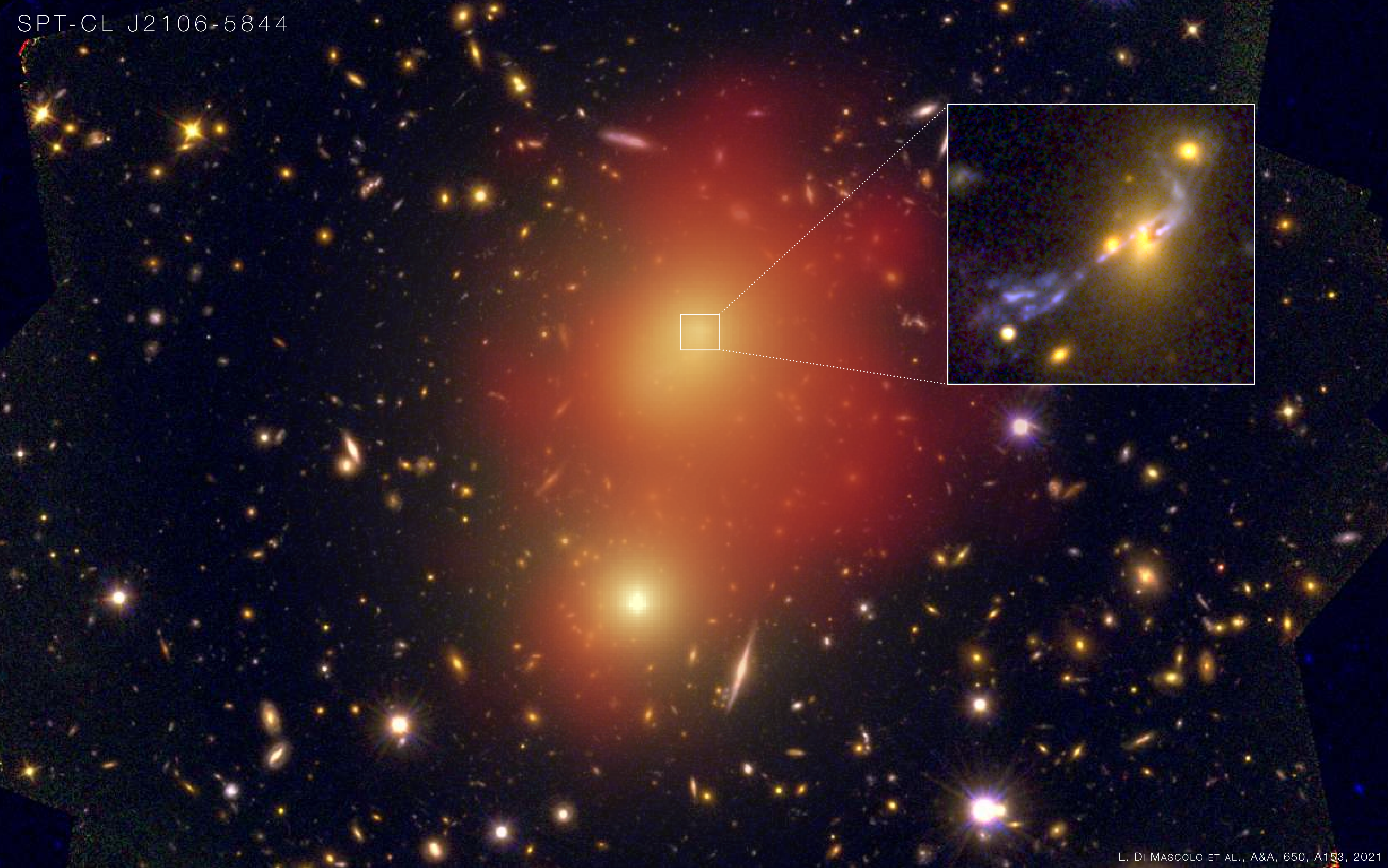

SPT-CL J2106-5844
L. Di Mascolo et al., A&A, 650, A153, 2021

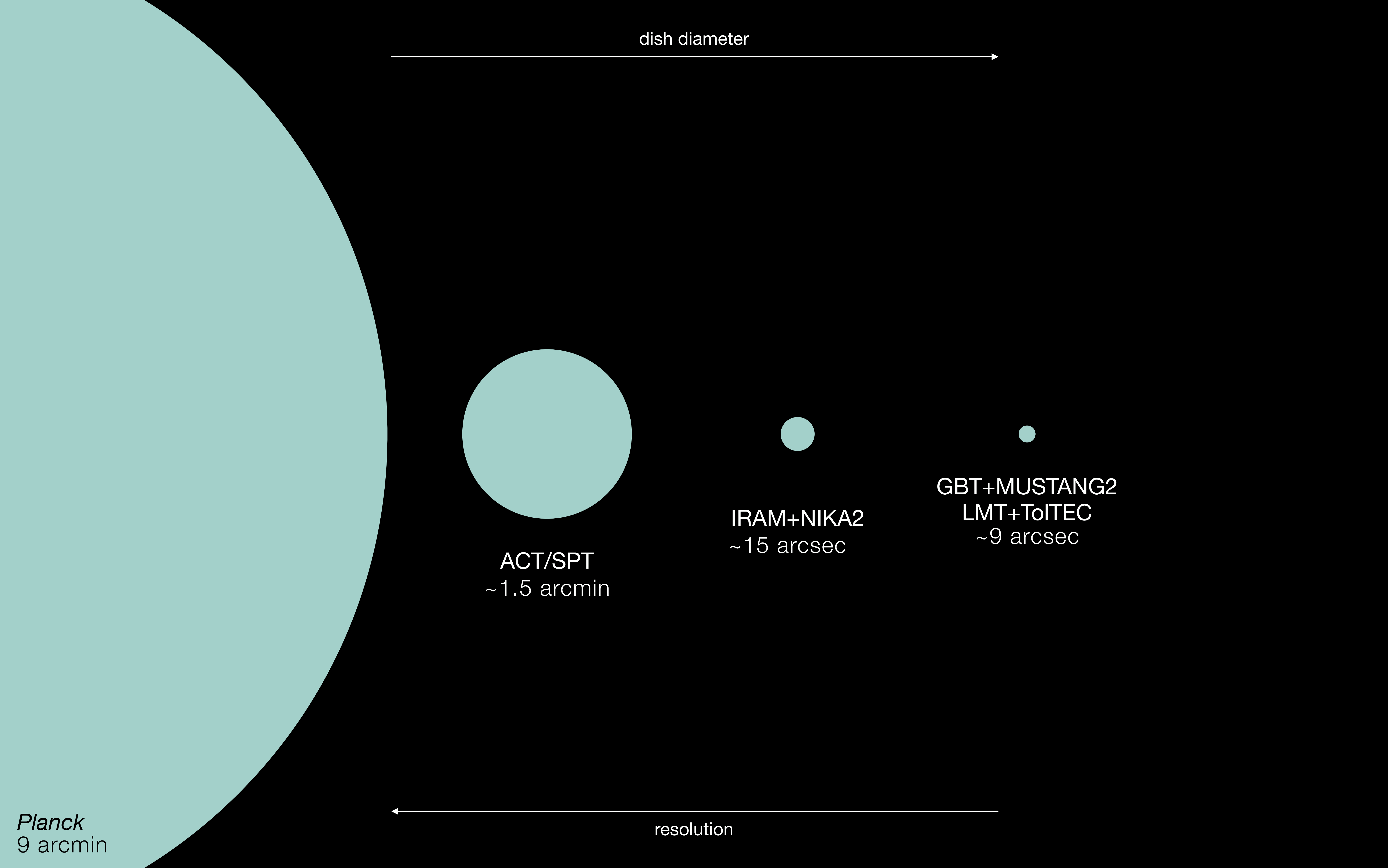

dish diameter
ACT/SPT
~1.5 arcmin
IRAM+NIKA2
~15 arcsec
GBT+MUSTANG2
LMT+ToITEC
~9 arcsec
resolution
Planck
9 arcmin

Single-dish facilities

- Parametric and non-parametric reconstruction of pressure profiles

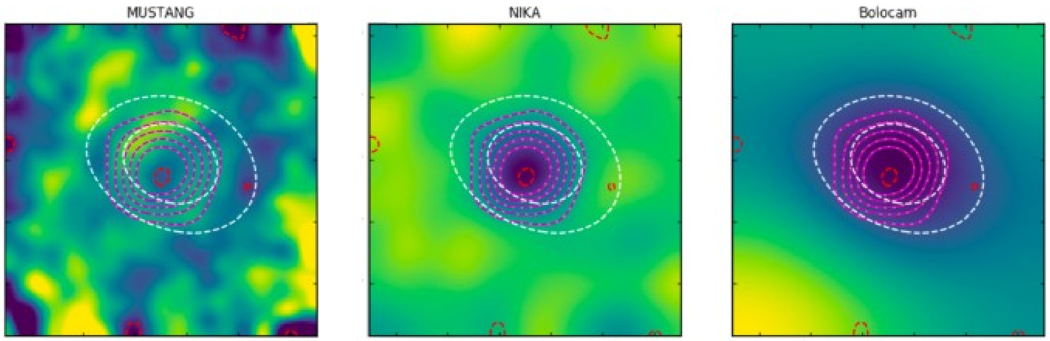

Romero+2017

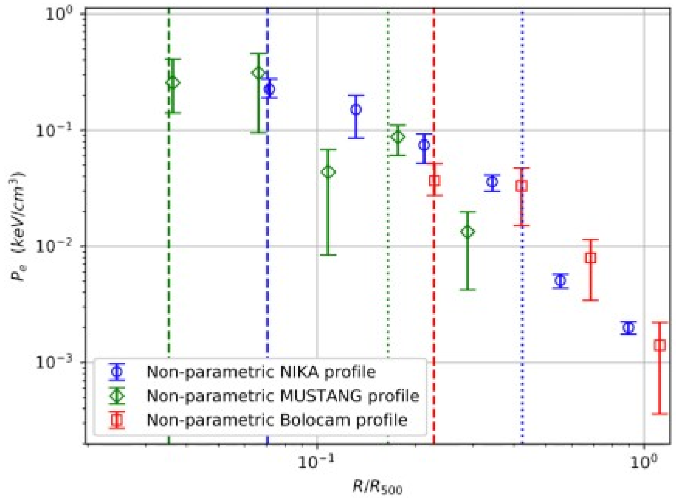

- Substructure detection

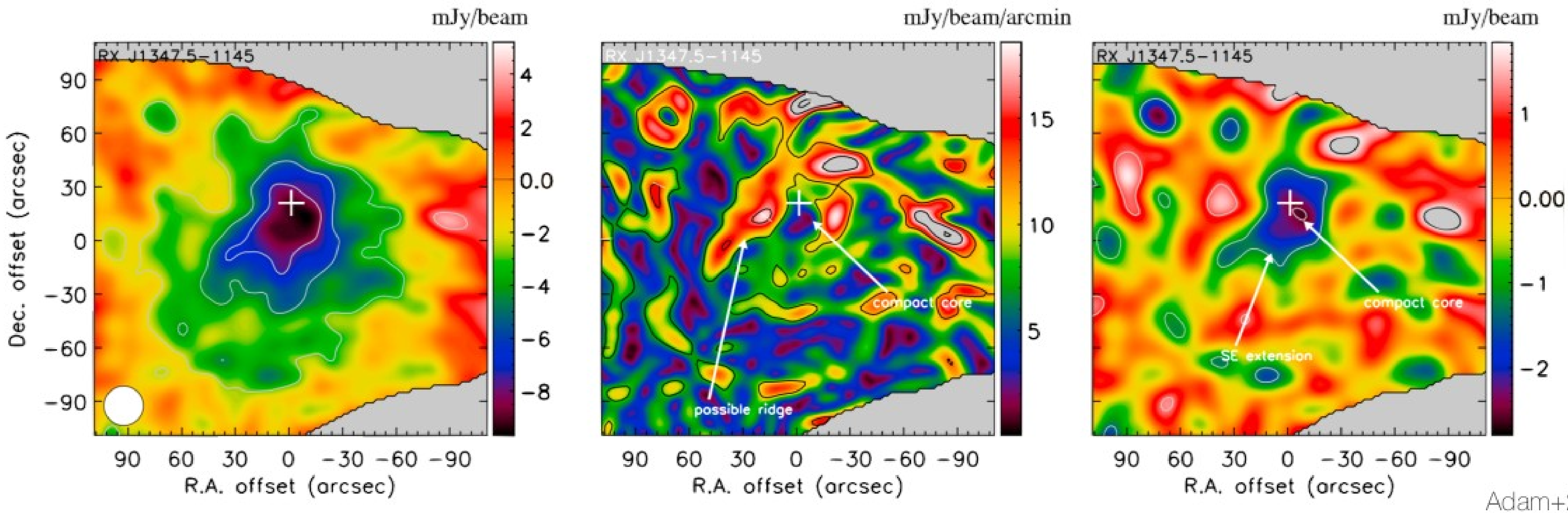

Adam+2018

A cosmic train wreck

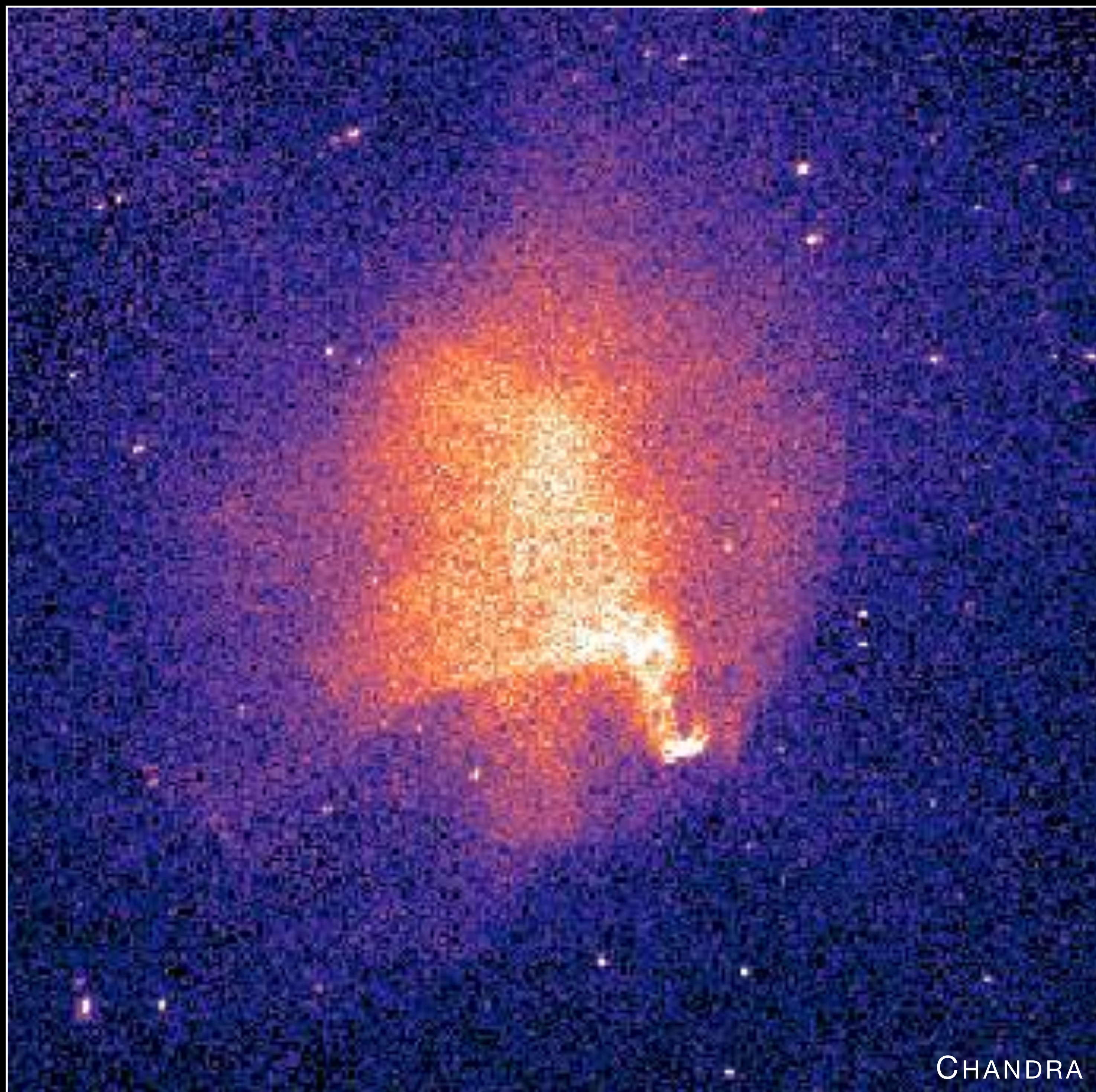

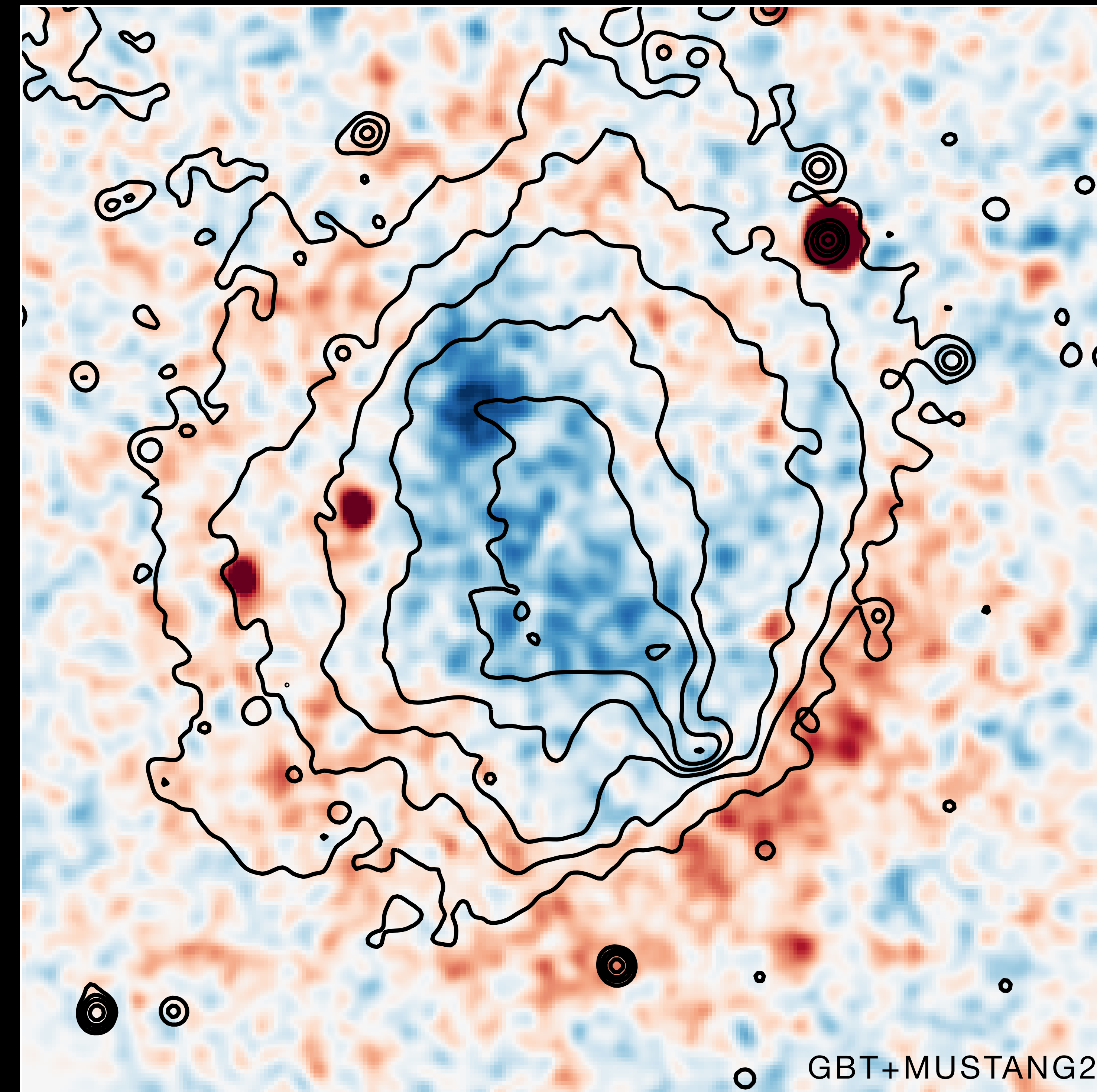

TRAIN WRECK CLUSTER

ADAPTED FROM WANG ET AL., 2018, APJ, 856, 2, 162

High-redshift mergers

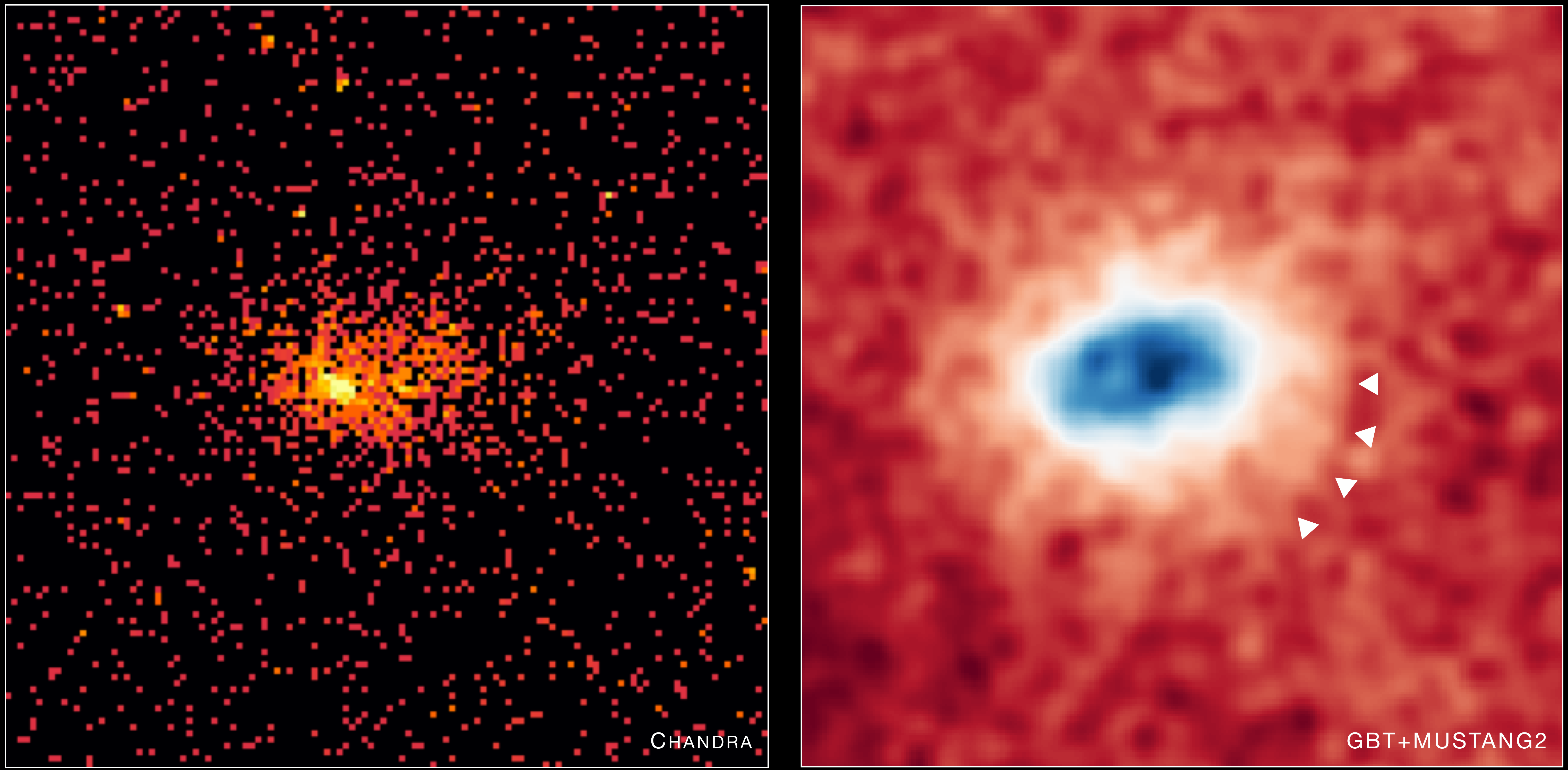

MOO J1142+1527

RUPPIN ET AL., 2019, APJ, 893, 1, 74
ADAPTED FROM DICKER ET AL., 2020, APJ, 902, 2, 144


A worldwide collaboration
22 countries involved
2816 papers
>1000/year new projects
One telescope, many antennae
x54 12-meter (ALMA)
x12 7-meter (ACA)

Let’s talk radio-interferometry

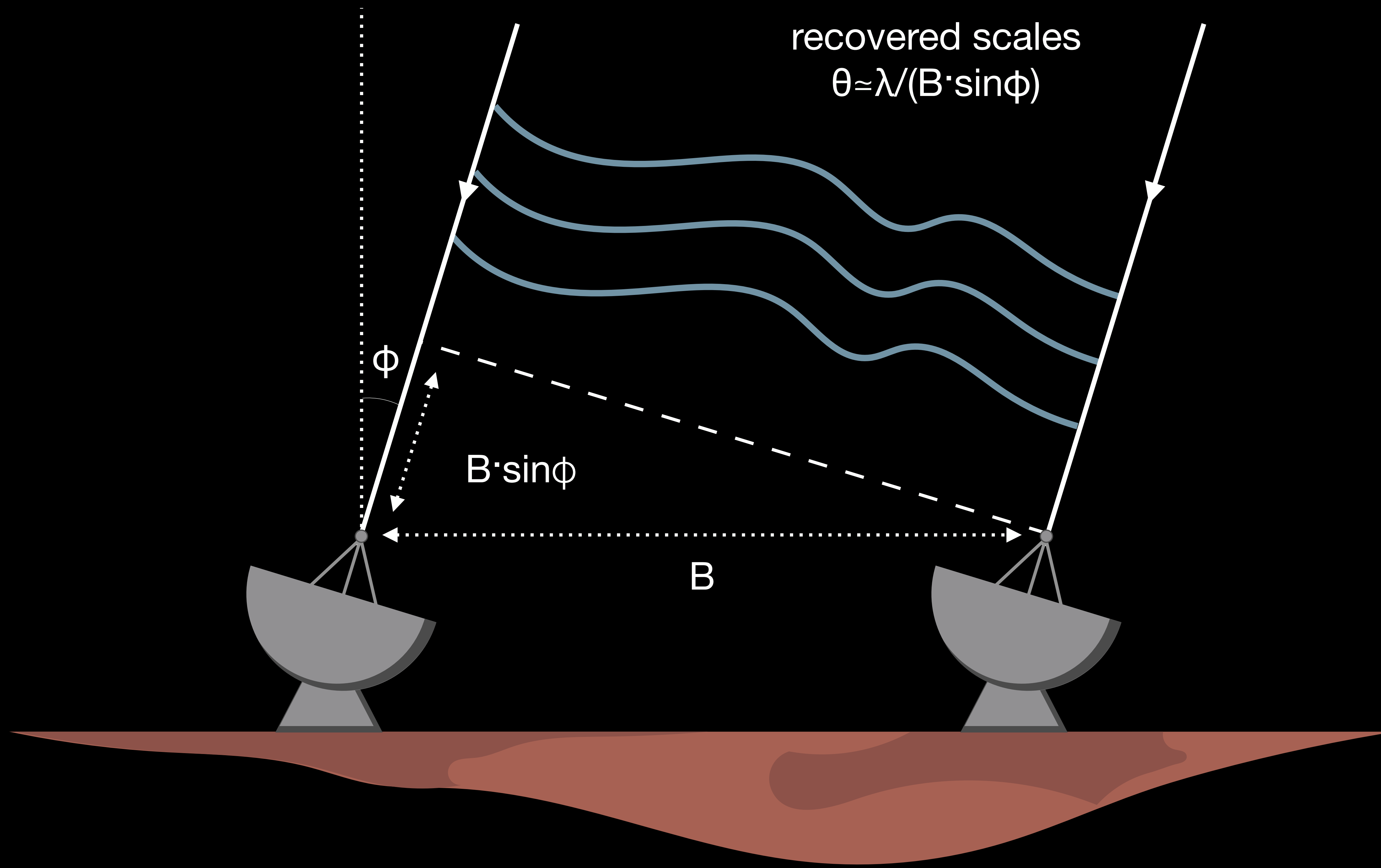

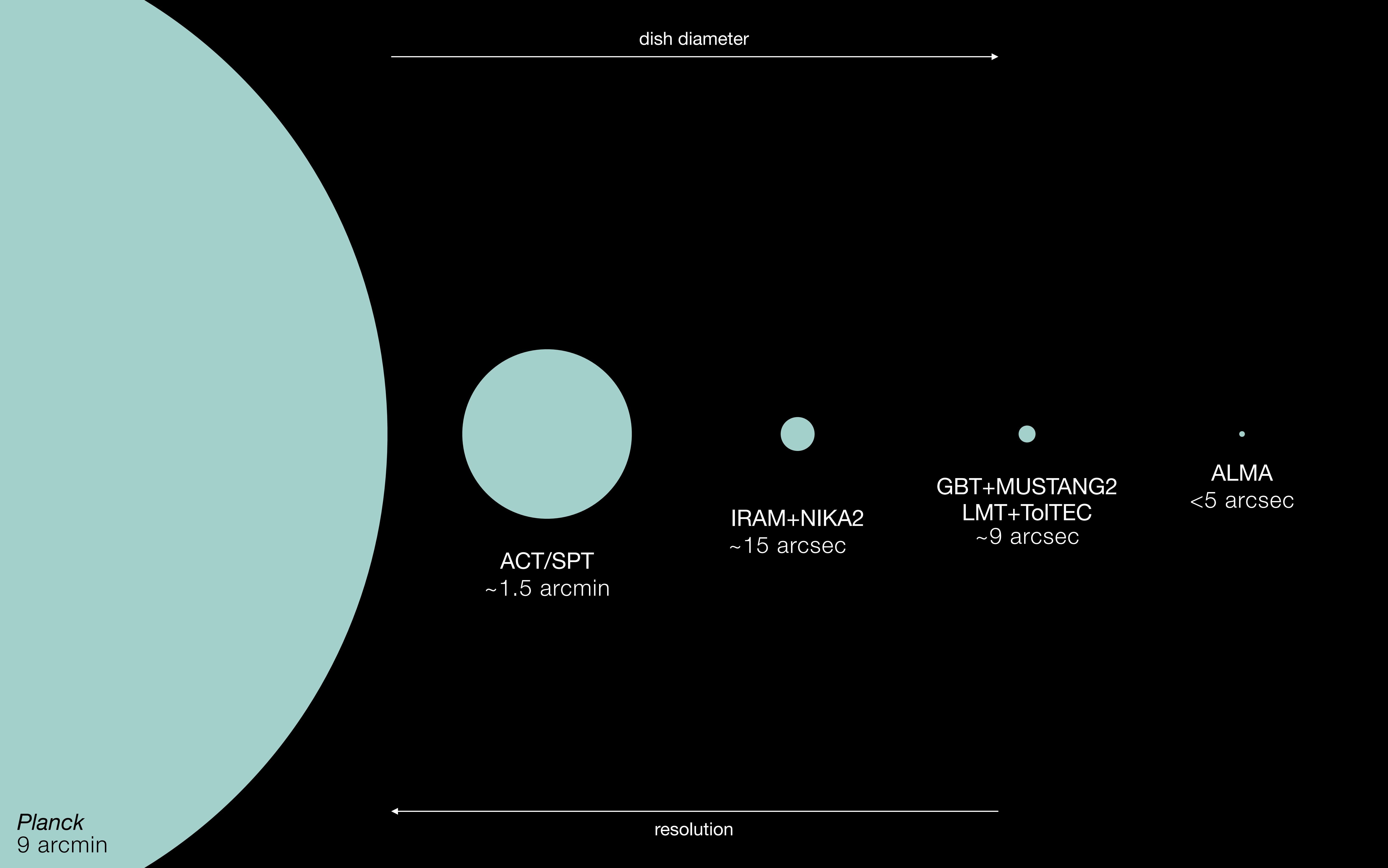
dish diameter
Planck
9 arcmin
ACT/SPT
~1.5 arcmin
IRAM+NIKA2
~15 arcsec
GBT+MUSTANG2
LMT+TolTEC
~9 arcsec
ALMA
<5 arcsec
resolution

Atacama Large Millimeter Array (ALMA)

So far, ALMA is the only instrument with an angular resolution ≲5 arcsec

- A large aperture is *synthesized* by combining the signals from separated small telescopes
- Measures the Fourier transform of the sky surface brightness

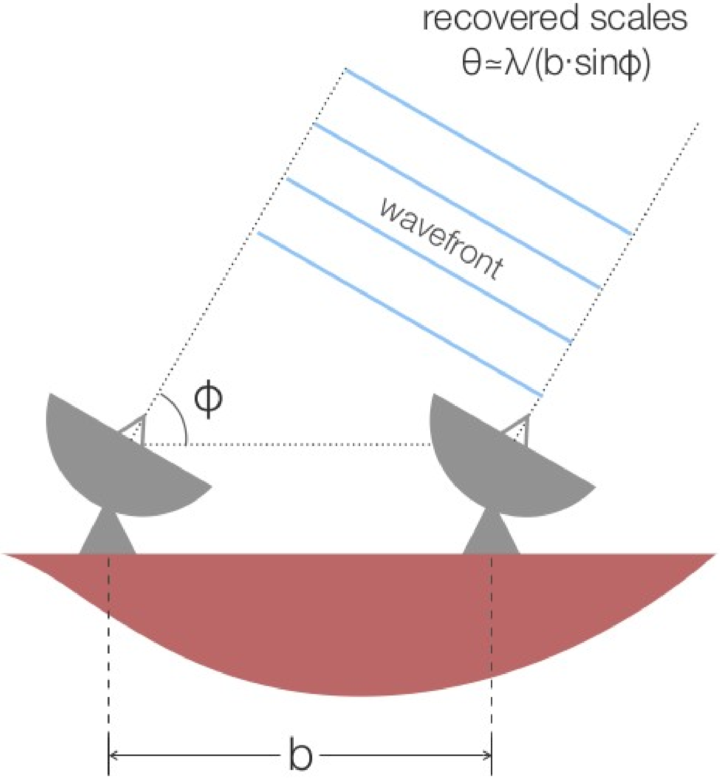

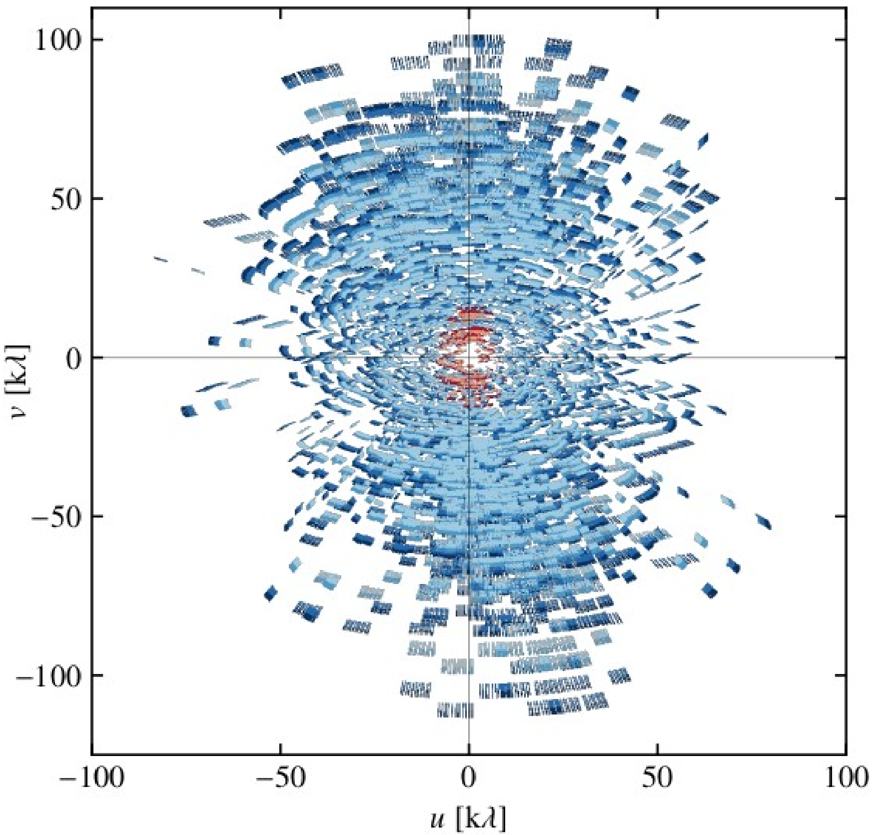

DM+2019 (arXiv:1812.01034)

Missing flux and large-scale filtering

Consequence of incomplete coverage of the *uv*-plane

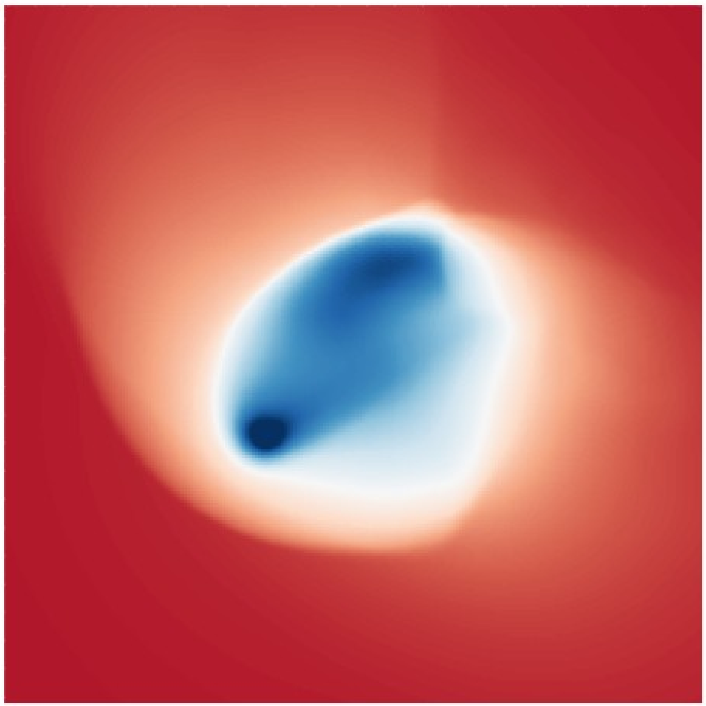

Congyao Zhang (MPA)

Missing flux and large-scale filtering

Consequence of incomplete coverage of the *uv*-plane

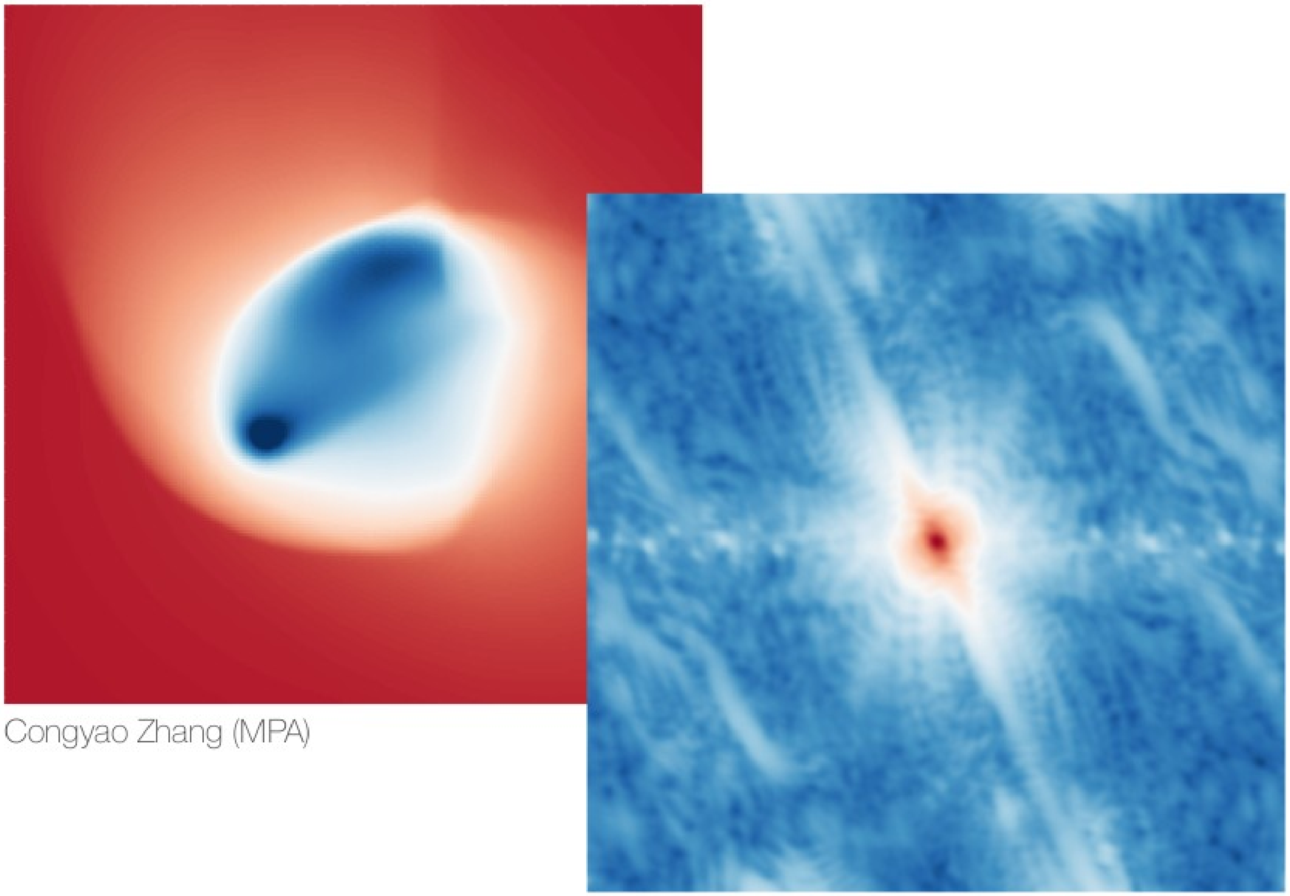

Congyao Zhang (MPA)

Missing flux and large-scale filtering

Consequence of incomplete coverage of the *uv*-plane

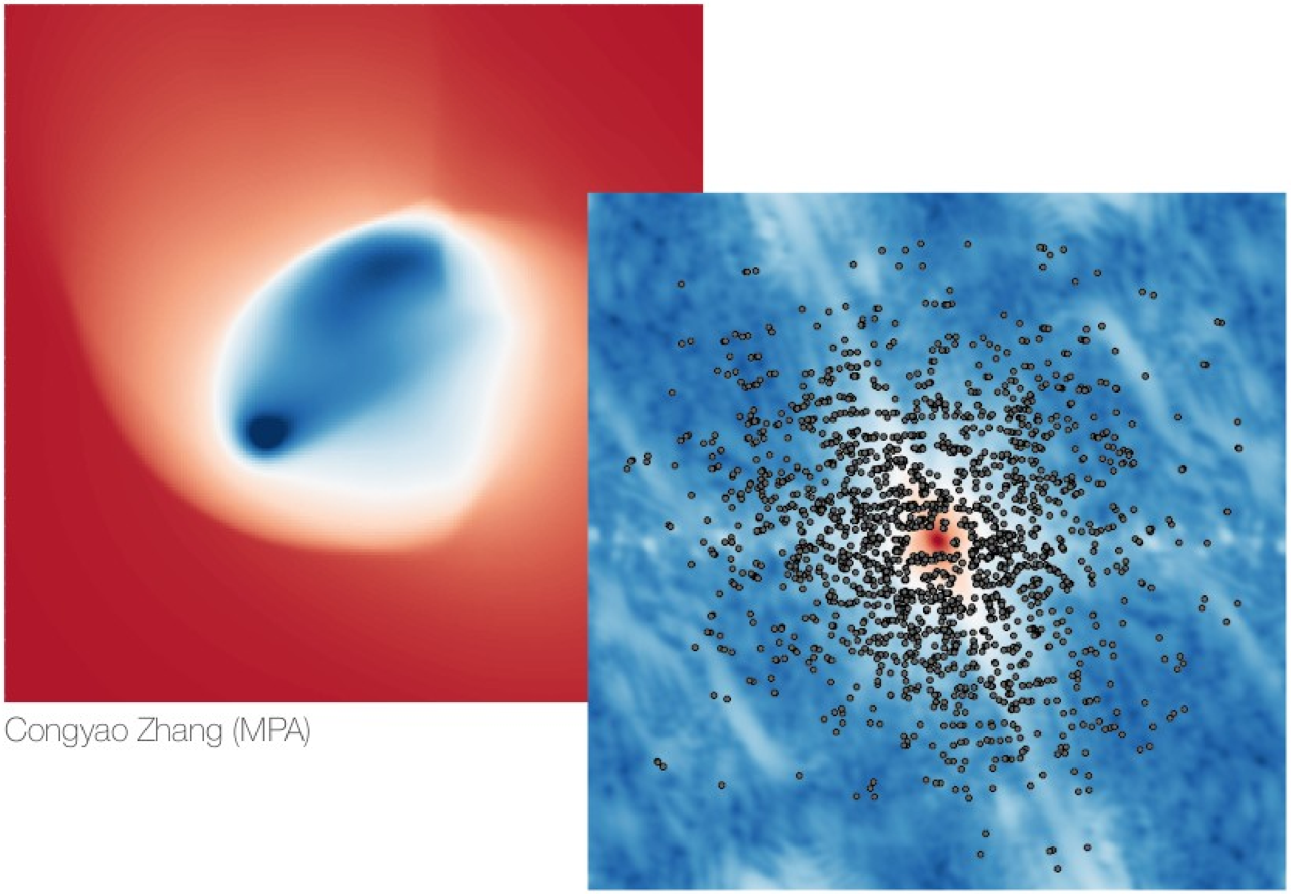

Congyao Zhang (MPA)

Missing flux and large-scale filtering

Consequence of incomplete coverage of the *uv*-plane

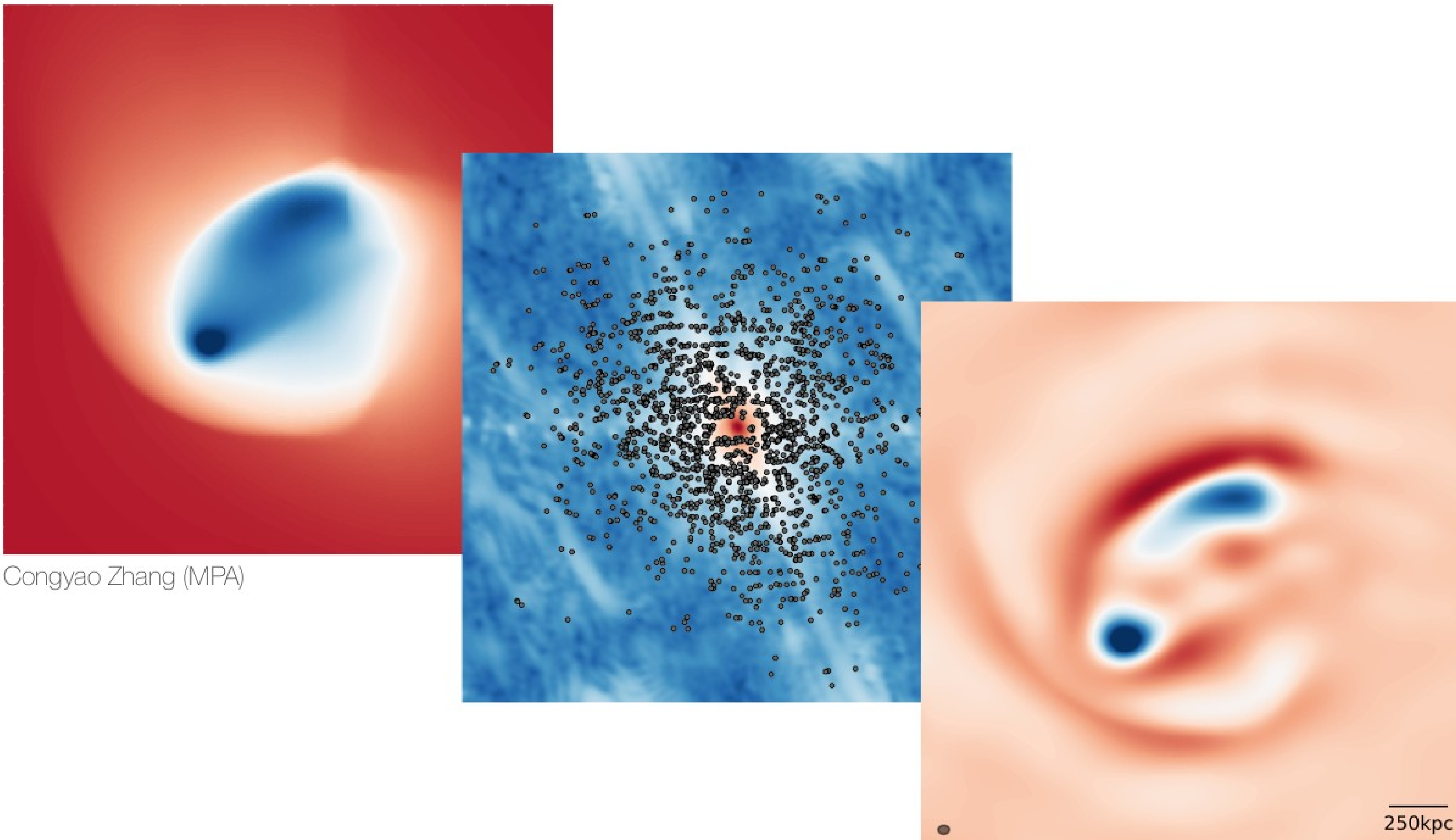

Congyao Zhang (MPA)

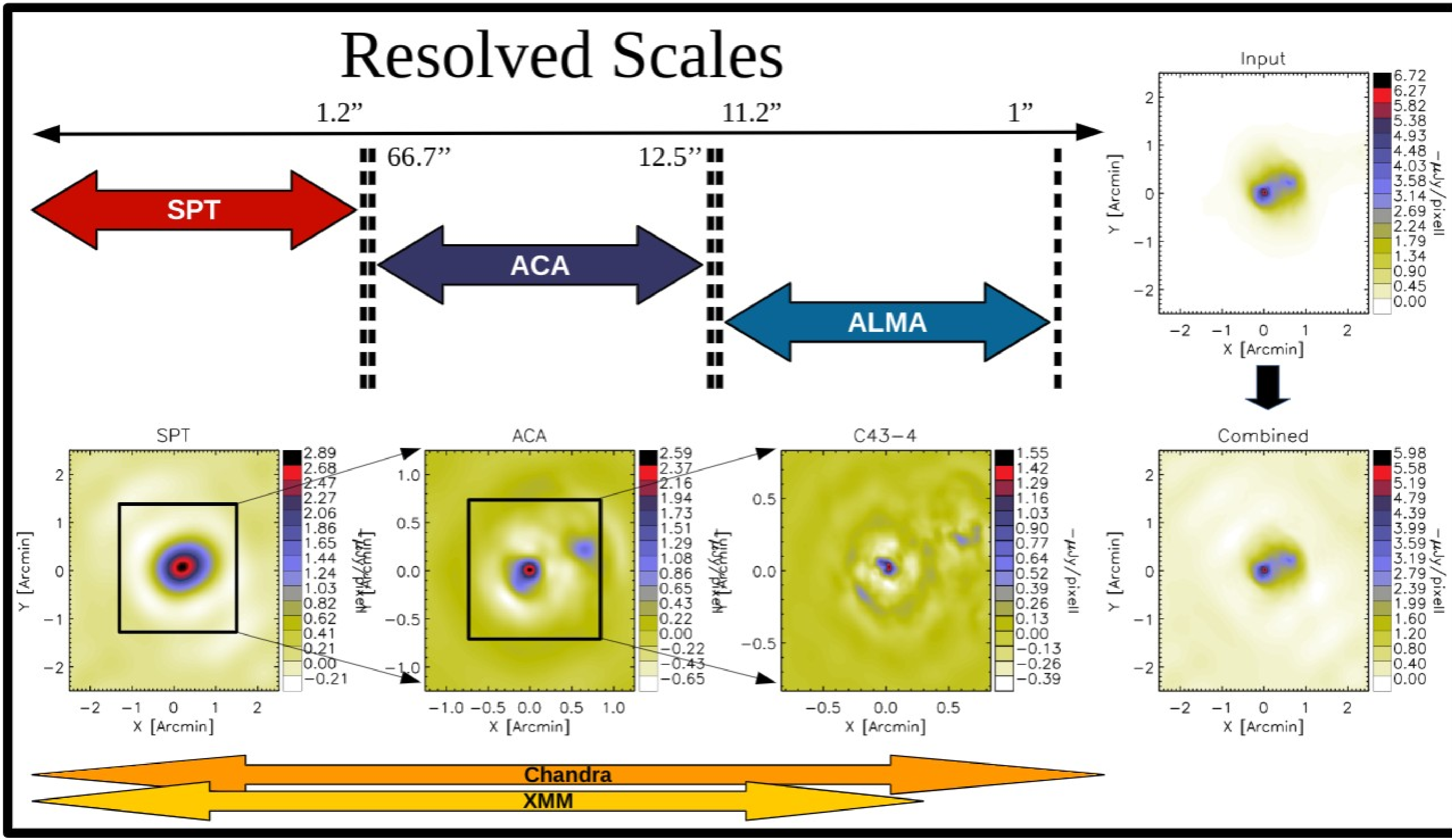
Resolved Scales
1.2”
11.2”
1”
66.7”
12.5”
SPT
ACA
ALMA
Input
Combined
C43−4
X [Arcmin]
Y [Arcmin]
−μJy/pixel
Chandra
XMM

The South Pole Telescope (SPT)

10-meter
submm wave telescope

100 150 220 GHz and
1.6 1.2 1.0 arcmin resolution

2007: SPT-SZ
960 detectors (UCB)
100,150,220 GHz

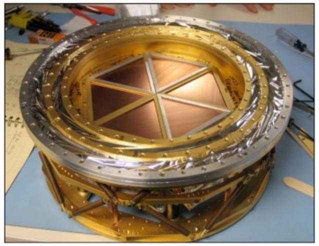

2012: SPTpol
1600 detectors
100,150 GHz
+Polarization

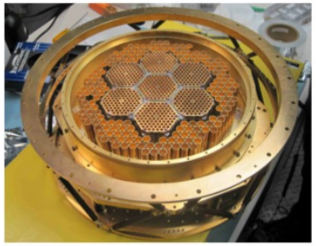

2016: SPT-3G
16,000 detectors
100,150, 220 GHz
+Polarization

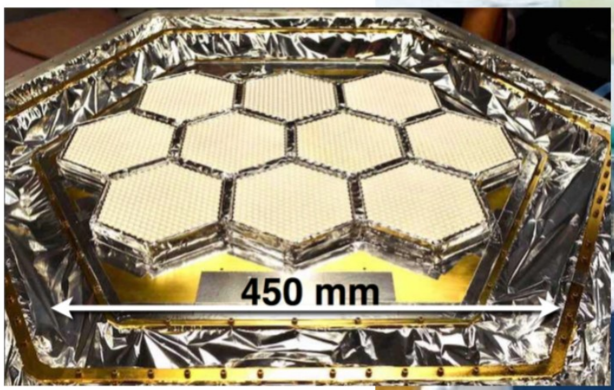

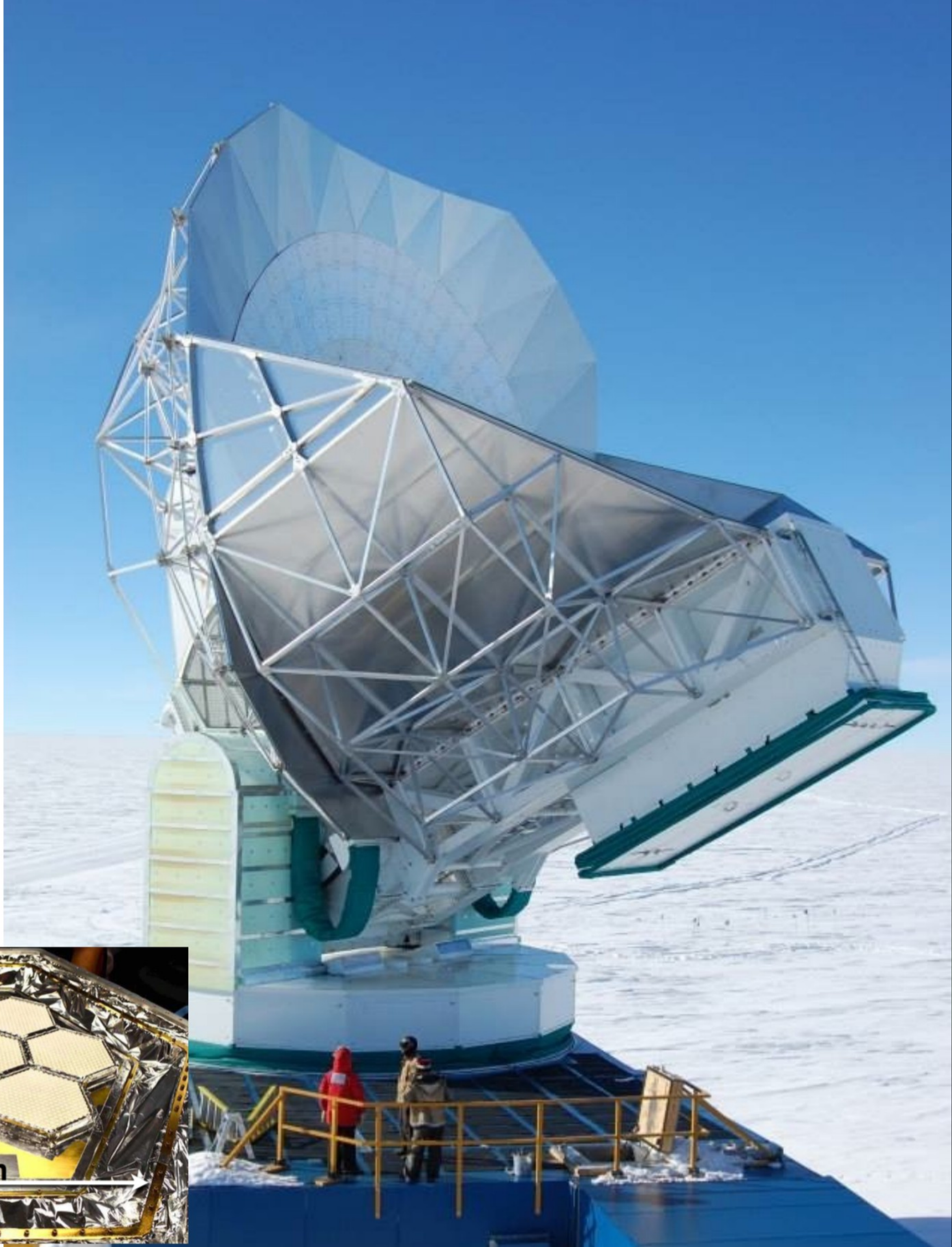

South Pole Telescope

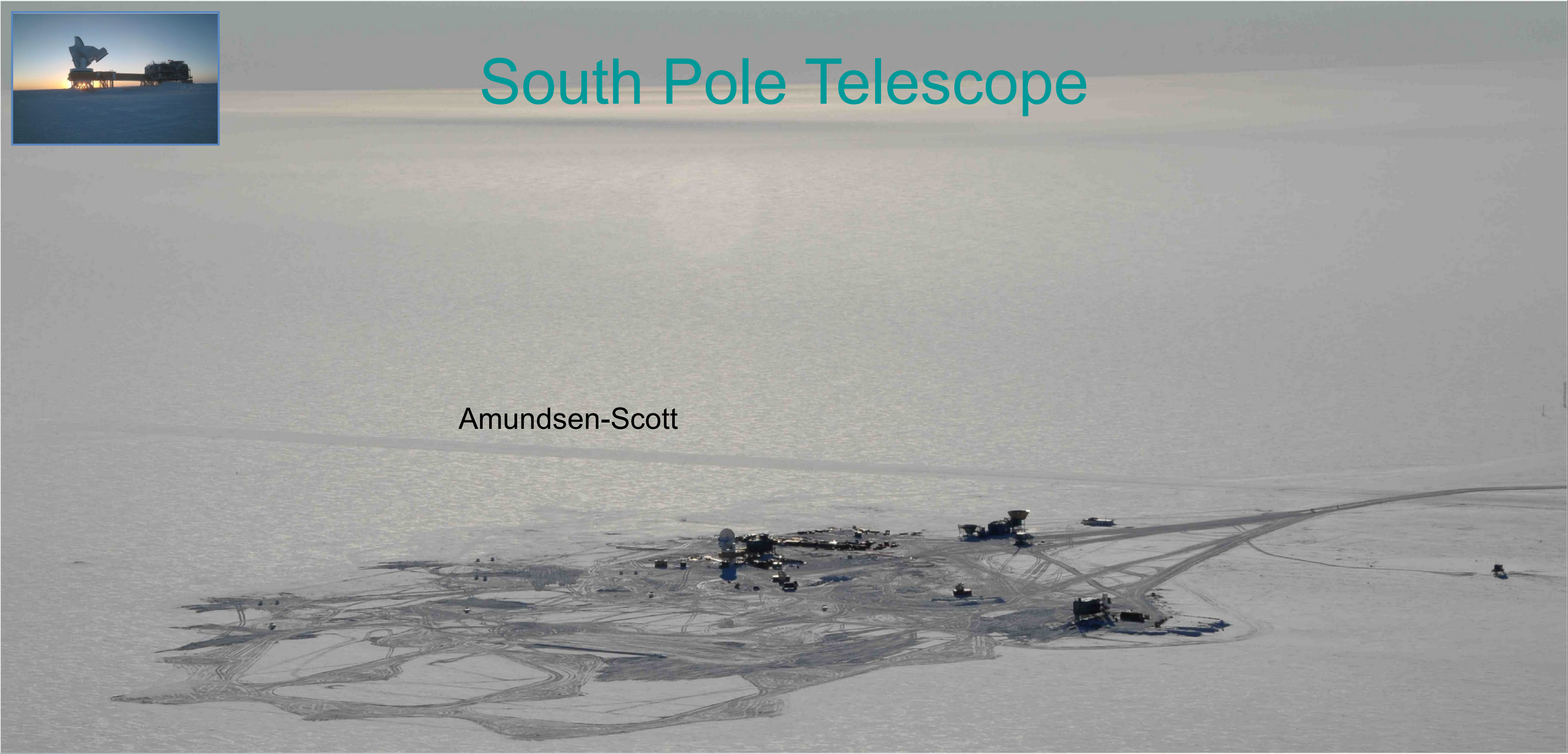

SPT data

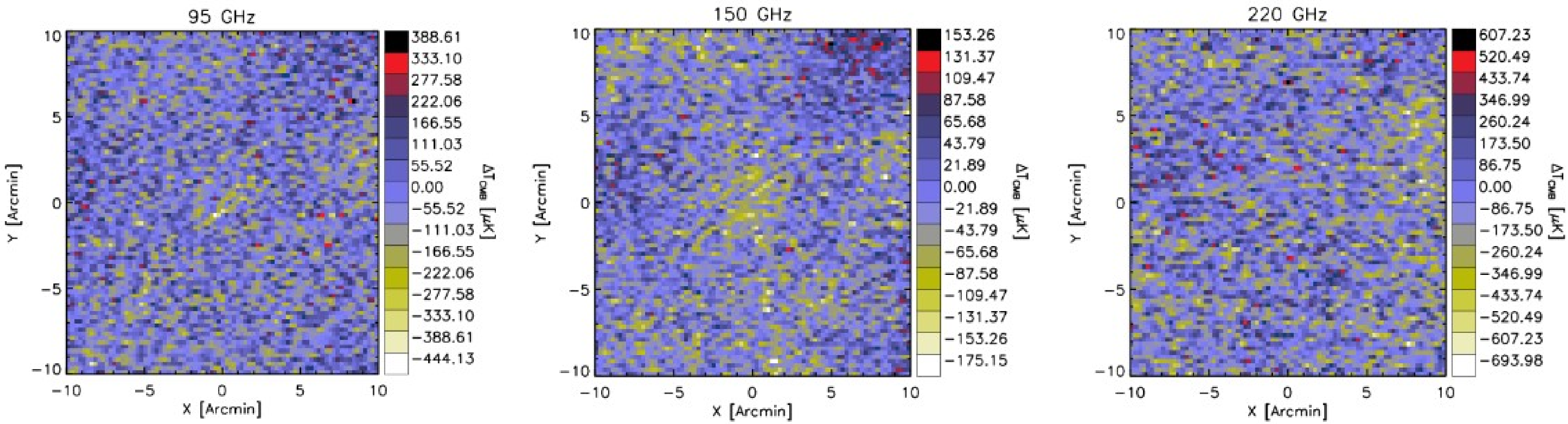
95 GHz
388.61
333.10
277.58
222.06
166.55
111.03
55.52
0.00
−55.52
−111.03
−166.55
−222.06
−277.58
−333.10
−388.61
−444.13
150 GHz
153.26
131.37
109.47
87.58
65.68
43.79
21.89
0.00
−21.89
−43.79
−65.68
−87.58
−109.47
−131.37
−153.26
−175.15
220 GHz
607.23
520.49
433.74
346.99
260.24
173.50
86.75
0.00
−86.75
−173.50
−260.24
−346.99
−433.74
−520.49
−607.23
−693.98
X [Arcmin]
Y [Arcmin]
ΔT_CMB [μK]

Optimal Matched Filter

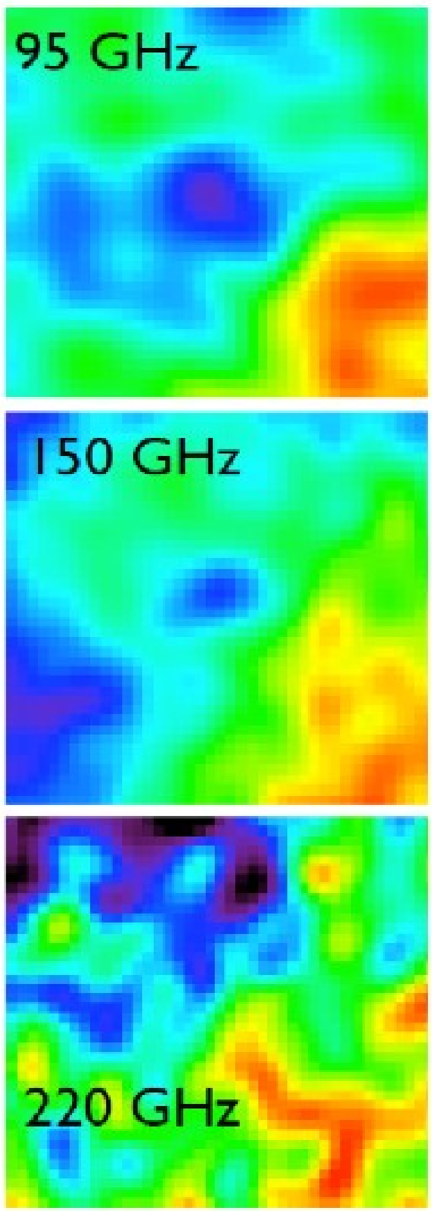

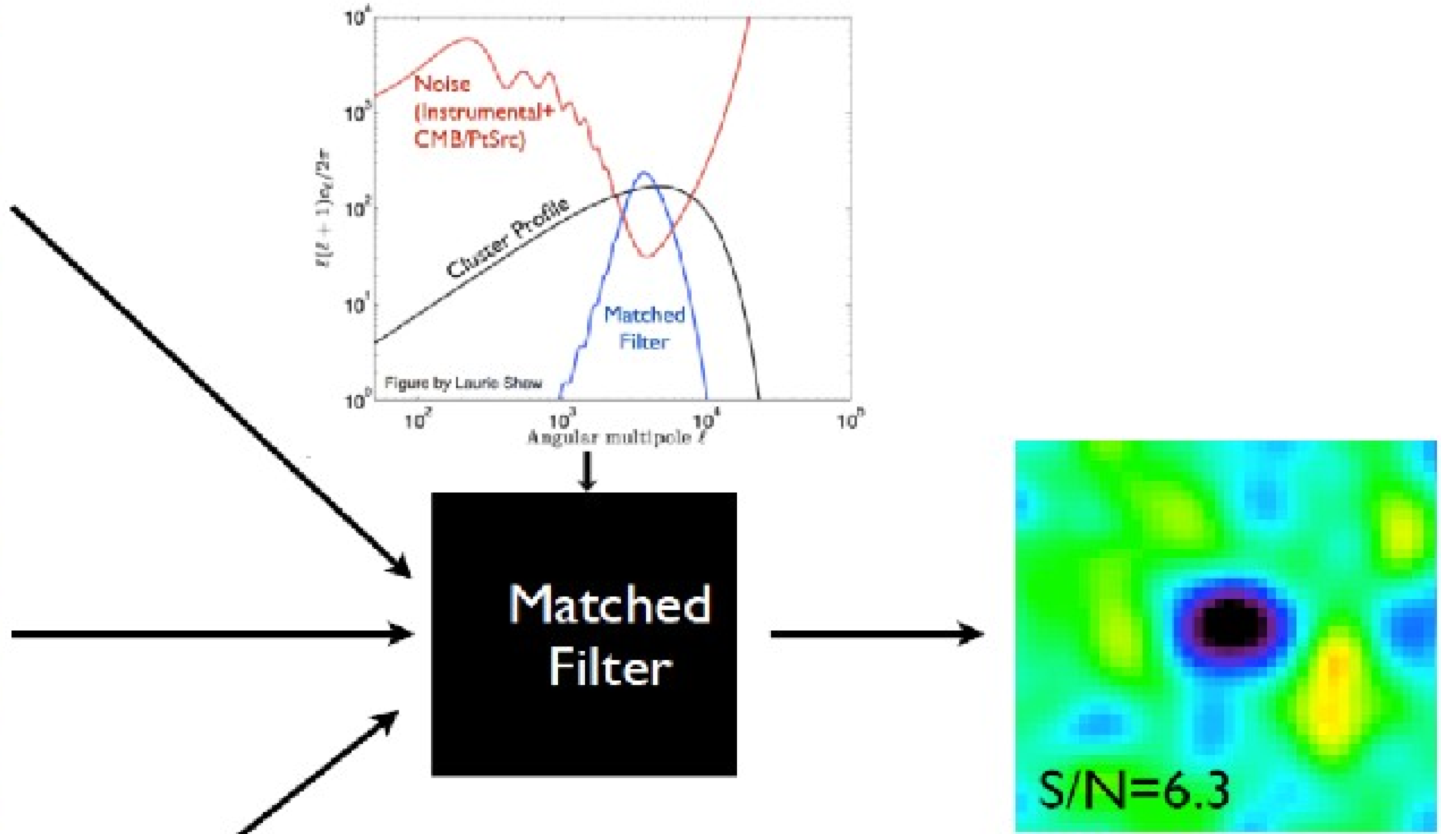

$$\psi(\vec{k}) = \frac{B(\vec{k})S(|\vec{k}|)}{B(\vec{k})^2 N_{\mathrm{astro}}(|\vec{k}|) + N_{\mathrm{noise}}(\vec{k})}$$

$$S(\vec{\theta}) = \Delta T_0 (1 + |\vec{\theta}|^2/\theta_c^2)^{-1}$$

- Matched-filter multi-frequency cluster finder (Melin et al. 2006)

SPT filtered maps

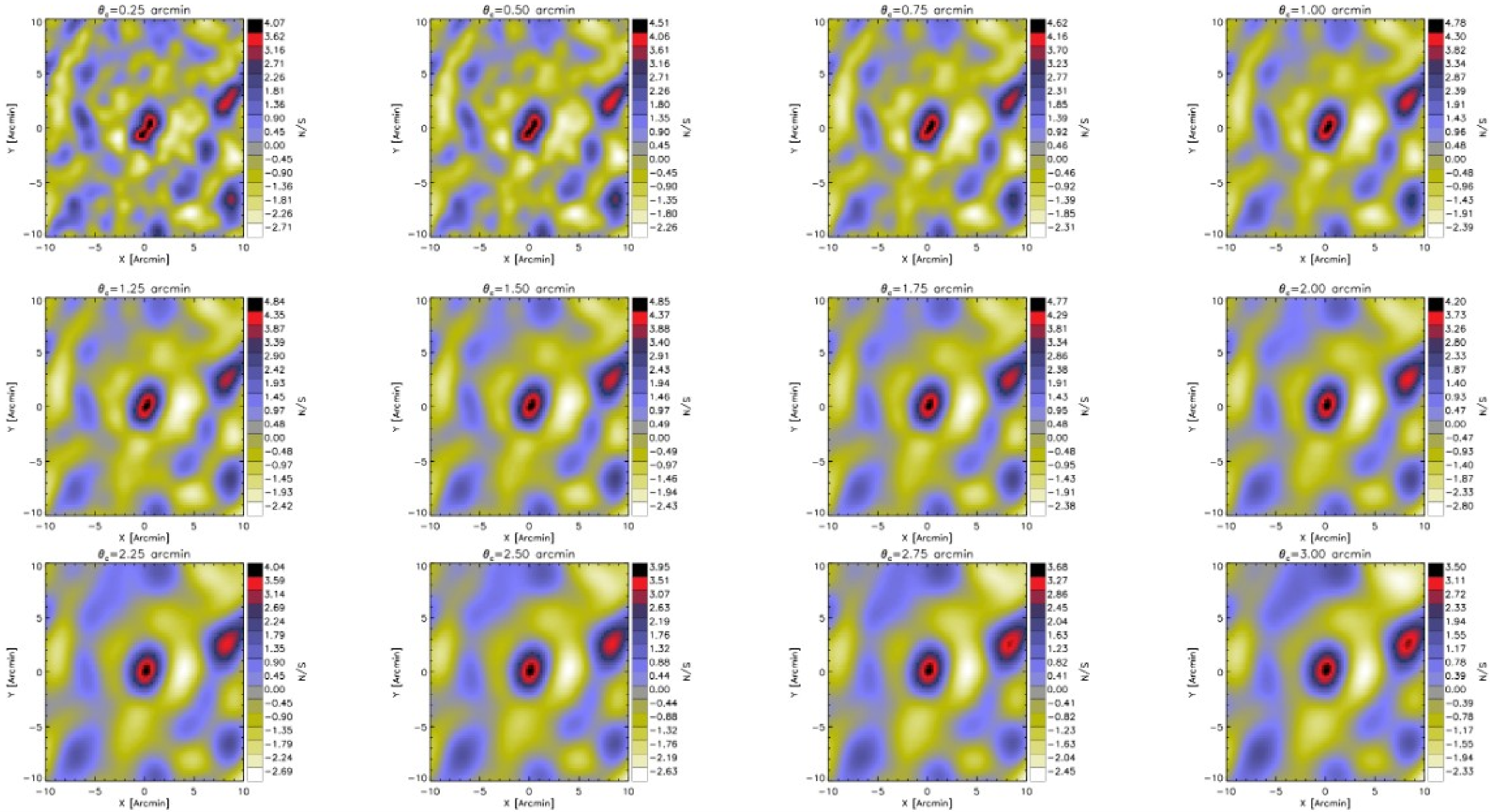

S/N = 5

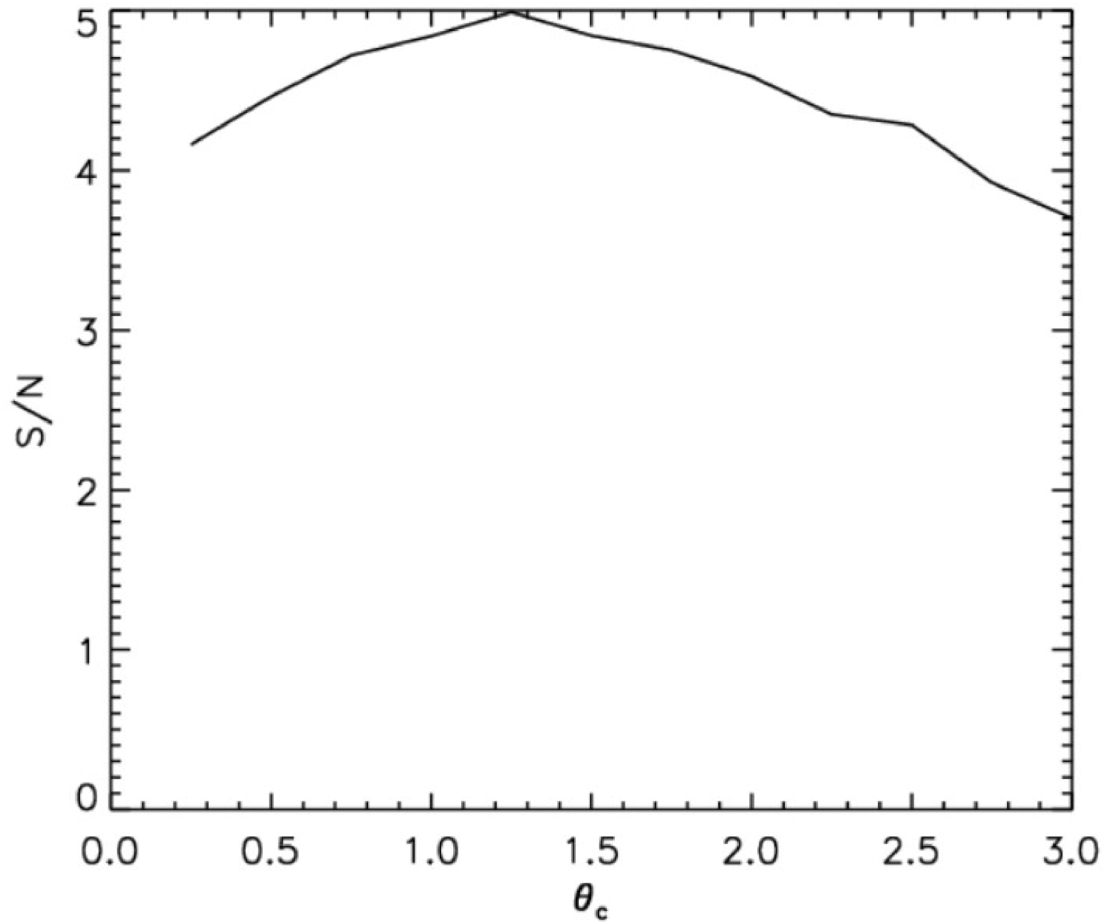

Confirmation of Galaxy Population

- Over the broad redshift range of the sample, we use optical and NIR imaging to probe for the galaxy population (Strazzullo+)

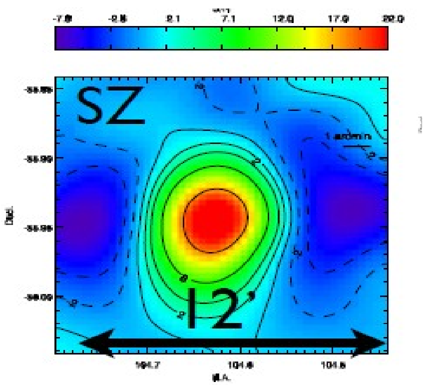

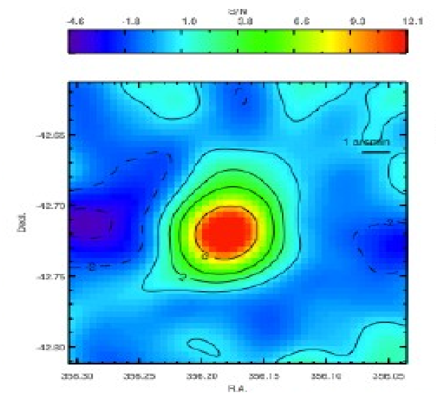

116

Confirmation of Galaxy Population

- Over the broad redshift range of the sample, we use optical and NIR imaging to probe for the galaxy population (Strazzullo+)

0658-5358 (z=0.30)
(Bullet)

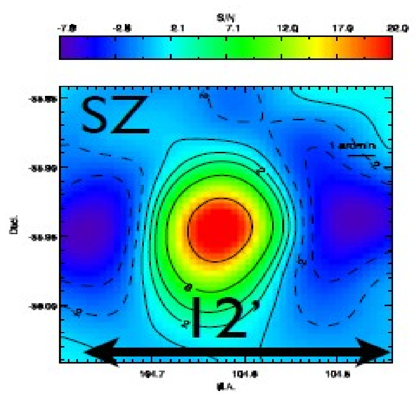

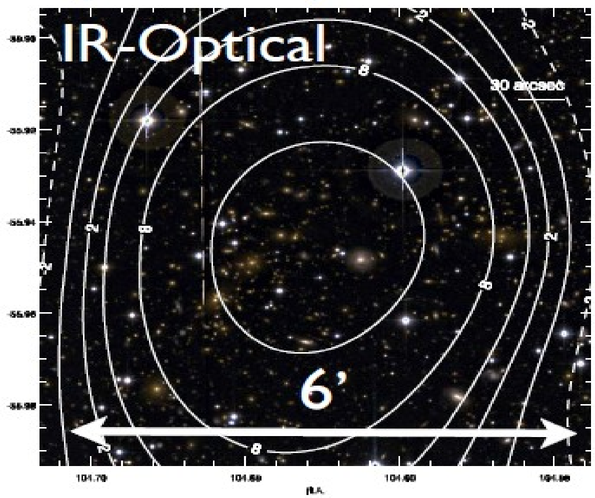

2344-4243 (z=0.62)

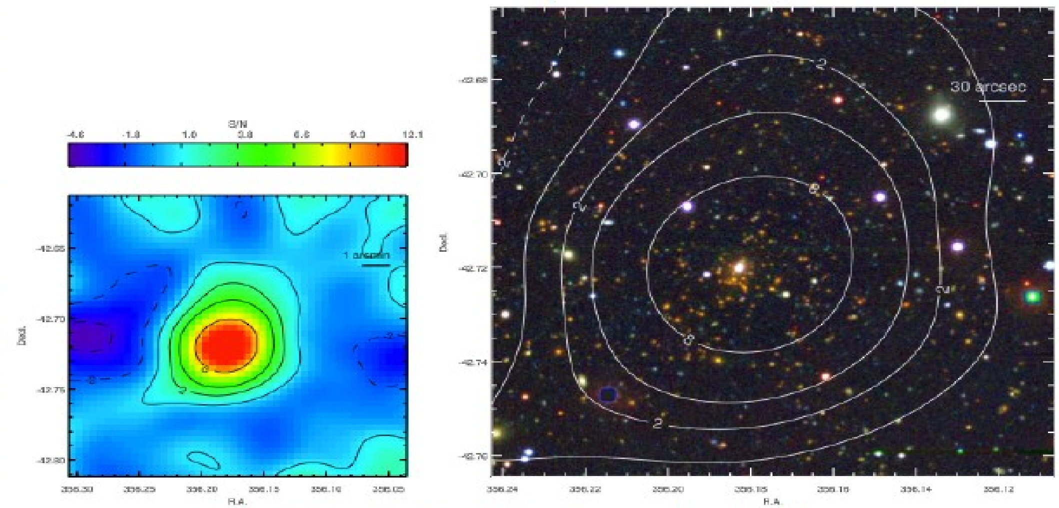

Multiple-facility Imaging Campaign for Cluster Confirmation

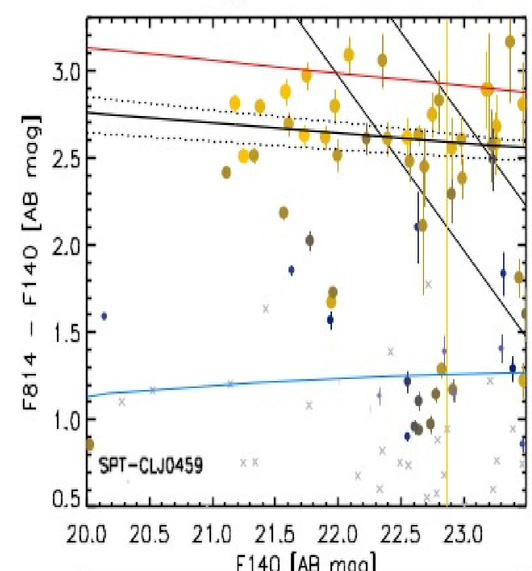

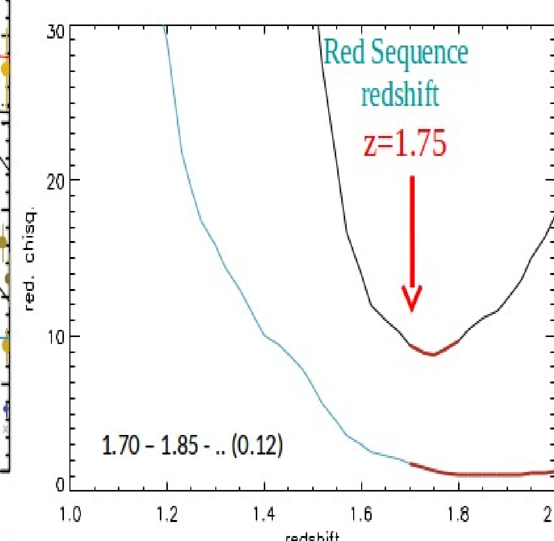

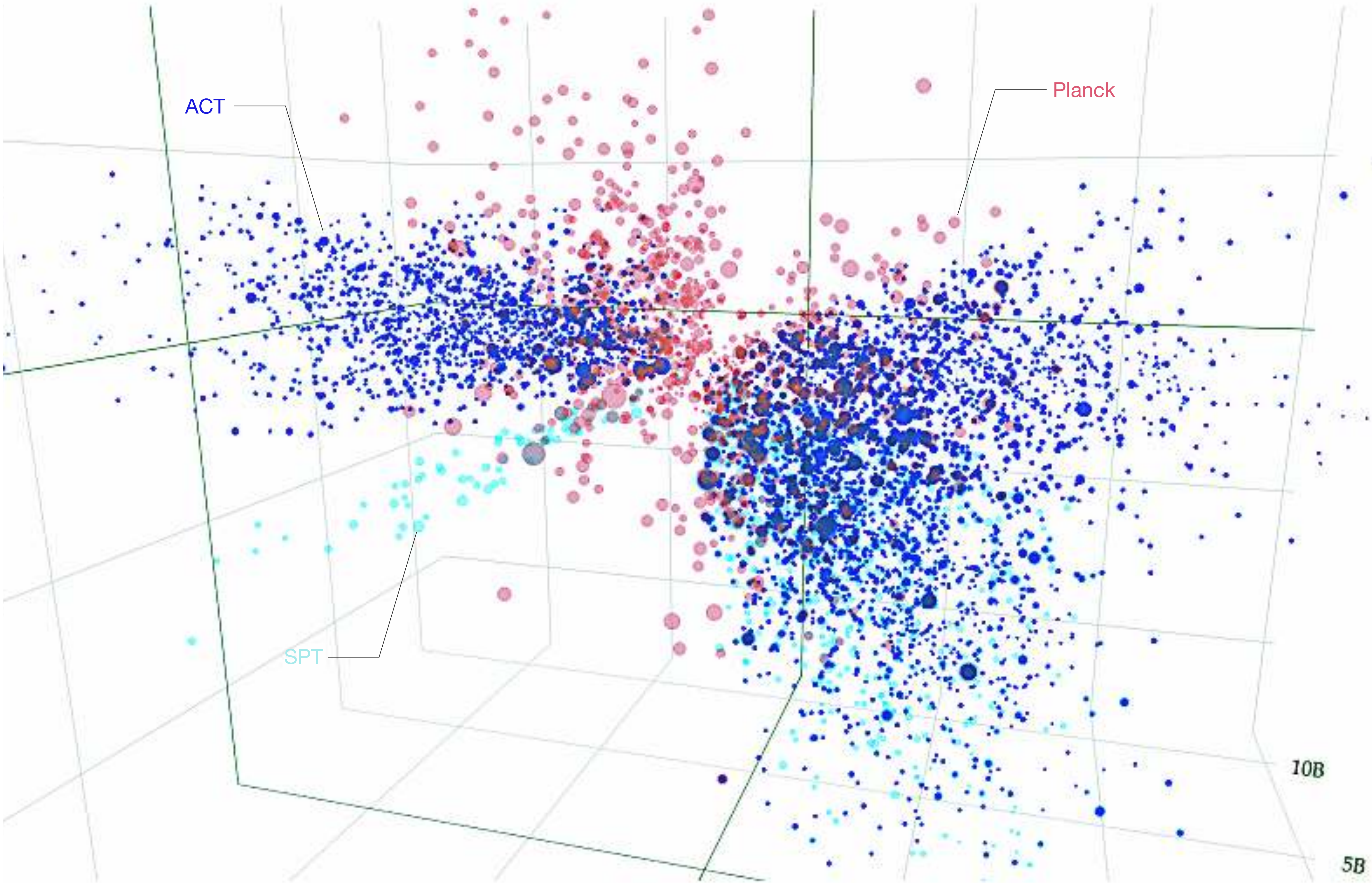

ACT collaboration (private)

clusters across cosmic time

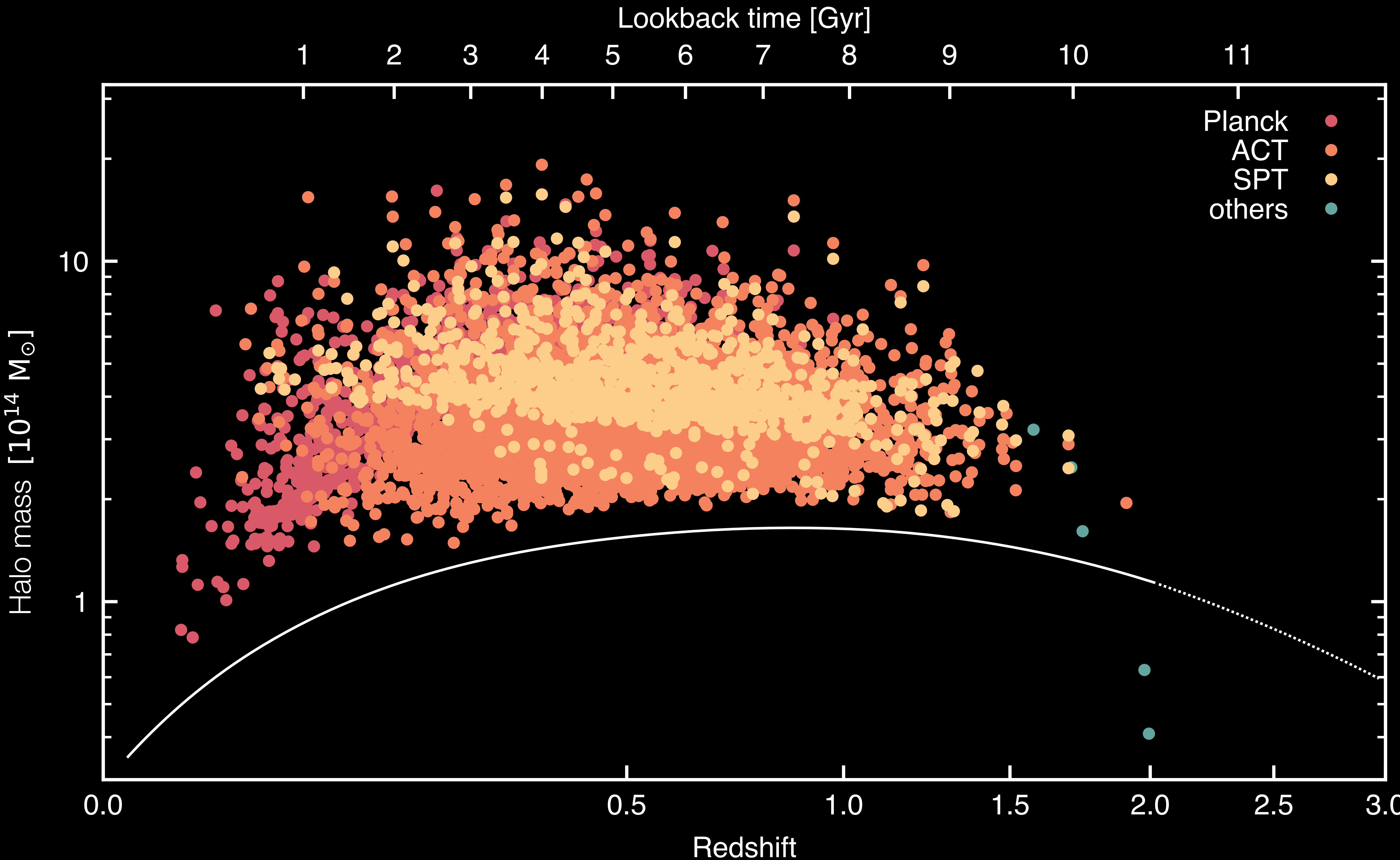

PlanckXXVII 2016, Hilton+2021, Bocquet+2019, Huang+2020, Bleem+2020

clusters across cosmic time

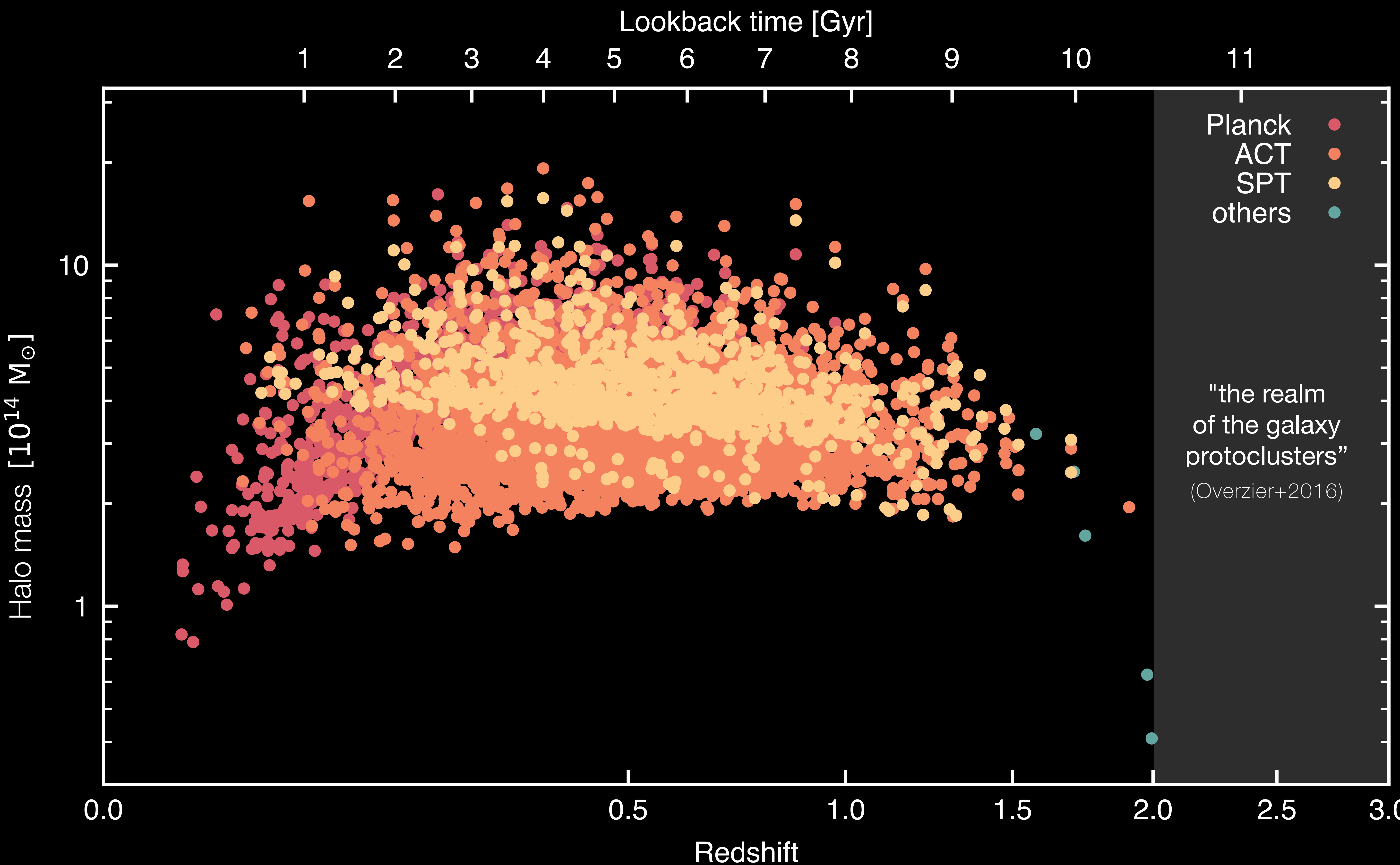

PlanckXXVII 2016, Hilton+2021, Bocquet+2019, Huang+2020, Bleem+2020

a turning point in cosmic history

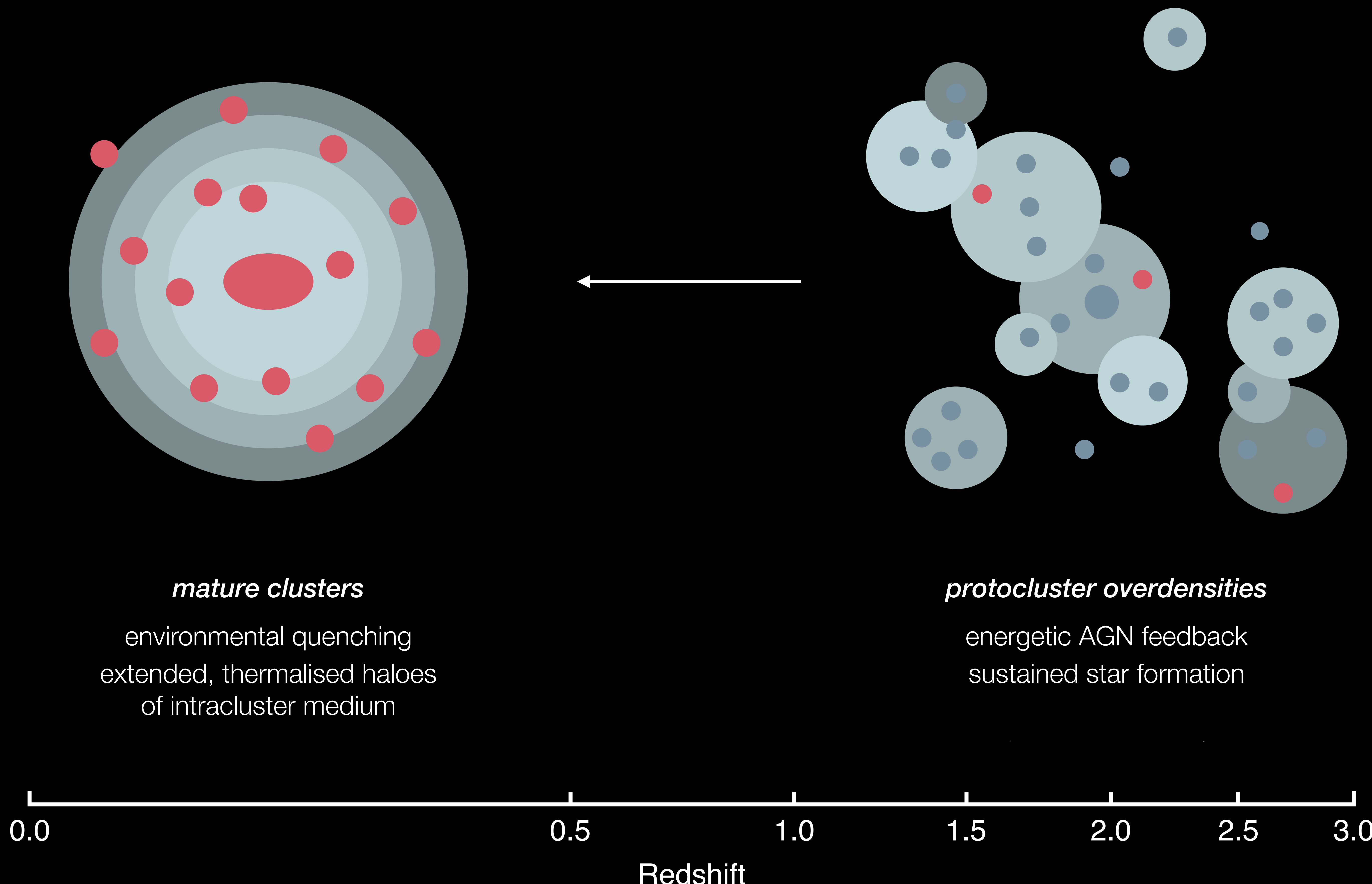

adapted from Chiang+2017 & Shimakawa+2018

confirmation of long-standing predictions

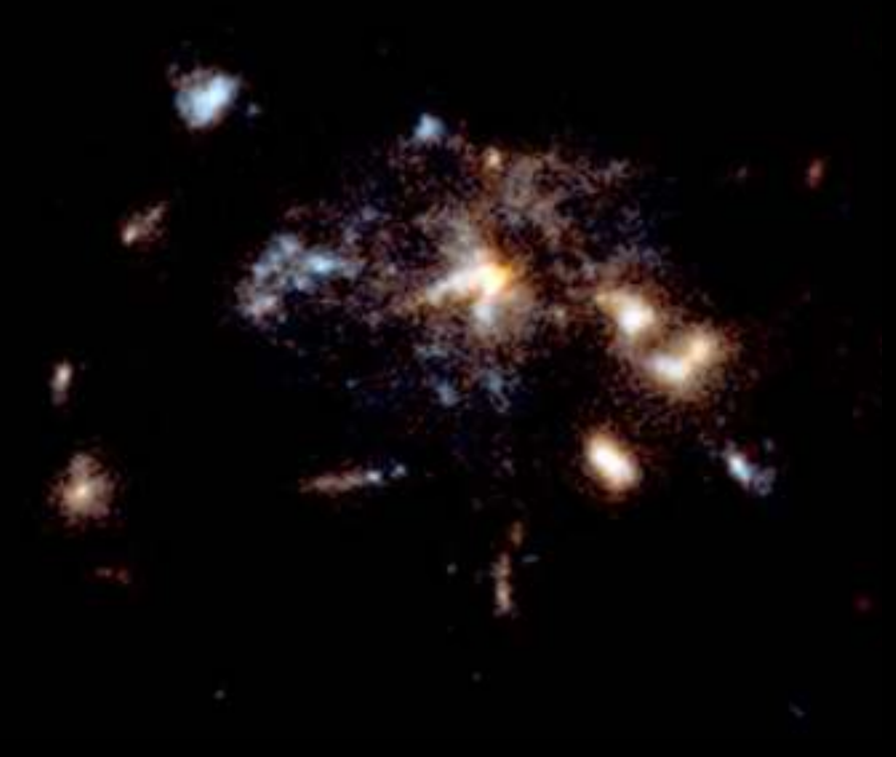

Pentericci+1997, Hatch+2009
Star-bursting proto-BCG fed by "cooling flow"-like precipitation (but not the only scenario)

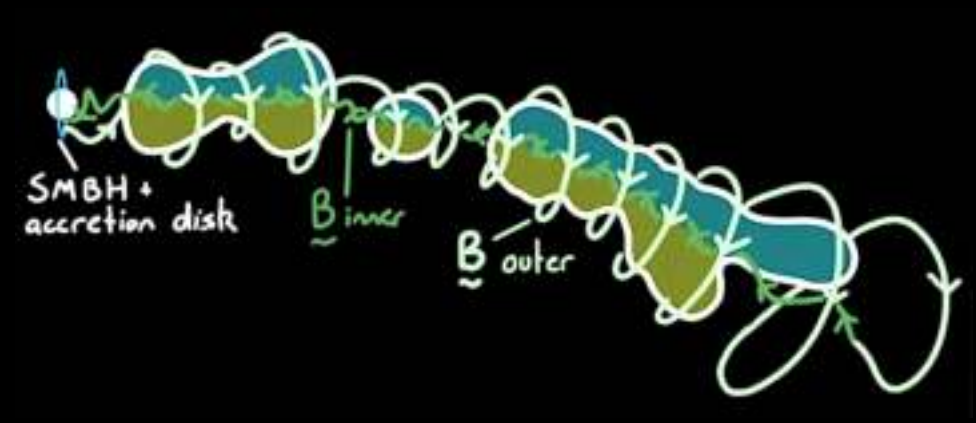

Carilli+1997, Anderson+2022
RMs generate in thin sheath of hot gas around the radio jet

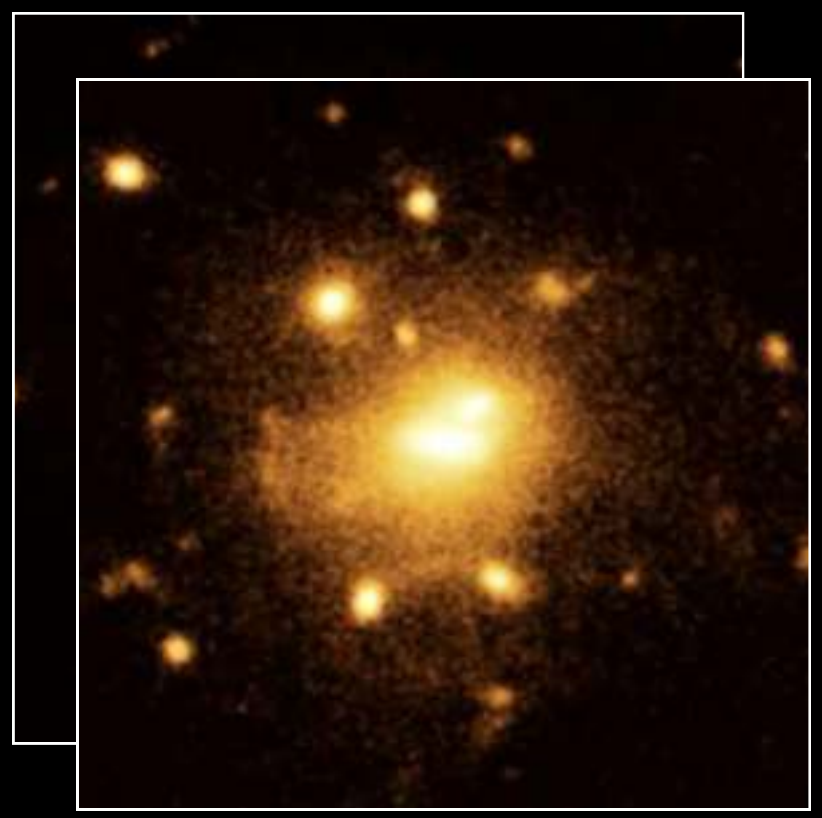

Saro+2009
simulated protoclusters with gravitational potential permeated by ICM at 2-5 keV

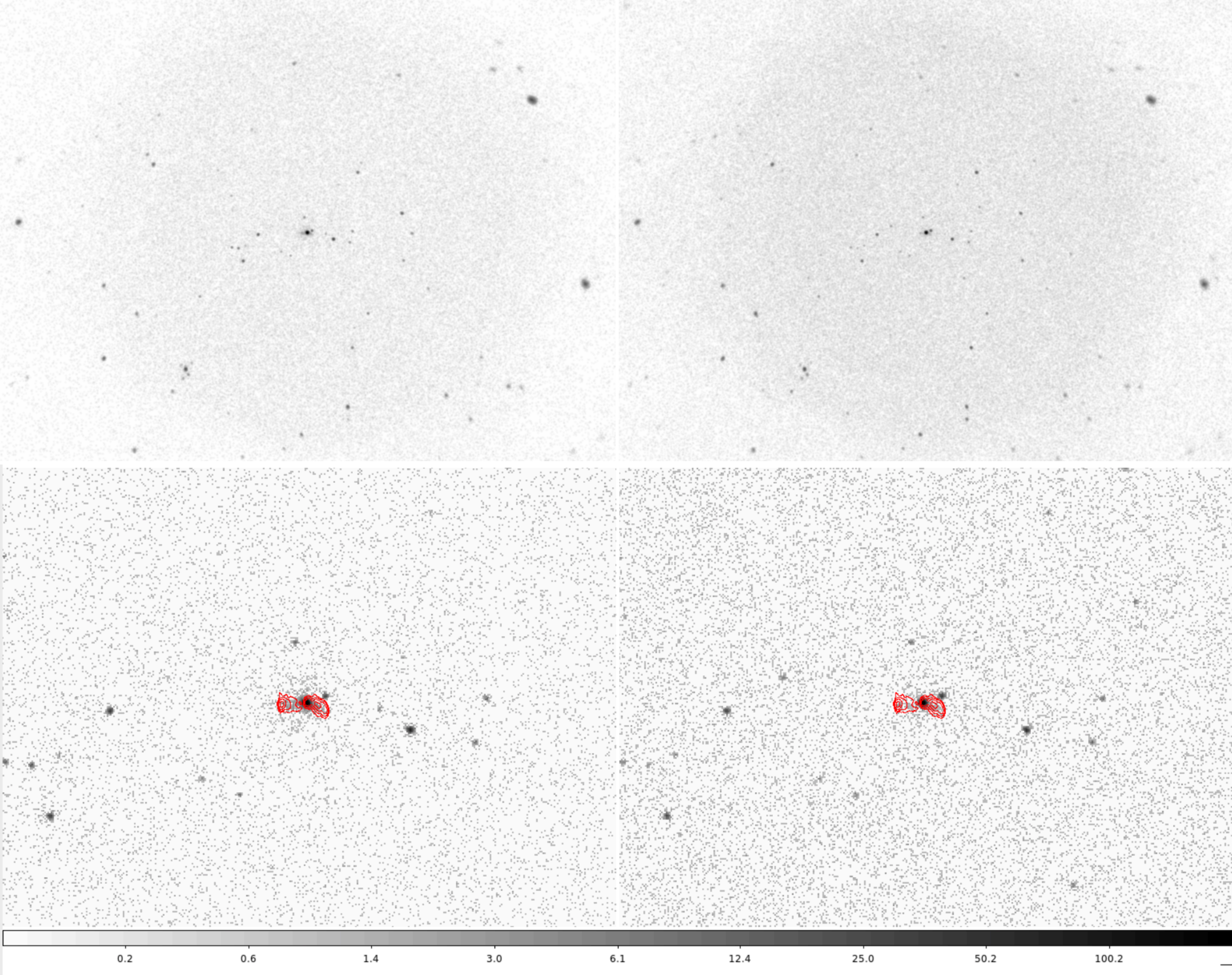
0.2
0.6
1.4
3.0
6.1
12.4
25.0
50.2
100.2

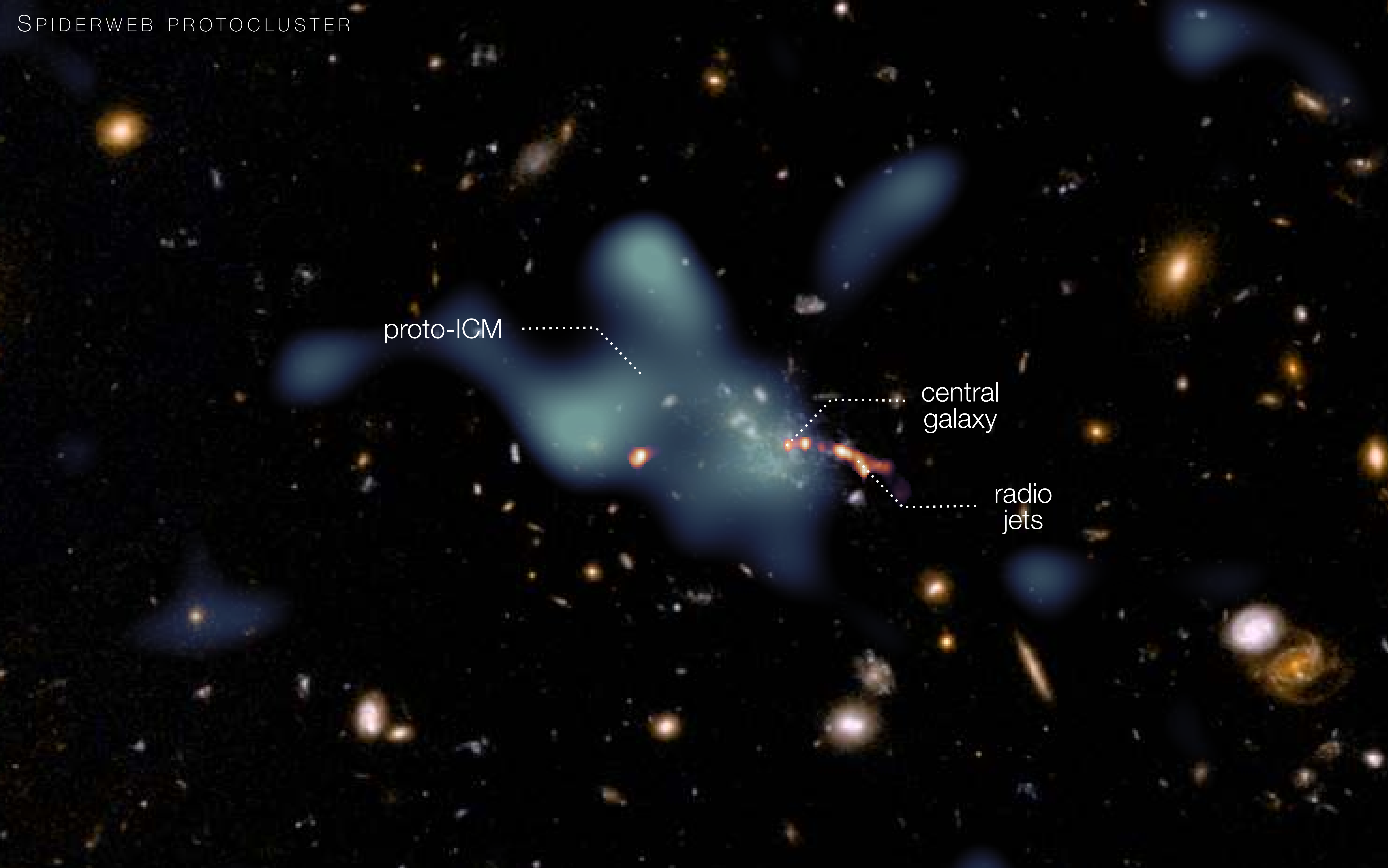
Spiderweb protocluster
proto-ICM
central
galaxy
radio
jets

What is the Mass of this objects?

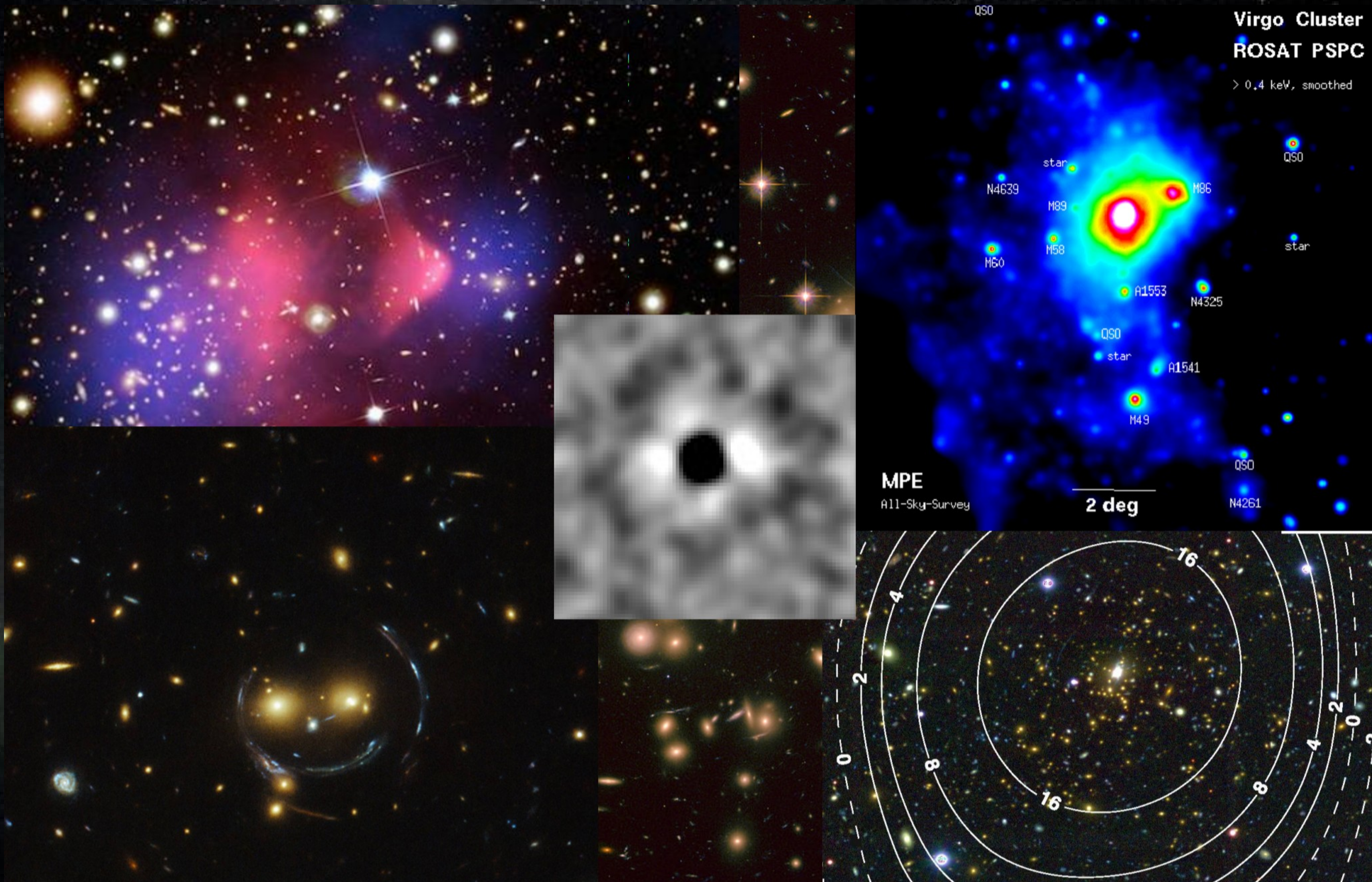

Multi-wavelength Observations: Mass Calibration

- Multi-wavelength mass calibration campaign, inclu
  - **Thermodynamical properties**
    - X-ray with
      - Chandra
      - XMM

Multi-wavelength Observations: Mass Calibration

- Multi-wavelength mass calibration campaign, including:
  - X-ray with
    - Chandra
    - XMM

Gravitational lensing from background galaxies

  - Weak lensing from:
    - Magellan ($0.3 < z < 0.6$)
    - HST ($z > 0.6$)
    - DES

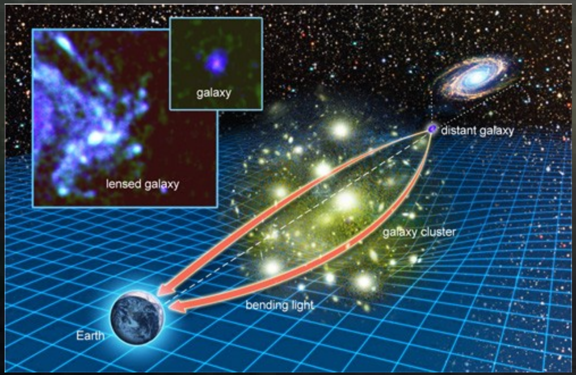

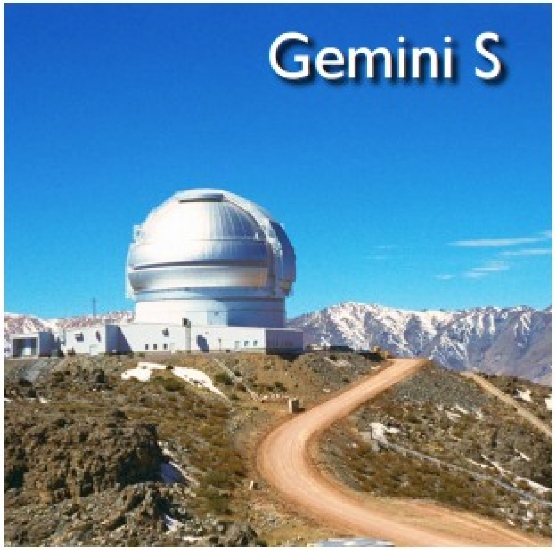

Multi-wavelength Observations: Mass Calibration

- Multi-wavelength mass calibration campaign, inclu
  - X-ray with
    - Chandra
    - XMM
  - Weak lensing from:
    - Magellan (0.3 < z < 0.6)
    - HST (z > 0.6)
    - DES

Velocity Dispersion of Galaxies

  - Dynamical masses from
    - Gemini (z < 0.8)
    - VLT (z > 0.8)
    - Magellan (z > 0.8)

CMB Cluster Lensing with SPT-SZ

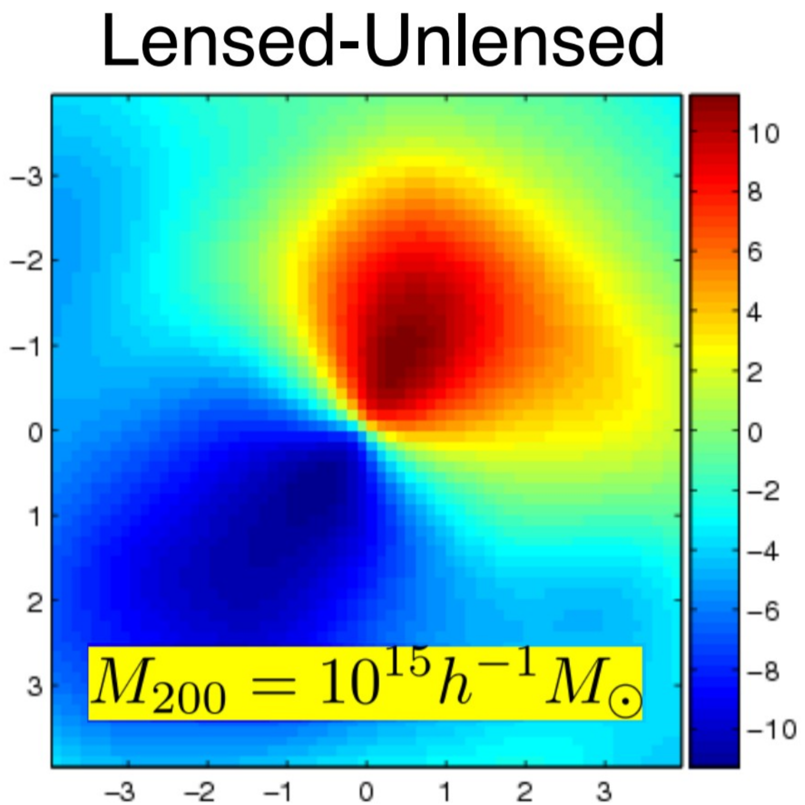

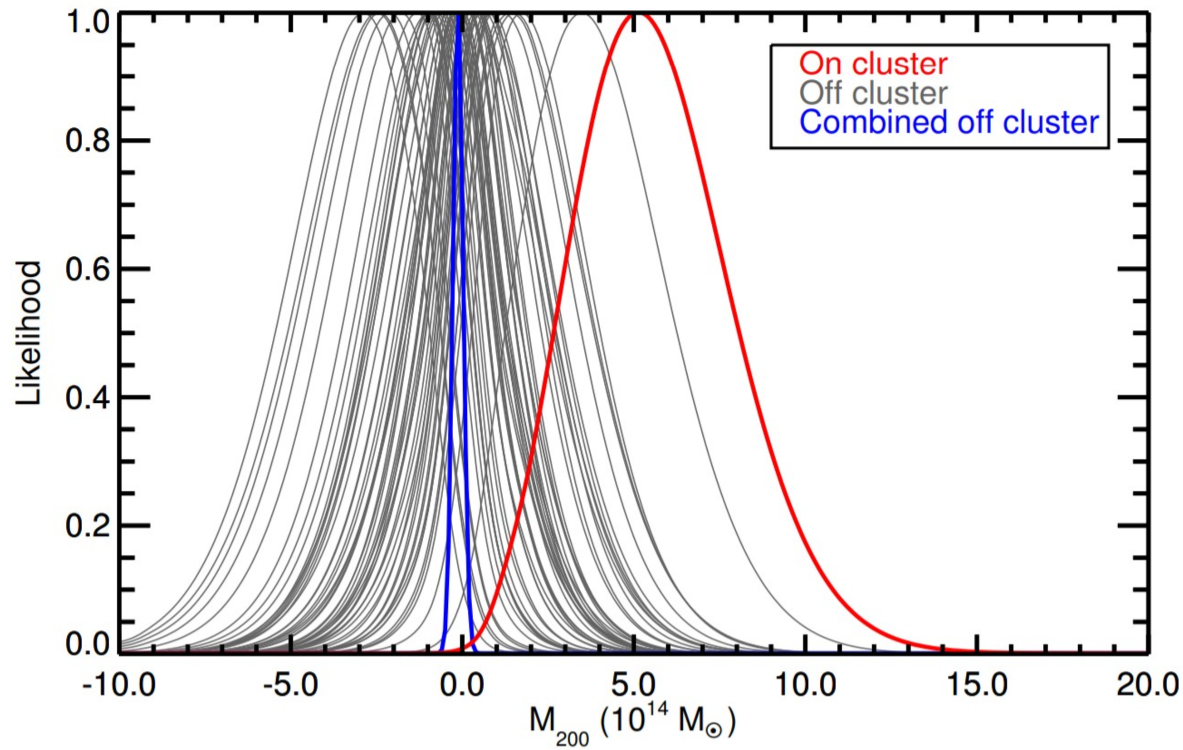

- A ~few uK "dimple" in the CMB caused by lensing of a ~10^{15} solar mass cluster

- A 3.1σ detection of CMB lensing using ~500 clusters measured by SPT-SZ

Baxter et al. 2015, ApJ, 806, 247

See also: Planck Collab. XXIV, 2016 A&A 594, A24 Madhavacheril et al. PRL 114, 15.